A Near-field Scanning Optical Microscope: Construction and Operation

by

John Philip Dunn

Thesis

Presented to the Faculty of the Graduate School of

The University of Texas at Austin

in Partial Fulfillment

of the Requirements

for the Degree of

Master of Science in Applied Physics

The University of Texas at Austin

August 2009

A Near-field Scanning Optical Microscope: Construction and Operation

Approved by
Supervising Committee:

John W. Keto

Alejandro de Lozanne

Dedication

For my family, in deeper appreciation than can ever be said.

Acknowledgements

I would like to thank the following people for their encouragement and support. My advisor, Professor John W. Keto provided inspiration. Tim Westbrook provided a very good start to the project. Ignacio Gallardo provided SEM images and some good conversations. Nathan Erickson was a great office buddy. I am also appreciative of the efforts of Carol Noriega, the graduate coordinator.

I would also like to thank the head of the student shop, Jack Clifford, and the machine shop supervisor, Allan Schroeder, and the machinists who gave good advice and made some of the parts.

August, 2009

Abstract

A Near-field Scanning Optical Microscope: Construction and Operation

John Philip Dunn, MSApplPhy

The University of Texas at Austin, 2009

Supervisor: John W. Keto

This thesis discusses the design and construction of a Near-field Scanning Optical Microscope (NSOM). Basic principles of operation, the characteristics of the hardware components, and the control software are discussed. A unique method of controlling the position of the probe is developed, and scans of a diffraction grating are presented. We show the influence that the surface topology and reflectivity and the interference of direct and reflected light have on the images. A second design of the instrument, for use in a vacuum chamber and with a flexure stage for lateral motion, is accomplished.

Table of Contents

List of Figures

Chapter 1: Introduction

1.1 Near-Field Scanning Optical Microscopy

The resolving ability of an optical microscope is limited by the fundamental inability to focus the light onto a sufficiently small spot. The diffraction limit is approximately half of the wavelength of light; features smaller than this limit cannot be distinguished from other nearby features when using far-field optics. Scanning Probe Microscopy (SPM), in general, uses either a very tiny aperture or a very sharp tip to obtain resolution beyond the diffraction limit. The basic methods used in SPM were conceived in 1928 [Synge] but suffered from a lack of ability to manufacture probes of the required dimensions.

The Near-Field Scanning Optical Microscope (NSOM) is an instrument that uses light to investigate the properties and especially the surface topology of materials. Unlike the typical optical microscope, an NSOM is not restricted by the diffraction limit to imaging objects that are larger than the wavelength of the light. Instead, it uses the properties of small apertures [Bethe] to obtain information beyond the diffraction limit: in the near-field region, the resolution of the image is limited not by the wavelength of the light, but by the size of the aperture at the probe fiber tip. (You must also be able to reliably position the tip in sub-wavelength increments.)

The probe fiber can be used to either deliver light to the sample or to collect light from the sample. Transparent materials can have the source and collection of light on opposite sides of the sample, but opaque materials must have the source and collection on the same side of the sample. Our instrument described here operates in the “Reflection” mode as in Figure 1.1(d), with the probe fiber as the source of light and with far-field collection optics. With modification, it could work in the “Illumination” mode.

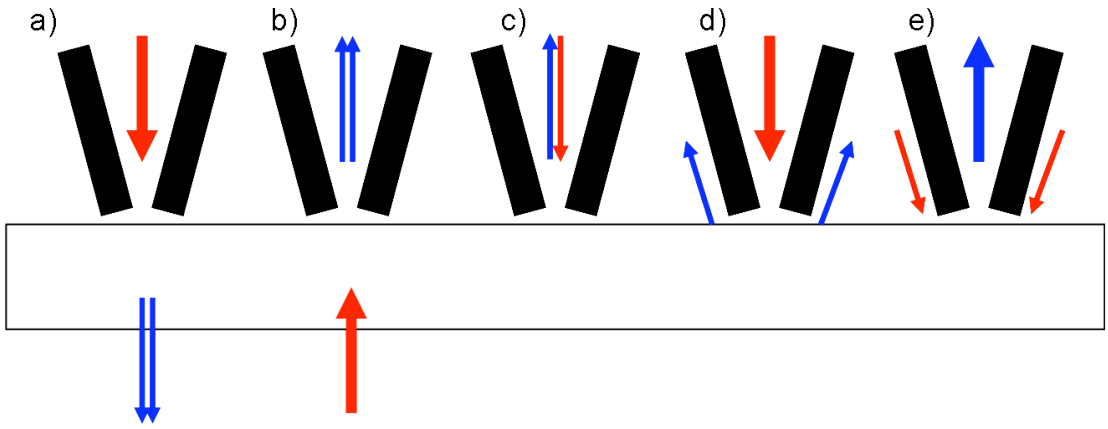

Figure 1.1: Possible NSOM Operating Modes (a) Illumination (b) Collection (c) Illumination/Collection (d) Reflection (e) Reflection Collection

Since the instrument detects a change in the light, there are several contrast mechanisms that are available, among them topography, index of refraction, fluorescence, reflectivity, stress, magnetism, material species, and birefringence. High-resolution spectroscopy is also possible. Our instrument described here operates on the topography and reflectivity of the sample, although with minor modification it could also work with fluorescence.

The probe tip needs to be positioned close enough to the surface that the light does not spread appreciably before it reflects (or is collected). Most commercial instruments use shear force microscopy to detect the close approach of the surface. The tip is "dithered," or vibrated parallel to the surface, at some amplitude. An external system monitors the amplitude of the vibration, and when the tip experiences the drag of the water layers adsorbed on the surface [Bout], the positioning system knows it is within the near-field range. Since our instrument is designed to work in an ultra-high vacuum (UHV), which does not have adsorbed water layers, we use a different method of detecting the distance to the surface.

When the light-emitting aperture is less than a wavelength away from the surface, the amount of light detected is a strong function of the distance to the surface because the gap between the probe tip and the surface becomes a second small aperture. Constructive and destructive interference affect the detected light too. The reflected light can be picked up in the far-field, and the distance from the surface to the tip can be calculated from the light intensity.

1.2 NSOM System Overview

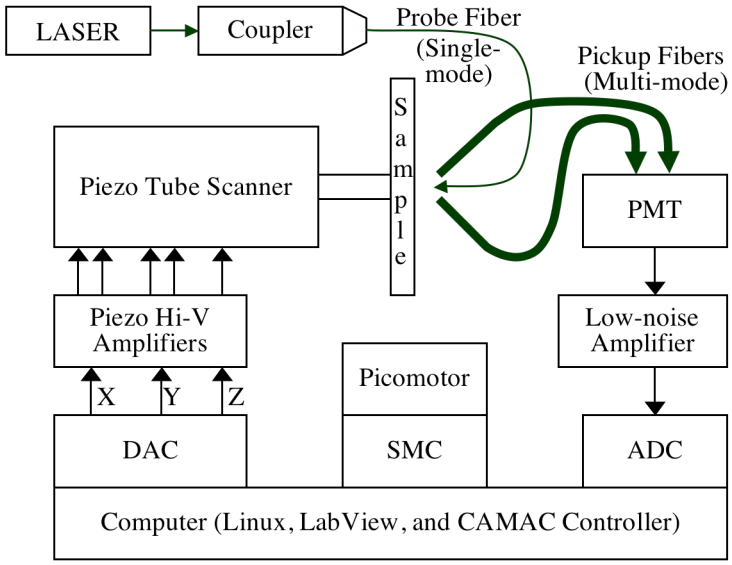

Figure 1.2: NSOM System Configuration

Our NSOM allows us to reliably position a probe tip within fractions of a nanometer of a sample surface. We illuminate the tip with a laser, detect the reflected light from the sample, amplify the result, and display the picture of the surface, all under software control.

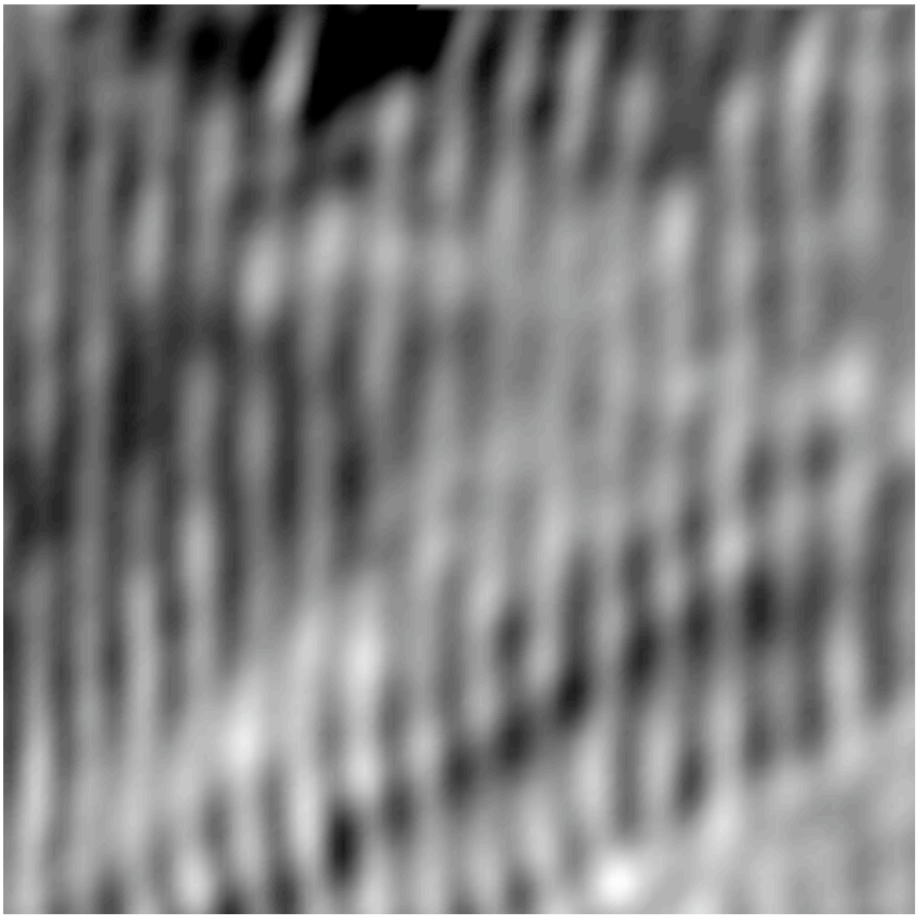

Figure 1.3: An NSOM Scan of a Diffraction Grating (22Aug07s2r)

Figure 1.3 is a scan of a diffraction grating, 127×127 pixels. The lines are 278 nm apart, and are resolved using 532 nm light.

This thesis will discuss the design and construction of an NSOM, and the modifications for a temperature-compensated vacuum chamber version. It will begin with a discussion of the basic properties of the probe tips and the piezoelectric nanopositioners. Next will be a description of the hardware and software of the microscope. Finally, it will include the results of our scans and the adaptations for the temperature-compensated vacuum chamber version.

Chapter 2: Probe Tips

2.1 Operating Tips

The fiber tip that emits the light is formed from a single-mode optical fiber that has been heated by a laser and pulled to a point. (An alternative method is to etch the tip with hydrofluoric acid.) As the fiber diameter is reduced below the waveguide cut-off dimension, light escapes from the sides of the fiber. Therefore, a 50-100 nm thick aluminum coating is applied to the fiber [DunnR], forming a tapering waveguide. The aluminum is deposited onto the tip in such a direction as to leave a hole, typically 50 to 80 nm in diameter, at the end of the tip from the shadow of the fiber. The laser light cannot propagate out of this aperture, but the evanescent field can and does; however, if a is the radius of the aperture, only $(a/\lambda)^4$ (10^{-4} to 10^{-5}) of the light can escape [Bethe]. Once the light leaves the tip, it can propagate unless the surface of the sample is within a wavelength of the tip. When the evanescent light reflects from the surface and is finally able to propagate as an electromagnetic wave, it is collected by the multimode optical fibers leading to the photomultiplier tube. Below, in Figure 2.1, is an SEM image of a well-formed tip [rdunngroup]. The tip on the right has been improved by Focused Ion Beam (FIB) milling to have a flat end.

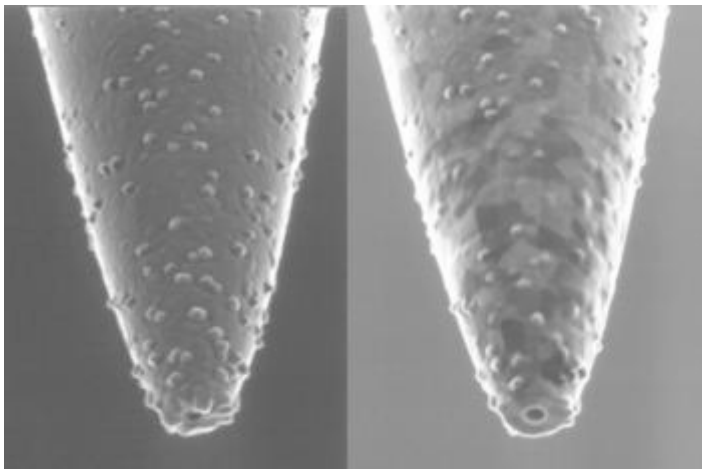

Figure 2.1: Well-formed NSOM Probe Tips

Commercial NSOM instruments will use Shear Force Microscopy (SFM) to detect the sample location. They vibrate the probe fiber at the mechanical resonance frequency with an amplitude of about 10 nm and detect the change in amplitude as it approaches the sample, experiencing the viscosity of the adsorbed water near the sample [Bout] [DunnR]. They are able to operate in constant height (above the surface) mode since they have this independent method to determine the height. The instrument described in this thesis is intended for eventual operation in an ultra-high vacuum. Our method does not dither the tip to detect distance to the surface, and so it is expected to have slightly better XY resolution than instruments that do.

The light that reflects from the surface may vary in intensity according to how close the tip is to the surface, by the geometry of the surface (blocking or scattering the light in directions that are not detectable), and by the intrinsic reflectivity of the surface. The tip itself can even block the reflected light.

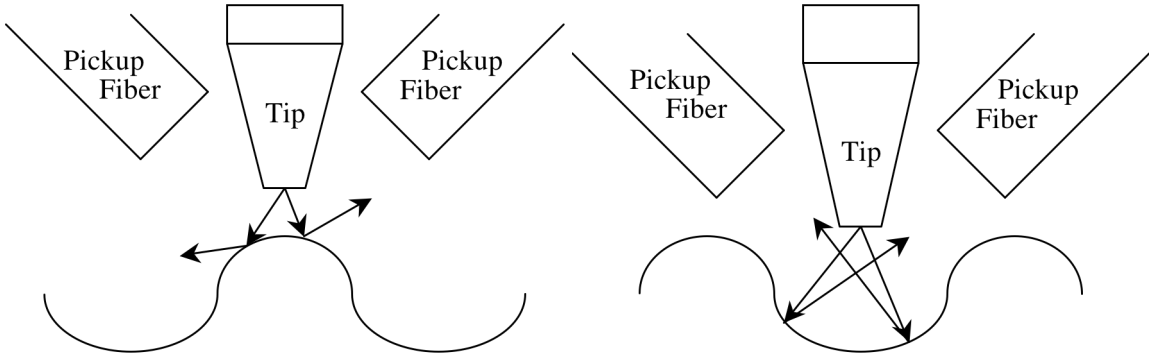

Figure 2.2: Dark (left) and Light (right) Regions of a Surface (not to scale)

2.2 FAR FIELD INTERFERENCE

The tip is close to a point source radiator, with light visible over more than 270°. The light that travels directly from the tip interferes with light that bounces off the sample surface. This interference provides some useful information. First, seeing the interference at all shows that the tip is nearing the sample surface, and its amplitude increases the closer to the surface it gets. Second, the period of the interference can calibrate both the picomotor steps and the piezo d_{31} constant. Third, the rapid change in intensity can provide an enhanced contrast for sample height values, *i.e.* the intensity is not just a property of the evanescent light propagation out of the tip, but the total distance too.

Since the direct light from the tip is seen at such large angles, the light must not be coming directly from the aperture. Instead, it comes from a few microns behind the aperture, where the electromagnetic field in the coating is at its greatest intensity. The light passes as an evanescent wave through the aluminum coating, since the coating is only a few skin-depths deep. The skin depth for aluminum is 13 nm for 500 nm light [DunnR], so the fraction of the light passing through is about 10^{-2} to 10^{-4}, comparable in intensity to the light from the aperture. This is the location where the tips exhibit damage,

as seen in the SEM images later in this chapter. The actual location of the direct light does not affect the period of the interference.

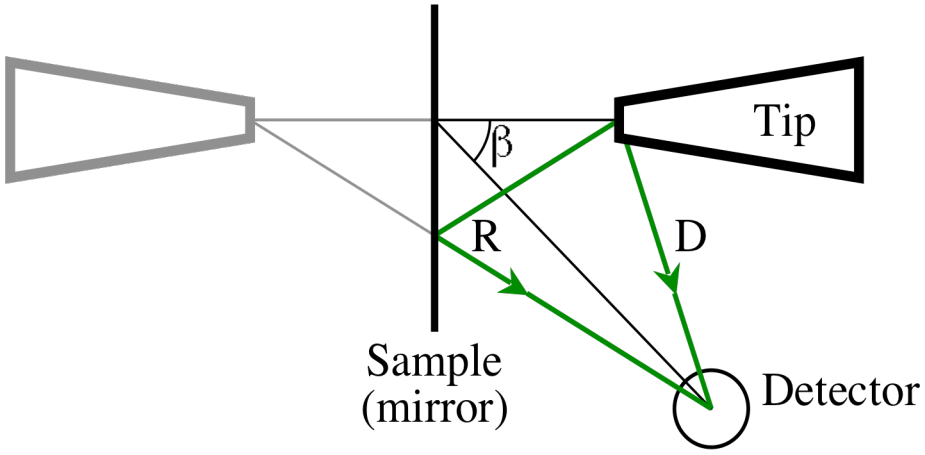

Figure 2.3: Light Path Interference

The fluctuation of the light occurs as the path length differences change some amount with a period of λ, the wavelength of the light. The difference in path lengths between the direct and reflected paths as the z distance changes is $d(D-R)/dz$, with the distance to the detector much greater than the tip-to-sample distance, and therefore the period of the fluctuation is

$$\Delta z = \frac{\lambda}{2\cos\beta}. \qquad (2.1)$$

For this instrument, the pickup fibers are positioned 45° to the normal and the wavelength of light is 532 nm, so the period of interference is 376 nm. The equation is valid regardless if the instrument has the pickup fibers stationary with respect to the tip holder or to the sample holder.

We have two pickup fibers, one on each side of the probe tip. It is likely that the interference distance is different on each side, and the intensity seen by each pickup is different. The intensities would be averaged at the detector; this effect may be the cause

of occasionally non-sinusoidal behavior of the approach curve. If we used only one pickup, this averaging would disappear, but we would have a "shadowing" effect as the sample topology would have a greater chance to block light from reaching the pickup fiber. One pickup also reduces the total light seen by the PMT and thus reduces the signal-to-noise level.

The approach curve has a final peak of intensity before it drops to a minimum (see Chapter 6). This final peak occurs where the path difference between the direct and reflected light is half the wavelength fluctuation, or 188 nm. This is not necessarily the distance between the tip and surface, since the strongest light from the tip is not from the aperture (as mentioned above), and the strongest reflection is not necessarily from the closest portion of the sample (possibly due to shadowing, topography, or material variations).

2.3 VARIATION IN REFLECTED LIGHT INTENSITY

An example of the variation in intensity is shown in Figure 2.4 on the next page.

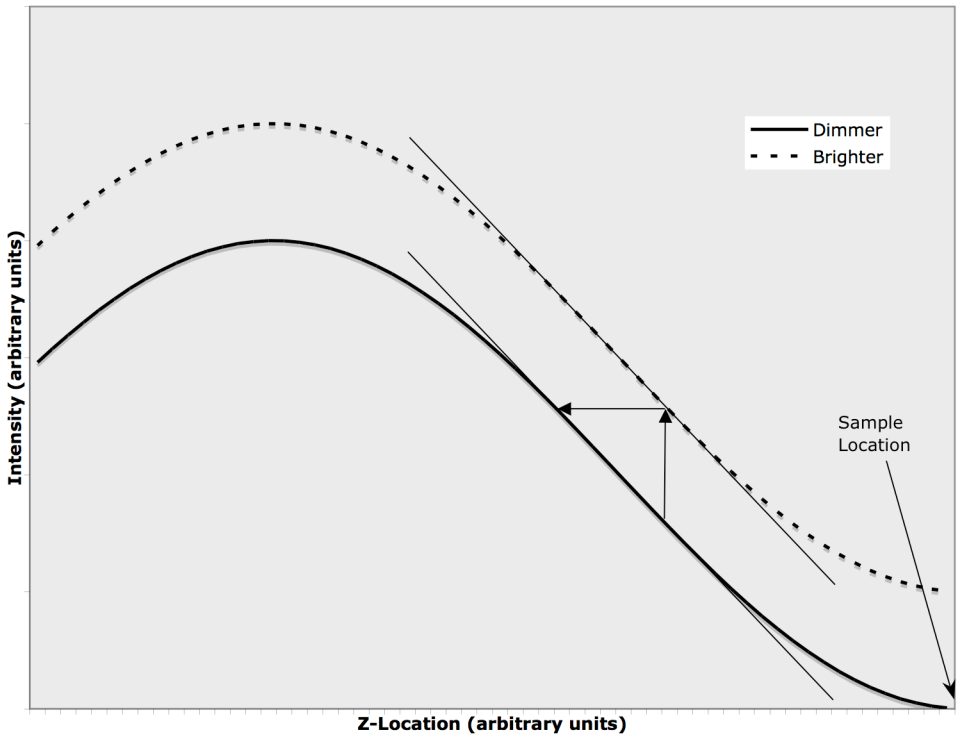

Figure 2.4: Intensity Variation with Position and Reflectivity

The algorithm pursued in previous work ([Gerbracht]) was to assume that the linear portion of the approach curve was a good judge of distance to the sample (here, the sample is to the right). As Z varies in that region, the intensity does vary almost linearly, and the intensity reading can be converted to distance [Carminati]. Unfortunately, any change in reflectivity, either intrinsic or topologically caused, is also interpreted as a change in Z position. To establish the true intensity curve after moving in X or Y, it would be necessary to sample the curve at enough points to locate the actual linear region. This requires a prohibitive (in time) number of sample points, which is why the peak-location algorithm is preferred (see Chapter 5).

2.4 DAMAGED TIPS

The laser is coupled to the probe fiber, but there is no way for the light to leave the fiber in meaningful amounts; it is mostly absorbed in the last few hundred microns of the tip, with some light being reflected back along the fiber and a tiny fraction exiting the tip through the aperture or through the cladding. There are multiple reflections of the light as the fiber narrows, and the aluminum cladding absorbs light at each reflection. This is a known problem, such that radiative heating of the sample or thermal expansion of the tip is sometimes a concern [DunnR].

Extrapolating from work by [Stahelin], adjusted for our input power, we can expect a temperature rise of up to 180°C at the tip. Temperatures much lower than the melting temperature of aluminum (660°C) can damage the tips. In the literature, stress caused by the different thermal expansion coefficients of quartz and aluminum usually causes the aluminum coating to flake off, but our experience is that more often the entire tip will crack off.

The predominant cooling mechanism is convection and conduction, rather than by radiation. This has some obvious implications for vacuum operation.

With our current setup (two pickup fibers and maximum signal amplification), we have not experienced tip damage if the output is 0.5 V or less at its maximum. We do not know how much power is actually entering the fiber, only that it can be more than enough to cause damage after some time.

Following are several tips that were damaged in the process of operating the NSOM described in this report. SEMs in this section are courtesy of Ignacio Gallardo.

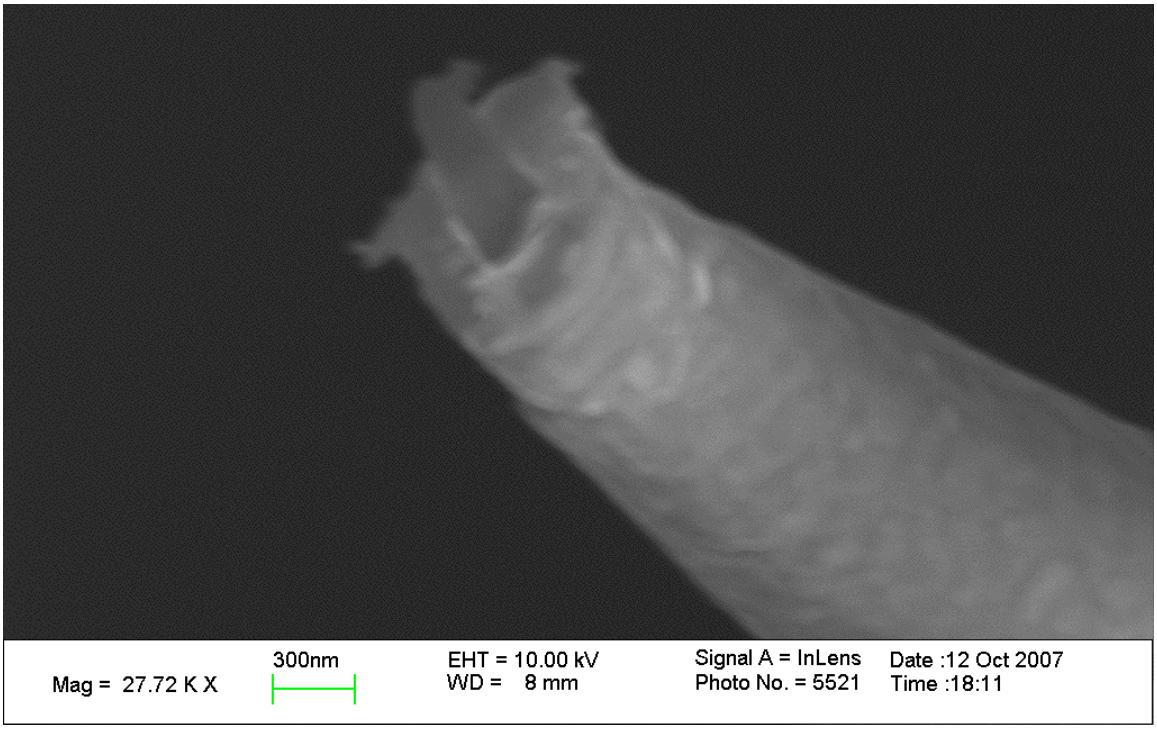

Figure 2.5: Tip Rammed Into Sample

This tip was accidentally driven into the sample surface by excessive picomotor movement. The aluminum coating appears extra thick because it has been pushed back around the tip.

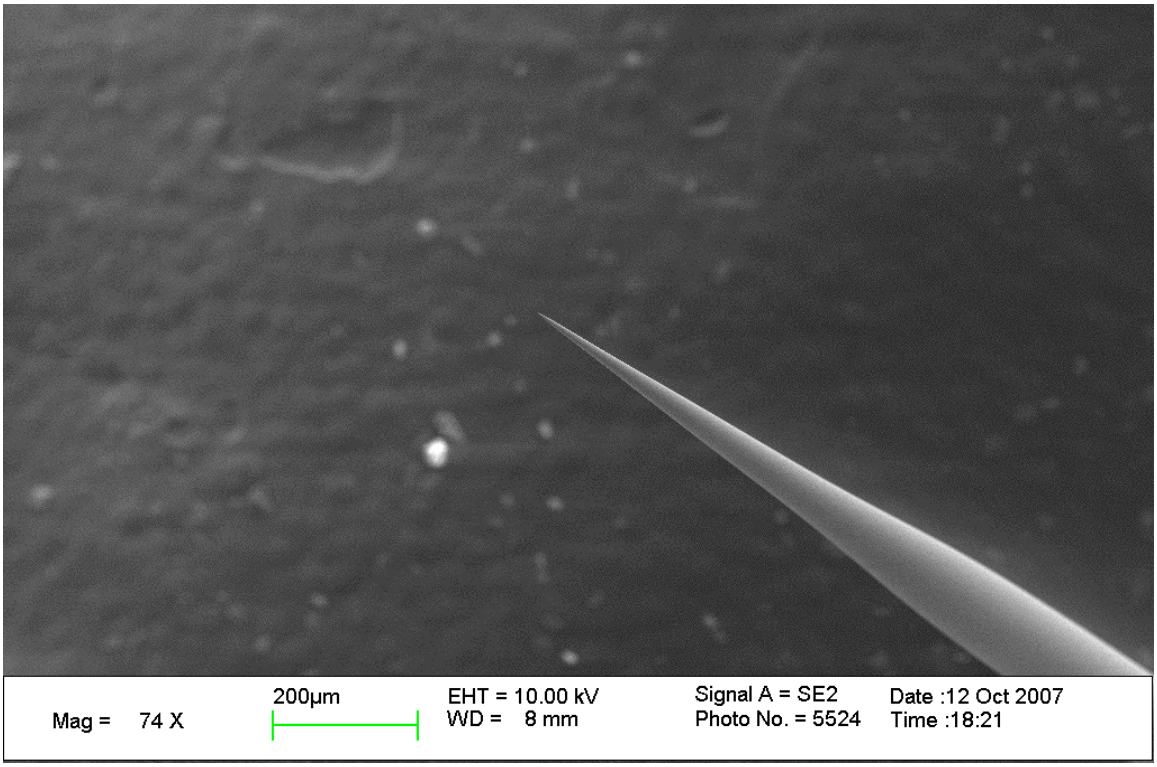

Figure 2.6: Large-scale Image of Tip

The tip in this SEM image is the same one as in the previous image, but the scale is such that the entire Figure 2.5 is just a few pixels in this image. The fiber attains its full diameter at the lower right. The fiber is inclined at about 45°.

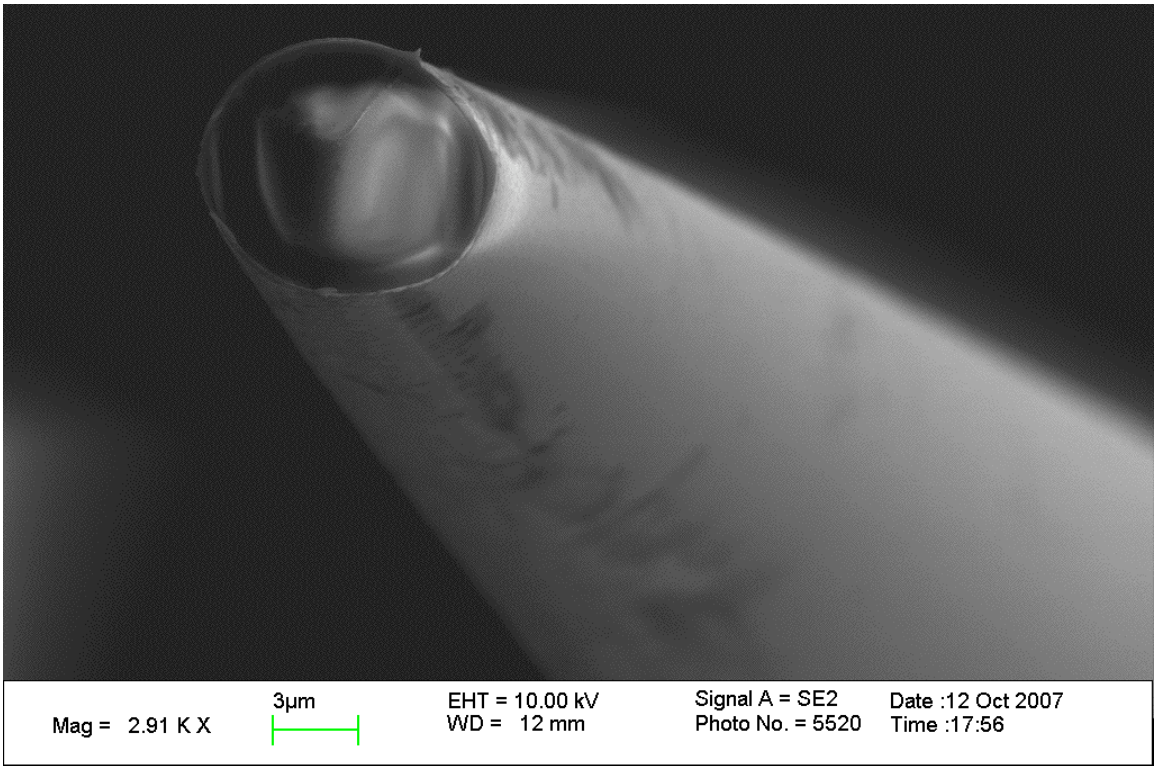

Figure 2.7: A Clean Break

This tip is has a flat, clean break. The fiber is almost vertical.

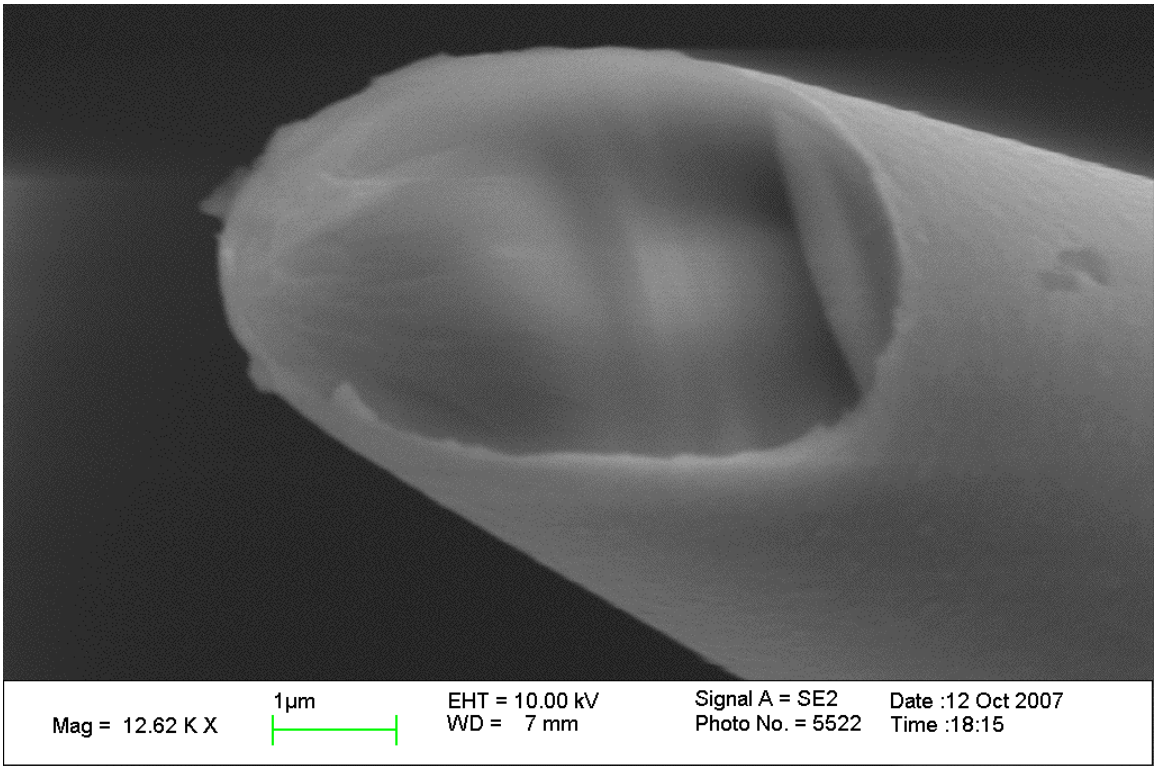

Figure 2.8: Tip Cracked Off

This tip appears to have cleanly cracked off, without any evidence of mechanical contact. It was stationary and some distance from the sample when it became much brighter. It was probably damaged by thermal stresses. The fiber is inclined at about 45°.

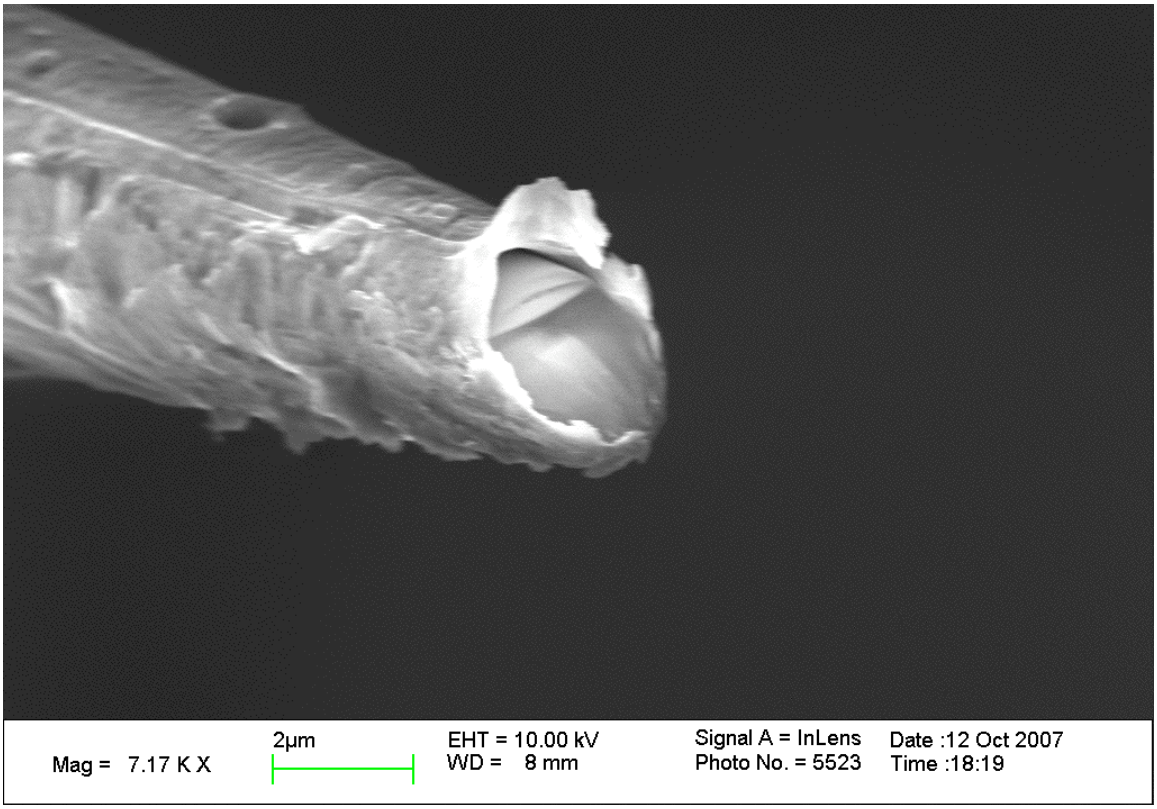

Figure 2.9: Cracked Tip with Mechanical Damage

This tip has both a clean glass surface and mechanical damage to the aluminum coating. It may have suffered thermal cracking during scanning, and the scanning algorithm approached the surface too closely (a brighter signal was interpreted as being farther from the surface, prompting a closer approach), causing the tip to drag along the sample surface. Note the thickness of the aluminum cladding is on the order of 100 nm, and it appears untypically rough. The fiber is inclined at about 45°.

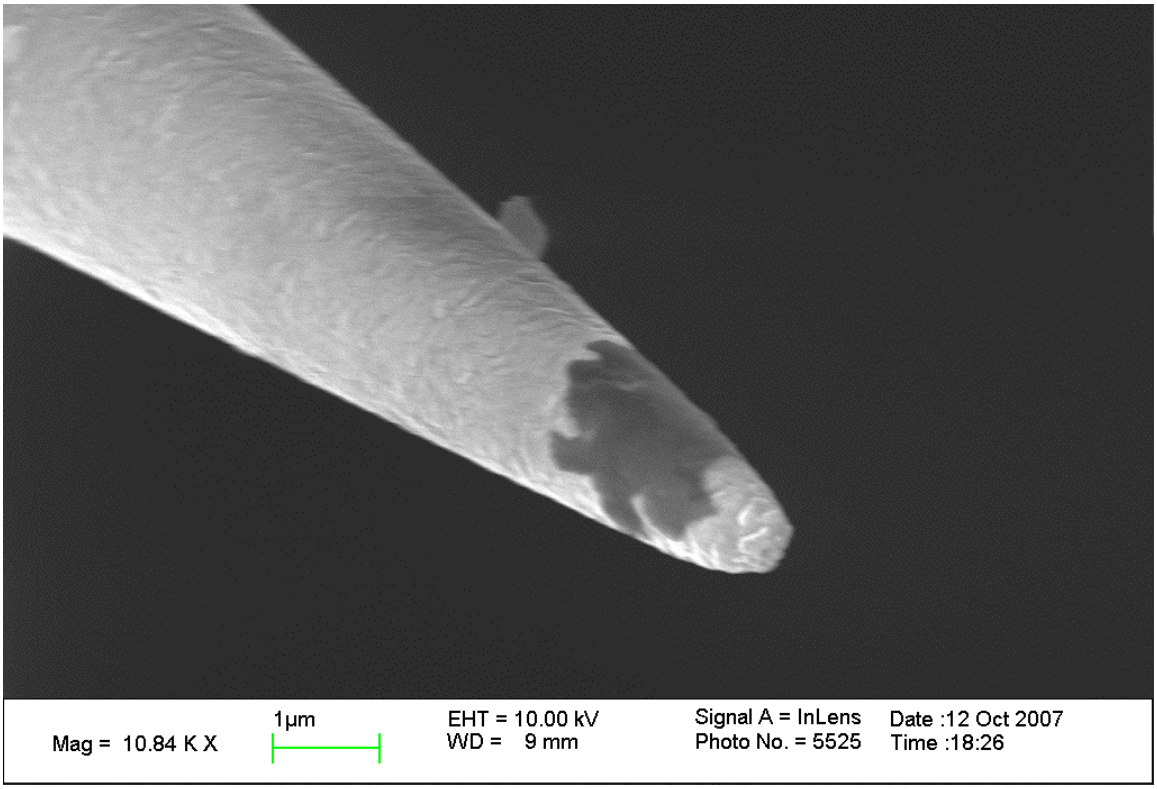

Figure 2.10: Tip with Missing Cladding

This tip was initially satisfactory, but became a poor quality tip during use. The aluminum cladding either flaked off or evaporated due to high heat. The cladding appears very thin near the damaged area. The damaged area is between 1.5 μm and 5 μm from the end of the tip, where the fiber diameter is about 1.5 μm. The aperture is not apparent, possibly due to the viewing angle. The fiber is inclined at about 45°.

Chapter 3: The Piezo Tube

The piezo tube scanner is composed of lead zirconate titanate (PZT). This material has the property of changing in physical dimension depending on the electric field applied to it. The direction of elongation/contraction is at right angles to the applied electric field. It is very lightweight and fragile, so care must be taken in handling.

PIEZOELECTRIC PROPERTIES

The tube scanner is a hollow tube, with axial nickel electrodes on the outer and inner surfaces. The outer electrodes have been segmented so that differential voltages may be applied, causing the tube to bend. The inner electrode is not segmented, and forms the main Z movement control. The tube has been "poled" so that a radial potential will contract or expand the tube in the axial direction.

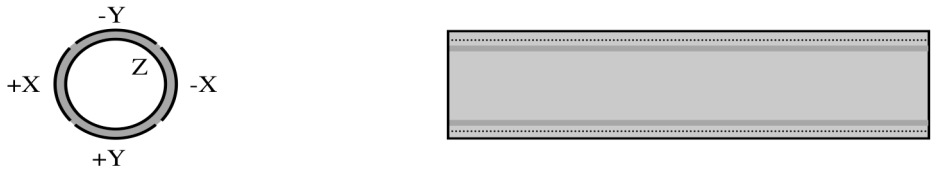

Figure 3.1: Axially Segmented Piezo Tube Scanner

When a voltage differential is applied to the inner and outer electrodes, the tube will elongate according the formula

$$\Delta L = \frac{d_{31} L}{t} V . \qquad (3.1)$$

If the tube has axially segmented electrodes (as we do) then it can bend if different voltages are applied to the opposite electrodes on the exterior. The movement of the tip is approximately on the surface of a sphere. The amount of deflection (for opposite and equal voltages on the two electrodes) is given by

$$\Delta X, \Delta Y = \frac{2\sqrt{2} d_{31} L^2}{\pi D_m t} V . \qquad (3.2)$$

For both equations, V is the applied voltage, t is the wall thickness $(O.D. - I.D.)/2$, L the tube length, and D_m the average tube diameter $(O.D. + I.D.)/2$ [Chen]. Note that Equation 3.2 applies to the tip movement only; if the sample or tip is attached to the tube (as it must be), then the extra length multiplies the lateral movement proportionately.

The parameter d_{31} is dependent on the exact composition of the PZT. Our tubes have a specified value of -1.27 Å/V but we have measured one tube to be -1.60 Å/V. The value also seems to diminish with time and/or use.

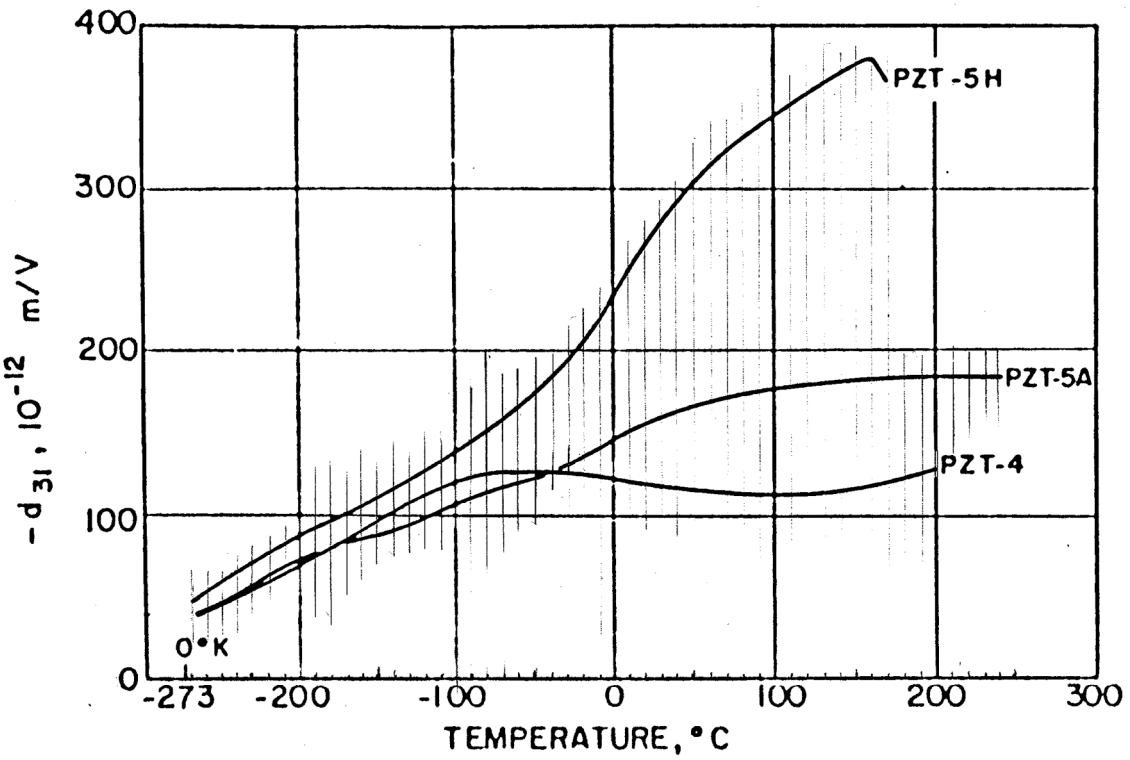

Figure 3.2: PZT d_{31} Variation with Temperature and Material

The maximum Z voltage (10 V at the DAC output) places -84 V on the inner electrode and +57±1 V on the outer electrodes, for a difference of 141±1 V. The

maximum change in length is ΔL_{max} = 877 nm. The minimum increment of length is 1/4095 of that, so ΔL_{min} = 0.214 nm. The approach curve, over the full Z range of the tube, will show 2.3 complete oscillations of the interference pattern.

The maximum X and Y voltage (±5 V at the DAC output) places ±150±2 V on opposite outer electrodes. The presence, in the instrument described here, of the sample holder adds approximately 0.6 inches to the length of the tube, and so the lateral movement of the sample is 60% greater than Equation 3.2 above would indicate. The maximum deflection is ΔXY_{max} = ±5384 nm. The minimum increment of lateral distance is 1/2046 of that, so ΔXY_{min} = ±2.63 nm.

The tube has a relatively high capacitance, given by

$$C = \frac{K_3^T \varepsilon_0 \pi D_m L}{t}. \tag{3.3}$$

The value of K_3^T is provided by the manufacturer as 1300, so the total capacitance of the tube, from internal electrode to the collective outer electrode is about 10 nF. It has been measured as 11.2 nF. The piezo amplifier must be able to drive this capacitive load and tolerate the heat dissipation.

The tubes will elongate if the outside electrode is at a lower voltage than the inside electrode. For historical reasons we operate the tubes with a negative voltage on the inner electrode and a positive voltage on the outer one so that the tube is normally contracted. This configuration works correctly, but the maximum tolerable field strength in contraction is approximately one third the extension value [Hicks]. The AC depoling tolerance for PZT-4 is 1000 V/mm [eblproducts]. When the tube is fully contracted and at the extreme lateral deflection, we are theoretically capable of applying at most 685 V/mm, so we do not exceed the maximum allowed voltage. We also have a software limitation on the tube movements so that the maximum amplifier output voltage is not

exceeded (the amplifiers have a 200 V supply, and the value listed above would require 207 V on one electrode); only one dimension (Z or X/Y) is permitted to exceed half its range at any time.

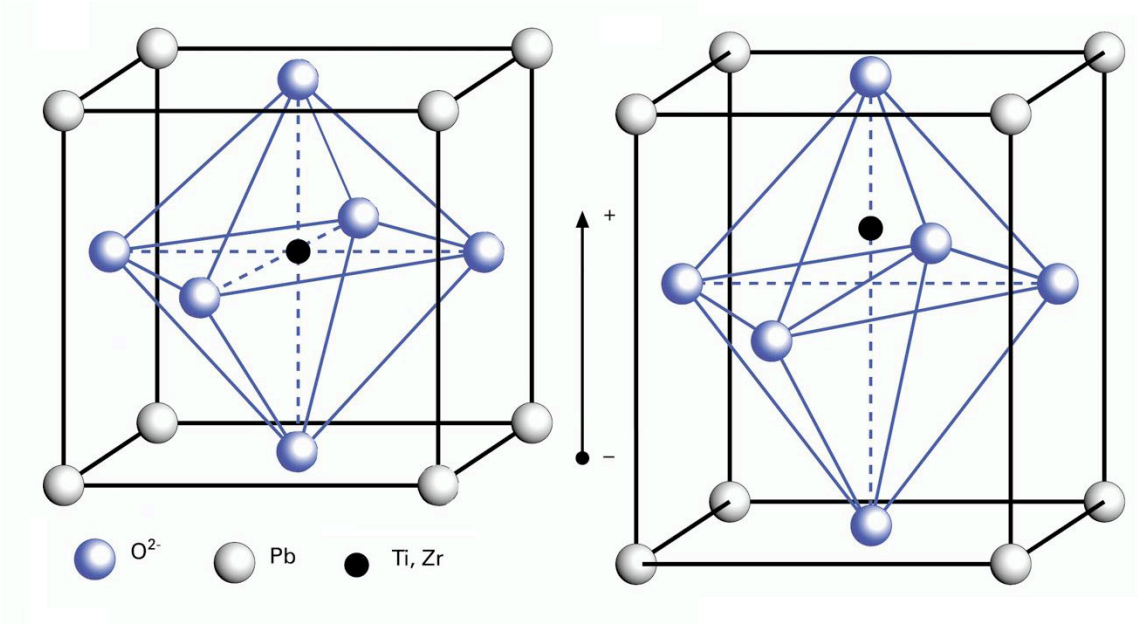

Figure 3.3: Elongation of PZT Crystal Structure [physikinstrumente]

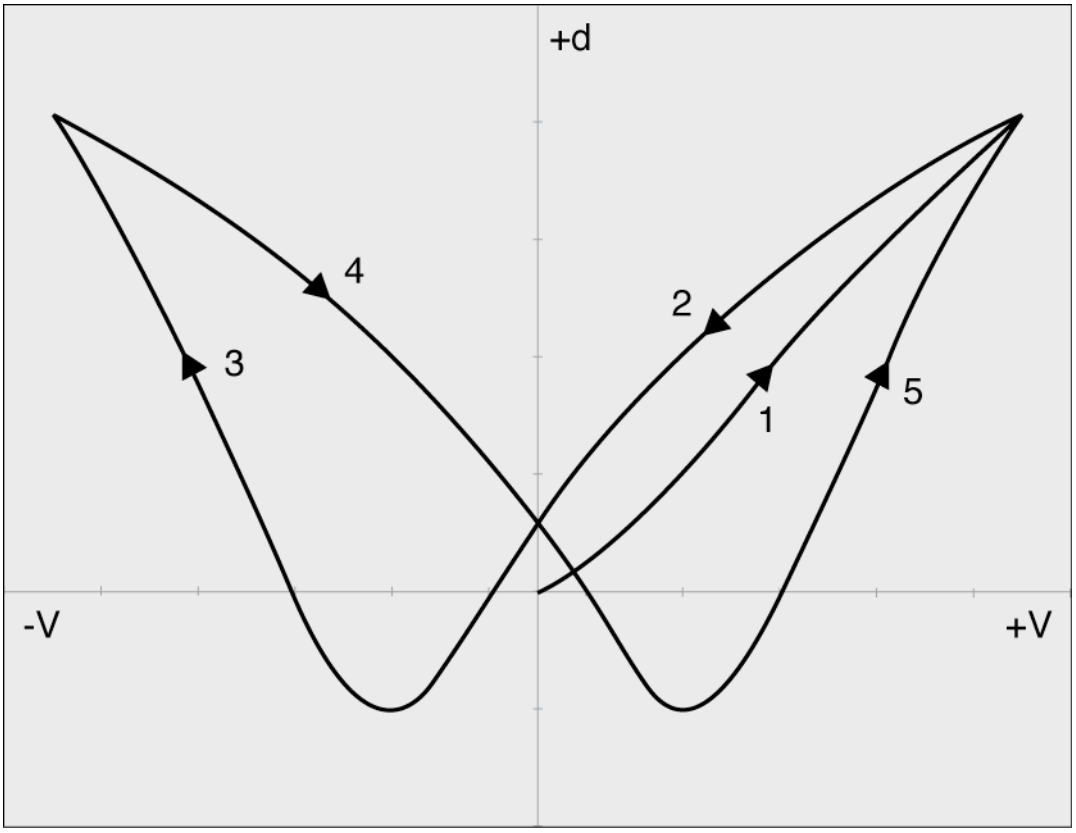

Figure 3.4: Butterfly Diagram for Large Voltage Range [Hicks]

Figure 3.4 illustrates the piezo expansion characteristics for a large input voltage range. Starting from unpoled material, as the voltage is increased, the material will begin to pole and expand. From the saturation point at maximum, as the voltage then decreases, the expansion follows path 2 to some negative voltage where the original polarization is lost, and the material will begin to repolarize in the opposite direction. It will continue to expand as the voltage becomes more negative, following path 3 to a saturation point.

The piezo tube will also expand in the radial direction when voltage is applied to the electrodes. The d_{33} parameter is 2.95 Å/V for our tube material. This expansion is irrelevant to our NSOM.

MOVEMENT

The tube cannot move faster than its first mechanical resonance frequency, which is usually near 10 KHz. To avoid excitation of this mode, the scanning speed is usually limited to 1% of this frequency [Moheimani]. We have observed the tube taking approximately 3 ms to move a commanded (large) distance. Reading the results of a change should either wait for the movement to mostly finish before taking data, or average the data over a long enough time that the majority of the reading is from the final position.

The actual movement is potentially inconsistent compared to the theoretical Equations 3.1 and 3.2. The tube is a machined material, and therefore the tube may not have perfect roundness or perfect wall thickness throughout (our tube thickness specification is ±0.001 inches out of 0.020" and an eccentricity of ±0.002 inches). In addition, the tube can have regions that do not respond identically to the applied electric field. These effects lead to inaccuracies in the scan position and unpredictable and irregular distortions in the results.

The piezo is very stiff, near 20% of the value for stainless steel, and can thus generate a lot of force [Hicks].

When the piezo force is applied in the contracting (pulling) direction, the tubes usually require pre-loading. We do not operate with pre-loading, as the sample has a relatively low mass.

HYSTERESIS

The piezo material exhibits hysteresis, or a path-dependent response to the input. Hysteresis is generally attributed to molecular friction at sites of material imperfections because of domain walls motion. When a small electric field is applied, domain walls motion is limited and reversible; hence hysteresis is not observed [El Rafai]. At higher

electric fields, the local energy barriers are overcome, and the domain walls move an extended distance. This provides an irreversible mechanism that contributes to observed hysteresis.

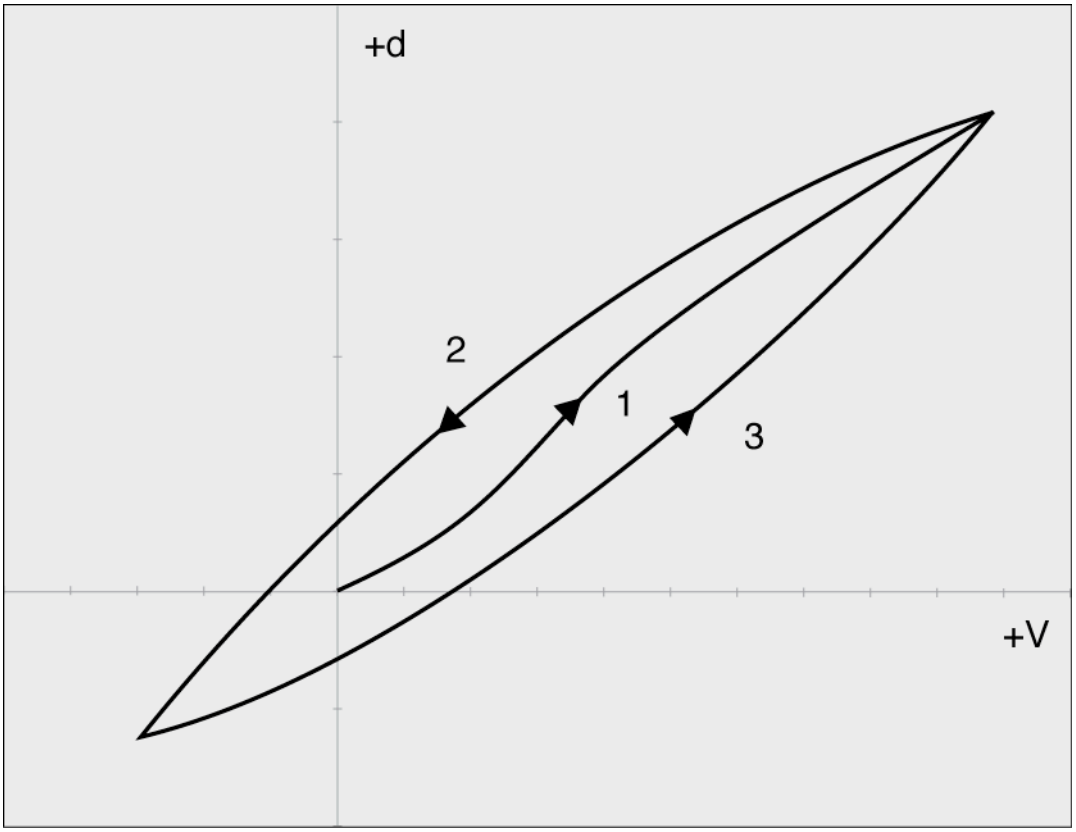

Figure 3.5: Movement Over Small Ranges [Hicks]

In practice, piezo actuators start with poled material and are used over a smaller voltage range than was shown in Figure 3.4. Figure 3.5 shows the operation for small voltages. Following path 1 from zero volts to the maximum, it will follow path 2 as the voltage is then reduced to some small negative voltage. (The negative voltage must not be sufficient to un-pole the material.) As the voltage increases again, it will follow path 3 back to the maximum extension. Regardless of the voltage range, during operation the movement path is unlikely to go through the origin.

To avoid distortions caused by hysteresis, commercial instruments usually scan in the same direction for each line, and it takes the same time to retrace a line as it took to scan it. This doubles the time to scan a line over the potential time.

The use of charge amplifiers [Comstock] [Fleming] significantly reduces hysteresis [Moheimani]. We would have to completely redesign our voltage amplifiers to convert them to charge amplifiers.

CREEP

The displacement of a piezoelectric actuator to a rapid change of input consists of two primary parts. The initial response is over a time scale controlled by the mechanical resonance of the actuator, typically a few milliseconds. This is followed by a slow creeping response over tens to hundreds of seconds which can amount to more than 20% of the total response, strongly dependent on the particular piezoelectric compound [El Rifai].

Creep will affect the position of the tip after it approaches the sample, and it will exacerbate the hysteretic effect at the turning points of the scanning trajectory [Moheimani]. Since its effects last so long, any variation in time in examining a point of the sample, *e.g.* a delay in returning control to the scanning subroutine or a repeated read, will show up as a distortion in the image.

MOVEMENT STRATEGIES

Since larger movements are more subject to the effects of hysteresis and creep, we recommend that movement of the tip should be kept to a minimum. Unfortunately, that is usually impossible. The lateral movement is essential, and a large movement in Z is, in our instrument, essential to locating the surface. The effects may be reduced by keeping consistent in all movements: starting from the same position and taking equal times for

all movements. No sample should be taken until at least the mechanical motion has mostly ceased. We also undergo a “soaking” procedure where the tip spends an extended period near the working distance before the scan operation to reduce the creep at the beginning of the procedure.

Chapter 4: The Microscope Hardware

4.1 Overview

The microscope hardware is designed to get the tip to reliably approach the sample within a distance of approximately 1 micron, which permits the tube scanner to approach even closer and then amplify and report the light intensity reflected from the sample. The hardware can be divided into three general categories: the control electronics, the mechanical movement, and the light source and detection.

The instrument is constructed on a standard optical table. The table has vibration isolating legs, and it is currently located on the building's basement floor. We have not noticed any vibration effects in our images.

4.2 Control Electronics

Computer System

The computer that controls the microscope is a rack-mount PC that runs the Linux operating system. The software that runs the experiment is described in the next chapter. The computer includes a model 2915 PCI bus to 3922 Controller card from KineticSystems (www.kscorp.com); it communicates with a CAMAC crate over a 40-conductor parallel ribbon cable using differential RS-485 signals. Three data transfers are required to perform one 24-bit cycle on the crate. The 2915 has the ability to address up to eight different crates, numbered 0 to 7, up to a total distance of 90 m from the 2915.

Figure 4.1: The Computer

The 2915 driver software was developed by a group in Japan [Haseno], and was modified to work with our system by Chris Boyd and John Keto. Boyd and Keto also developed our system's library interface of C driver calls named "KetoLib".

CAMAC Crate

The Computer Automated Measurement And Control (CAMAC) crate is a card cage with 25 slots. The backplane bus does one 24-bit data transfer in 1 microsecond, while the fastest consecutive driver I/O call takes approximately 15 microseconds to complete due to operating system overhead. The address of our microscope control crate is 0. The rightmost two slots are reserved for the parallel bus crate controller, a model 3922 card from KineticSystems. The control electronics for the microscope are inserted into the crate slots. The cards are a stepper motor controller, a digital-to-analog converter, and an analog-to-digital converter. The new NSOM that will use the flexure stage will require a different digital-to-analog converter, the "KetoLab DAC".

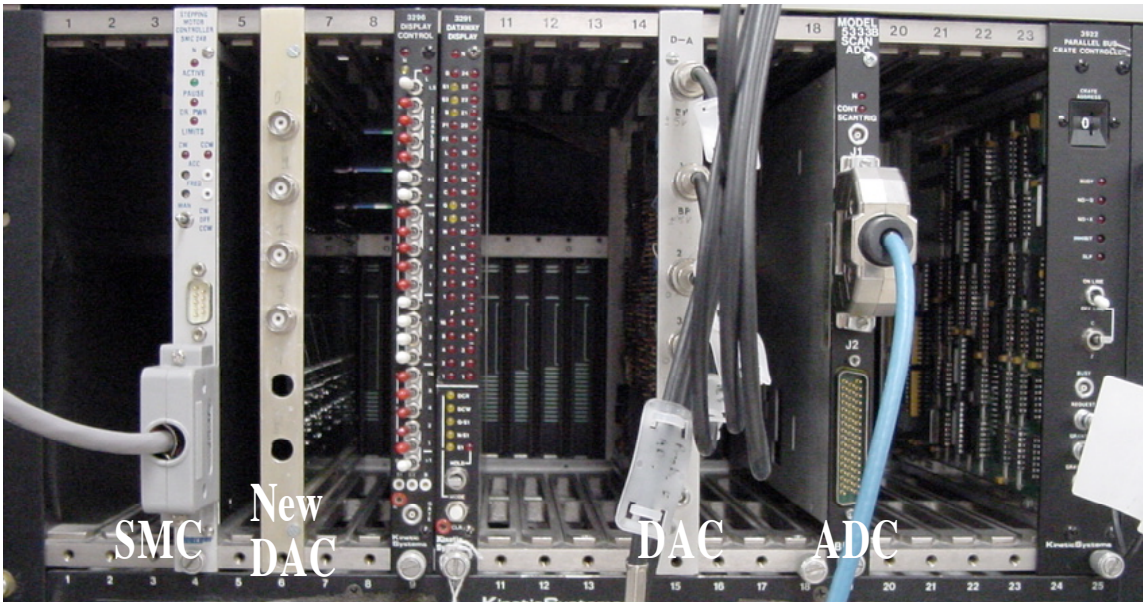

Figure 4.2: The CAMAC Crate

The Stepper Motor Controller (SMC)

The SMC-24B from Joerger Enterprises, Inc. (www.joergerinc.com) is used to control the picomotor (discussed below). It was modified to have an output of +12 VDC over the external 50-pin connector pins 14 and 15, instead of the original +24 VDC. The picomotor control box requires 12 VDC to operate. The cable hood includes a pullup resistor on one of the lines. The SMC cable is wired to provide direction/clock signals instead of separate stepper motor phase outputs. Writing a positive value to the SMC step register results in a clockwise motion of the picomotor.

The Analog Outputs (DAC)

The Digital-to-Analog Converter (DAC) is designed in-house. It accepts a 12 bit number from the CAMAC bus, although chips 0 and 1 take their uppermost bit from bus line W16 instead of W12 as might be expected. It includes six Burr-Brown DAC80 chips. Chips 0 and 1 control the piezo tube X and Y motions respectively; they output -5 to

+5 VDC. Chip 3 controls the piezo tube Z motion and outputs 0 to 10 VDC. These voltages are subsequently amplified (see below) to the high voltages as required by the piezo tube.

The Analog Input (ADC)

The BiRa Systems, Inc. (www.bira.com) model 5333B Scanning Analog-to-Digital Converter (ADC) digitizes the PMT signal. It is capable of one 12-bit conversion every 10 microseconds. It has differential inputs. For enhanced resolution, the card is configured to take the input as unipolar with 5 V full scale, but the card is capable of accepting 10 V as full scale. This application only uses a single channel, although it has the ability to digitize 32 channels. The software, using the device drivers in non-LAM mode, is capable of one ADC read every 15.6 microseconds. In LAM mode, the ADC card limits the read rate to one per 10 microseconds, which is a perceptible but not dramatic performance improvement. Since the limiting factor in the speed of scanning is the millisecond-long mechanical movement of the piezo, a faster read of the ADC would not reduce the time for a scan.

Analog Outputs for the Flexure Stage (DAC)

The KetoLab 6-Channel DAC is designed to produce the voltages to control the flexure stage. It is currently populated with four chips, Burr-Brown DAC715PK, at addresses 0 to 3. They are graded as 15-bit linearity (the output is accurate to ±2 LSB) and will accept a 16-bit number from the CAMAC bus, in two's complement format. The flexure stage requires 0 to 10 VDC to control its X-Y position, with 5 V being the center, or neutral, position. The command data to output 0 V to 9.99985 V is -32768 to +32767, with data 0 causing an output of 5 V. The chips are set to data 0 (5 V) by the "clear" operation of the CAMAC bus.

There is one important caution to using this card in that the conversion chips expect true data from the bus, but the data on the CAMAC bus is inverted; prior to any write to this card, the data to be written must be inverted in software. The chips are hardwired to use "transparent mode" which means that the output changes immediately upon the write to the chip; the latching capability of the chips is not used, so it is not possible to have multiple channels make simultaneous changes.

Piezo Amplifiers

The piezo tube requires high (circa ±165 V) voltages to obtain the greatest movement possible. The output of the DAC card goes to three amplifiers, designed and constructed in-house. The detailed description of these amplifiers can be found in [Gerbracht]. The amplifiers have selectors on their front panel to change the amplification, but the marked values do not correspond with the actual values; they have changed since the time they were constructed and must be experimentally determined.

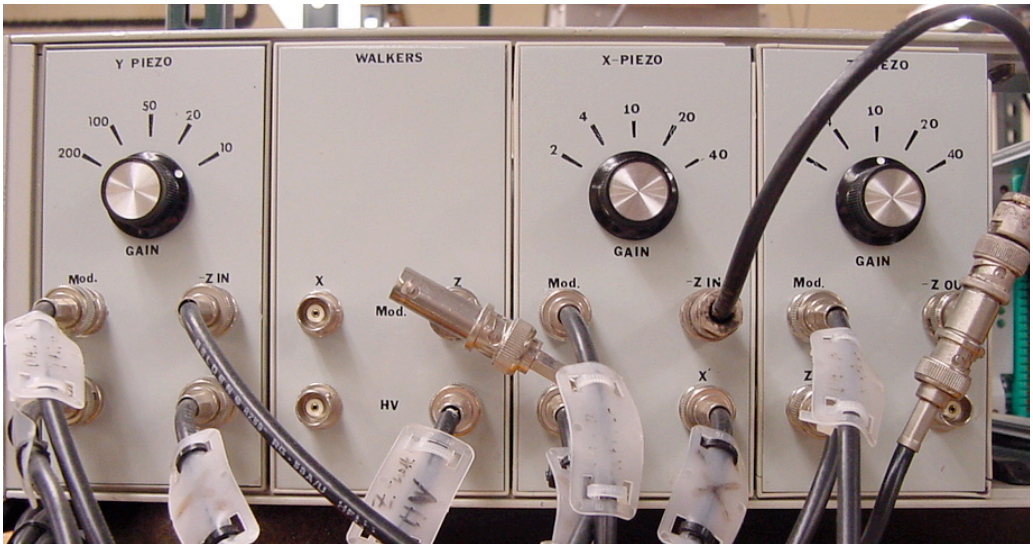

Figure 4.3: The Piezo Amplifiers

To reduce the maximum absolute output voltages for the amplifiers, the Z output is fed into the X and Y amplifiers (as well as Z). The maximum Z contraction, corresponding to a control voltage of +10 V, places -166 V on the inner electrode and +109 V on the outer electrodes; even at the most extreme contraction, the tube scanner is still able to move in X and Y, albeit not to the maximum range. At maximum X or Y deflection, as commanded by ±5 V (with Z at 0 V), the outer electrodes have ±149 V on them. The control software includes code to limit the movements of X and Y (or Z) when the tube is commanded to move to more than half the maximum movement in Z (or X or Y).

Any future NSOM may wish to reduce hysteresis by using a voltage-to-charge amplifier, rather than a voltage-to-voltage amplifier [Comstock] [Fleming]. Our amplifiers include simple low-pass RC filters on the power supplies to the opamps; this is probably counterproductive as the CMRR and PSRR for the opamps is quite good.

4.3 Mechanical Movement

The Translation Stage

The prior versions of the NSOM (see [Guttroff] and [Gerbracht]) used a "walker" stage to have the sample approach the tip. This stage used a piezo tube with a large mass glued to the end of it, and it rode on synthetic sapphire rods. By slowly extending and quickly contracting the tube, the quick movement would use the inertia of the mass to break the walker loose from the force of static friction; the slow movement would leave the walker stage in place. It was prone to sticking and inconsistent movement.

The present NSOM uses a commercial optical translation stage from New Focus (www.newfocus.com), model 9063-COM, with a picomotor for movement. The stage provides a highly stable platform and a repeatable movement to the same general location

on the sample. It is only 0.63 inches thick, which is essential for use in the small vacuum chamber.

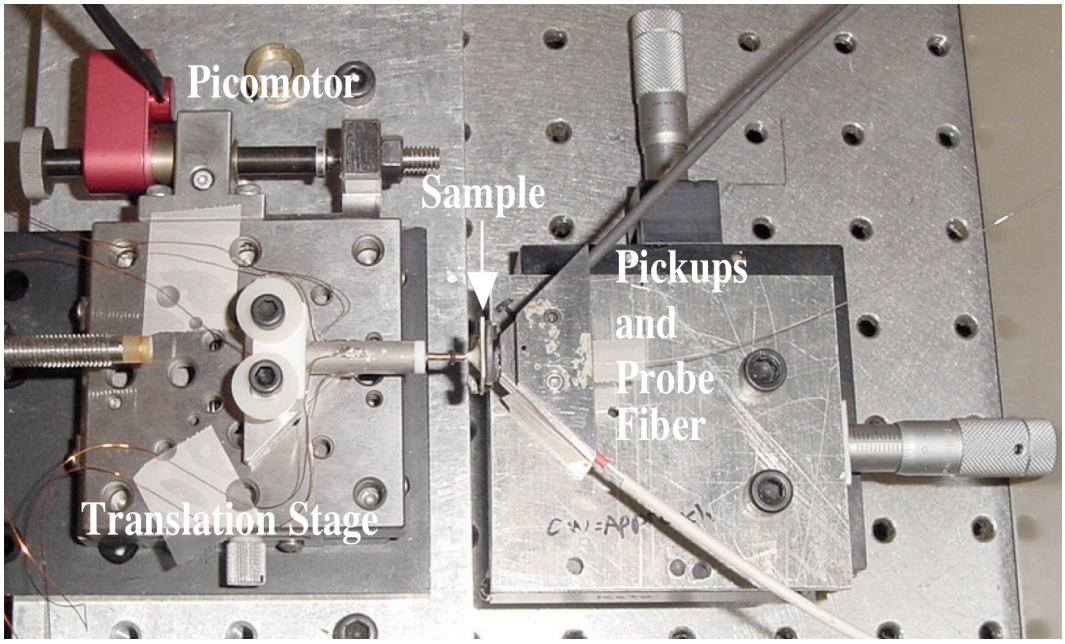

Figure 4.4: The Translation Stage and Fiber Mount

The translation stage does not move in X or Y. The fiber carrier is mounted on a separate manually operated translation stage that provides movement parallel to the table surface (X and Z).

The Picomotor

To provide gross movement, we use a picomotor from New Focus, model 8302, with its controller. This picomotor also uses a piezo and inertia, but in a more reliable fashion. It has piezo "jaws" that grip the 80 TPI screw and slowly extend to fractionally rotate it, then suddenly contract. During the slow expansion, the high static friction enables the screw to turn; in the sudden contraction, the inertia and low dynamic friction of the screw leaves it in place while the jaws slip. The picomotor movement is approximately 15 to 30 nm per step, and it can step at a maximum rate of 2 KHz.

Although the exact step distance is not perfectly consistent (changing with duration of use and region of the screw, among other factors), the movement characteristics are far superior to the previous "walker" method [Guttroff]. Clockwise motion of the picomotor results in a retreat of the sample from the fiber.

The picomotor controller, New Focus model 8703 integrated driver module, takes the control signals from the SMC card in the CAMAC crate and creates the high voltages waveforms in the precise sequences needed by the picomotor. It is configured to take a direction signal and a clock from the SMC, instead of a standard stepper motor waveform. It is powered by 12 VDC from the SMC card, and it creates the higher voltages needed by the picomotor. A minimum of three wires are needed to control the picomotor.

The controller creates noticeable amounts of electrical noise on the cable to the SMC. To help reduce the power supply noise and any potential problems, the power wires could incorporate a common-mode choke.

The Tube Scanner

The tube scanner is used to move the sample in all three dimensions. The specific tube scanner we use is composed of EBL#1 (type PZT-4), as manufactured by EBL Products, Inc. (www.eblproducts.com). PZT-4 has a relatively flat temperature dependence over -100 to +200 °C compared to other common PZT materials. It is a hollow cylindrical tube, 0.25 inches outer diameter, with wall thickness 0.02 inches, and length 0.98 inches. It has a d_{31} expansion coefficient specified as -1.27 Å/V; however, initial calibration of the tube resulted in a measured -1.60 Å/V. It has nickel-coated electrodes, one on the inner surface, but with the outer electrode segmented into four quadrants. It can tolerate a potential of 1 KV/mm before depoling.

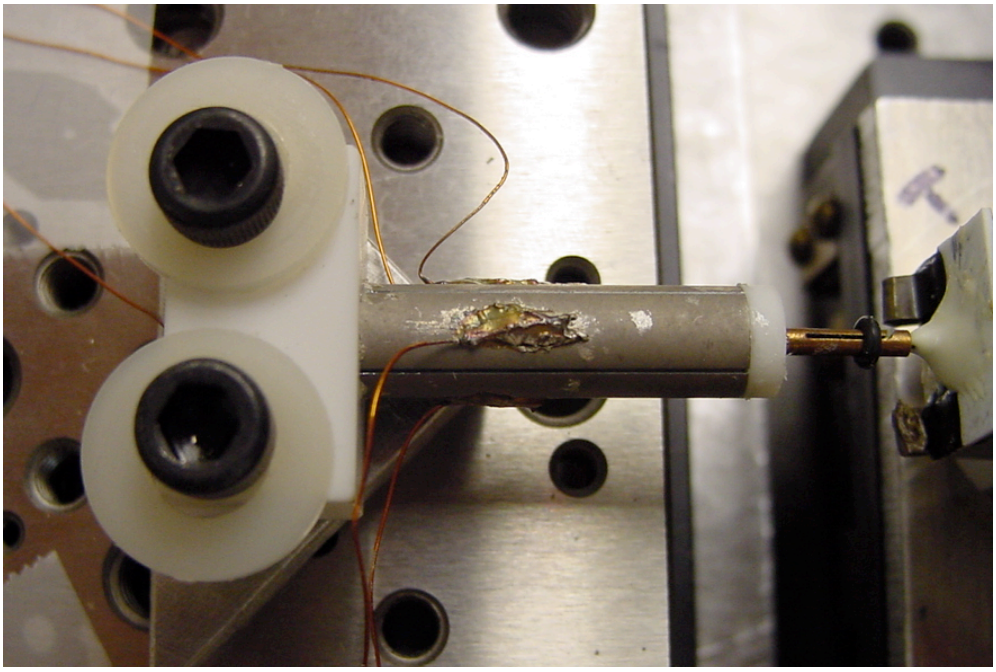

Figure 4.5: The Piezo Tube Scanner

To prevent depoling by high soldering temperatures, the wires from the amplifiers are attached to the tube by silver epoxy. We have used either MG Chemicals number 8331-14g, or for a UHV application, Epoxy Technology, Inc. (www.epotek.com) EPO-TEK H21D.

Since the piezo tube is very fragile, it is not held directly by screws or clamps. Instead, it is glued to a MACOR carrier; a good non-conductive epoxy for this purpose in UHV is EPO-TEK H72. MACOR is a machinable low-outgassing ceramic with thermal expansion characteristics that match the piezo material.

The Sample Holder

A sample holder is glued to the end of the tube scanner; the portion attached to the tube scanner is MACOR. This adds approximately 0.6 inches to the overall length of the

tube. It does not affect the Z movement of the tube, but it will exaggerate the X and Y movement by about 60% compared to the predicted value in Equation 3.2.

4.4 Light Source and Detection

The Laser Source

We use a green Nd:YAG laser as a light source. It is a Uniphase Corp. (www.jdsu.com) model μGreen 4301-010 class IIIB solid-state laser system at a wavelength of 532 nm and an output power rated at 10 mW but measured as 2.6 mW. It is coupled to the fiber by a New Focus model 9091 5-axis positioner and 5712-B-H (or 5713-B-H) aspheric microscope objective. Since the fiber is single-mode with a small input diameter, accurate positioning is essential. The lenses used can focus the laser to a waist size of 0.8 microns; partial rotations of the fine adjustment screws can radically change the coupling efficiency, and it is common to find the coupling efficiency changing over time and temperature. On a cautionary note, if the laser is well-coupled to the fiber, it will destroy the fiber tip. Reducing the light to safer levels is required to prevent destruction of the fiber. We already use a 50% attenuator after preliminary alignment. Deliberately reducing the coupling efficiency by adjusting the Z-position of the fiber is strongly recommended.

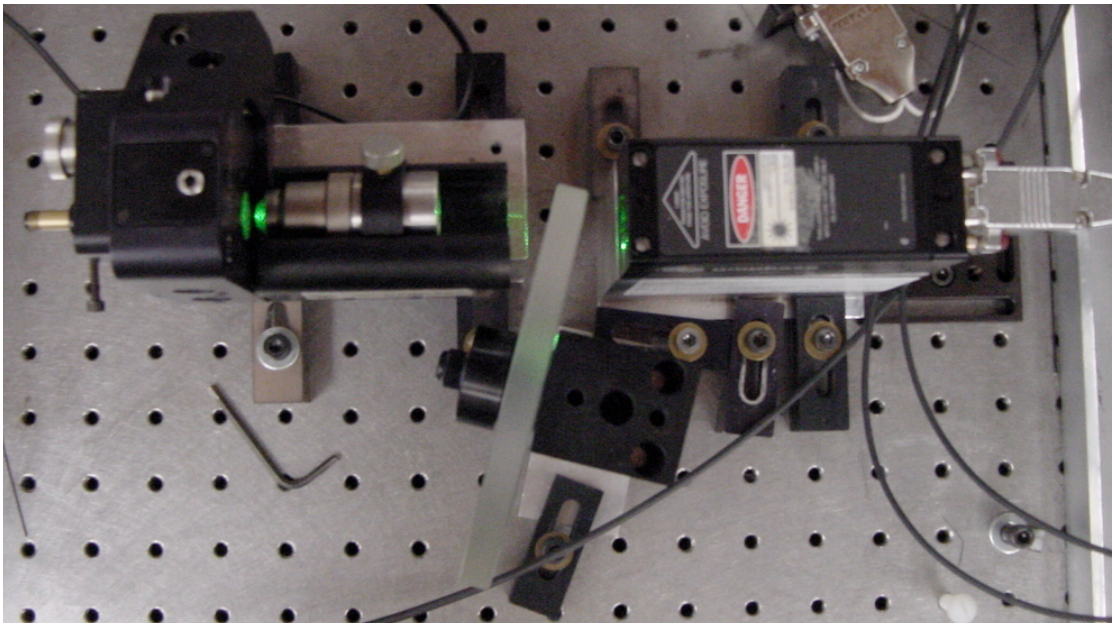

Figure 4.6: Laser Head, Attenuator, Focusing Lens, and Aligner (right-to-left)

The NSOM Probe Fiber

The fiber tip is the critical component of any NSOM system. We obtained the unmounted probes from Veeco, Inc. (www.veeco.com), part number 1730-00. These are single-mode fibers created by the pulling method and are coated with aluminum. The opening at the tip is 50 to 80 nm in diameter.

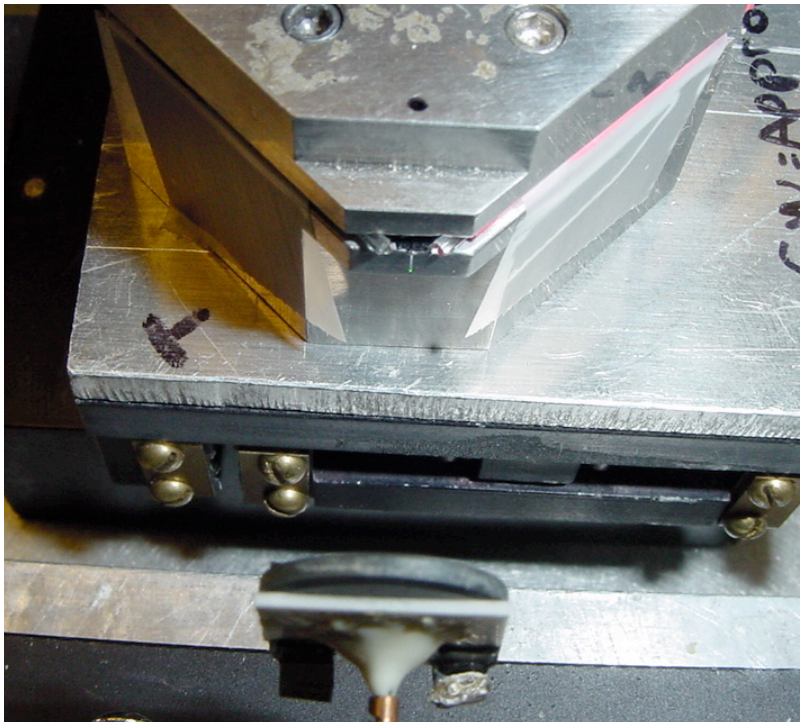

Figure 4.7: A Sample's View of the Tip

These fibers are designed for a cutoff wavelength of 650 nm, *i.e.* the fiber can propagate shorter wavelengths in a multimode fashion. Since we are using a 532 nm laser, the fiber leaks light over its entire length (where uncoated by aluminum), especially going around bends. The loss of light does not affect the imaging process since, we have too much light from the laser for the fiber to tolerate, but the lost light has the potential to reflect from the inside of the chamber and be picked up by the PMT. After installing a new fiber, the lost light makes it easier to locate the laser focus, since the fiber glows noticeably when the tip is only approximately near the focus.

The Pickup Fibers

The light scattered from the surface must be captured by multi-mode fibers which transmit the light to the PMT. The fibers used are from Thorlabs (www.thorlabs.com),

part number FT-1.0-URT (now superseded by BFH48-1000). These are 1 mm core diameter fibers with NA=0.48 for a ±28° capture angle. A pair of these fibers is positioned as close as possible to the NSOM fiber tip, stationary with respect to the tip and at an angle of 45° to it, pointing directly at the tip. Their optimal placement is no farther than $\tan(\arcsin(0.48))/0.5 = 1.09$ mm from the lit tip.

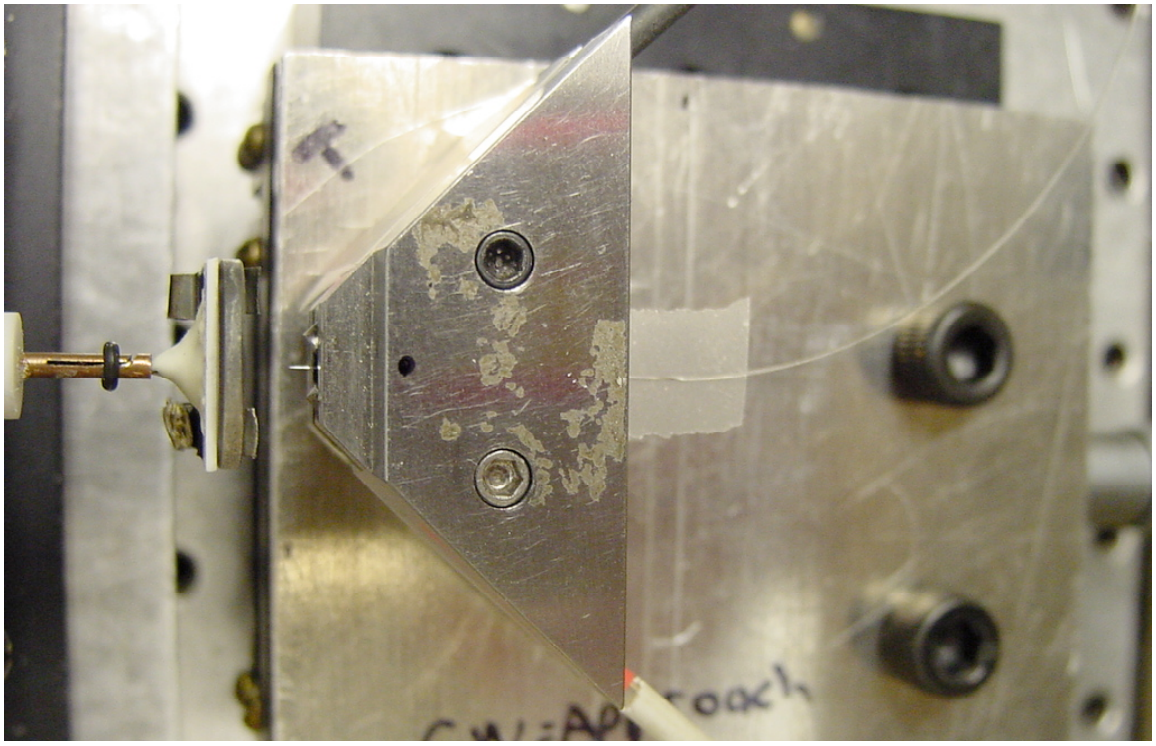

Figure 4.8: The NSOM Probe Fibers and Pickup Fibers

The Photomultiplier Tube

The photomultiplier tube (PMT) converts the light captured by the pickup fibers to a current. The RCA model IP28 PMT used in this project has had its resistor network modified to work with higher currents than is usual for a PMT. A PMT is typically used to detect individual photons, but in our case, we needed a light detector with low noise characteristics. Our sampling software can average the PMT readings over thousands of

samples, but averaging over more than a hundred samples does not reduce the dark current fluctuations in the output.

The PMT is expected to be linear for supply voltages up to 300 V [Gerbracht]. The PMT supply is typically operated at 400-600 V. Even in its uncalibrated and nonlinear condition, the PMT can qualitatively detect changes in the amount of light, and it is perfectly suitable for the "constant phase" mode of operation.

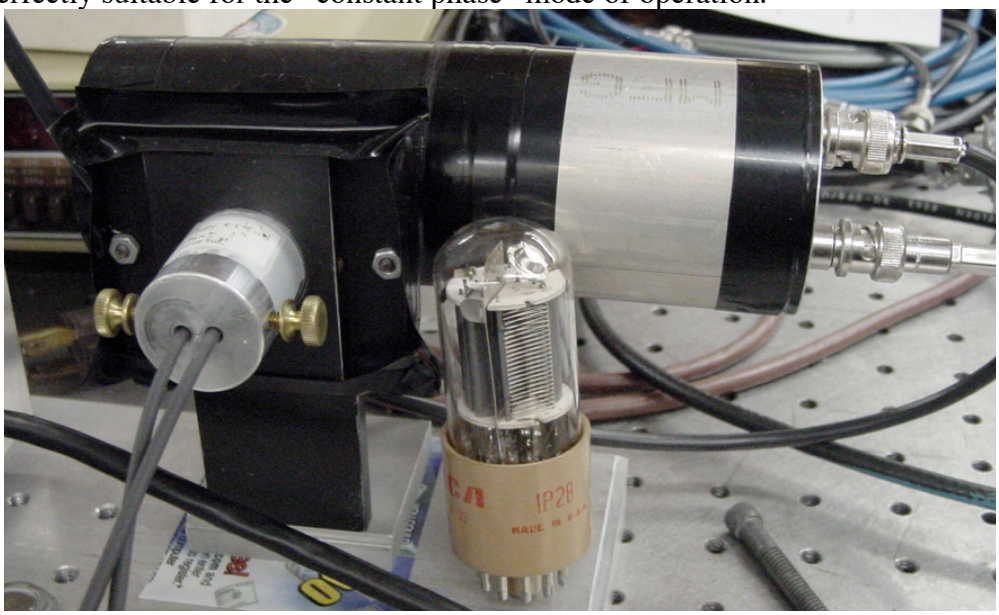

Figure 4.9: The PMT with Fiber Guide and Spare Tube

The power supply for the PMT has been observed to have detectable amounts of 120 Hz noise, although this frequency has not been detected in the ADC data. It has also been observed to go on occasional voltage "excursions". Should this happen during a scan, the scan is rendered useless.

The PMT Amplifier

The amplifier for the PMT is a low-noise, voltage-to-voltage, non-inverting 3-stage amplifier, designed and constructed in-house [Gerbracht]. The first stage uses an OPA111 opamp, and the second and third stages each use an OP177 opamp. The first

stage is inverting with a switch-selectable gain of -2000 or -20000 V/V. The second stage is non-inverting with a variable gain, controlled by a multi-turn potentiometer, of +2 to +12 V/V. The final stage has an inverting gain of -1 V/V. The output of this amplifier is a negative voltage because the overall gain is non-inverting and the PMT provides a negative current in the presence of light. Since the ADC only accepts positive voltages, the output of the amplifier's final stage is connected to the negative input of the ADC, and the ground of the output's power supply is connected to the positive input of the ADC.

Figure 4.10: The PMT Amplifier

The amplifier is typically operated at its maximum gain. At maximum gain, with the PMT supply at 400 V, the output has approximately 1% of 60 Hz noise. We typically average the PMT samples over approximately 1/60 of a second to average out the noise,

although this only improves the accuracy by 1%. The averaging process also allows time for the piezo tube to complete its movement so the majority of the samples are from the desired location.

The amplifier has provision for using a photodiode instead of a PMT as the sensor element. It includes an offset circuit for nulling the output.

Since the PMT provides a very small current as its output, this amplifier should probably be a transimpedance amplifier.

Chapter 5: The Controlling Software

5.1 Overview

The NSOM is controlled by two LabView applications: the Approach application and the Scan application; all software is located in the NSOMproject/new_nsom directory. These applications call the library functions written in C; the C functions are in the shared object library, "new_nsom.so". This file is created by a Makefile, so any time a change is made to the source code, the operator can simply issue the "make" command and the library is automatically rebuilt. The C functions call the library routines that are in KetoLib or are in the 2915 driver package.

The source files are separated into files that either deal specifically with a piece of hardware, or perform a specific type of function. Any software routine should talk to the underlying hardware strictly through the functions located in the file associated with that piece of hardware; only these specific files should need to understand the actual hardware communication protocols.

Source file	Purpose
new_routines.c vac_routines.c	Collected subroutines; faster than separate LabView operations. Move in X, Y, and Z and primary scan subroutines.
keto_dac.c	Interface to the new KetoLab DAC. Set piezo voltages and control of the flexure stage. Used only by vacuum system.
old_dac.c	Interface to the old DAC. Set piezo voltages.
bira_adc.c	Interface to the ADC. Contains routines to average readings.
smc24b.c	Interface to the SMC. Contains routines to step and to monitor SMC activity.
crate_ops.c	Collected CAMAC crate operations; understands how to write and read data through the system ioctl calls to the 2915 driver. Usually called from the hardware interface files.

Inside the DAC files is the provision for limiting the change in voltage per CAMAC write cycle, *i.e.* a restriction on the maximum movement speed of the piezos. Any commanded position change over the limit is accomplished in multiple writes. The result is to ramp the piezo voltage instead of a single massive change. The ramp occurs with the CAMAC write cycle time of 15 microseconds per step, and the piezo moves over a time of milliseconds, so this restriction on movement does not meaningfully affect the operating speed of the instrument. It is intended to accelerate the sample more slowly.

Some precise nomenclature is required to discuss these LabView applications without confusion. The piezo tube itself can "contract" and "expand"; these terms apply to the physical dimensional change of the piezo tube. The terms "retract" and "extend" apply to the relative movement of the tip and sample: retract means they are getting farther from each other, and extend means they are getting closer. A particular movement may be accomplished by either contracting or expanding the tube depending on the physical construction of the instrument. The picomotor can rotate either "clockwise" or "counterclockwise"; depending on the construction of the translation stage and mounting hardware, this rotation may result in an "approach" or a "retreat" where the sample and tip are getting closer together or farther apart, respectively. The software as discussed below will exclusively use the motional terms retract, extend, approach, and retreat. The specific detail of how this action is accomplished is hidden from the immediate knowledge of the user.

5.2 THE APPROACH APPLICATION

The Approach application is a LabView application with the express purpose of getting the tip within 100 nanometers (the near-field distance) of the sample. It is divided into three regions: a region that is applicable to all operations, a region concerned with

the picomotor control, and a region that moves the piezo tube in the Z direction, extending toward and retracting from the sample.

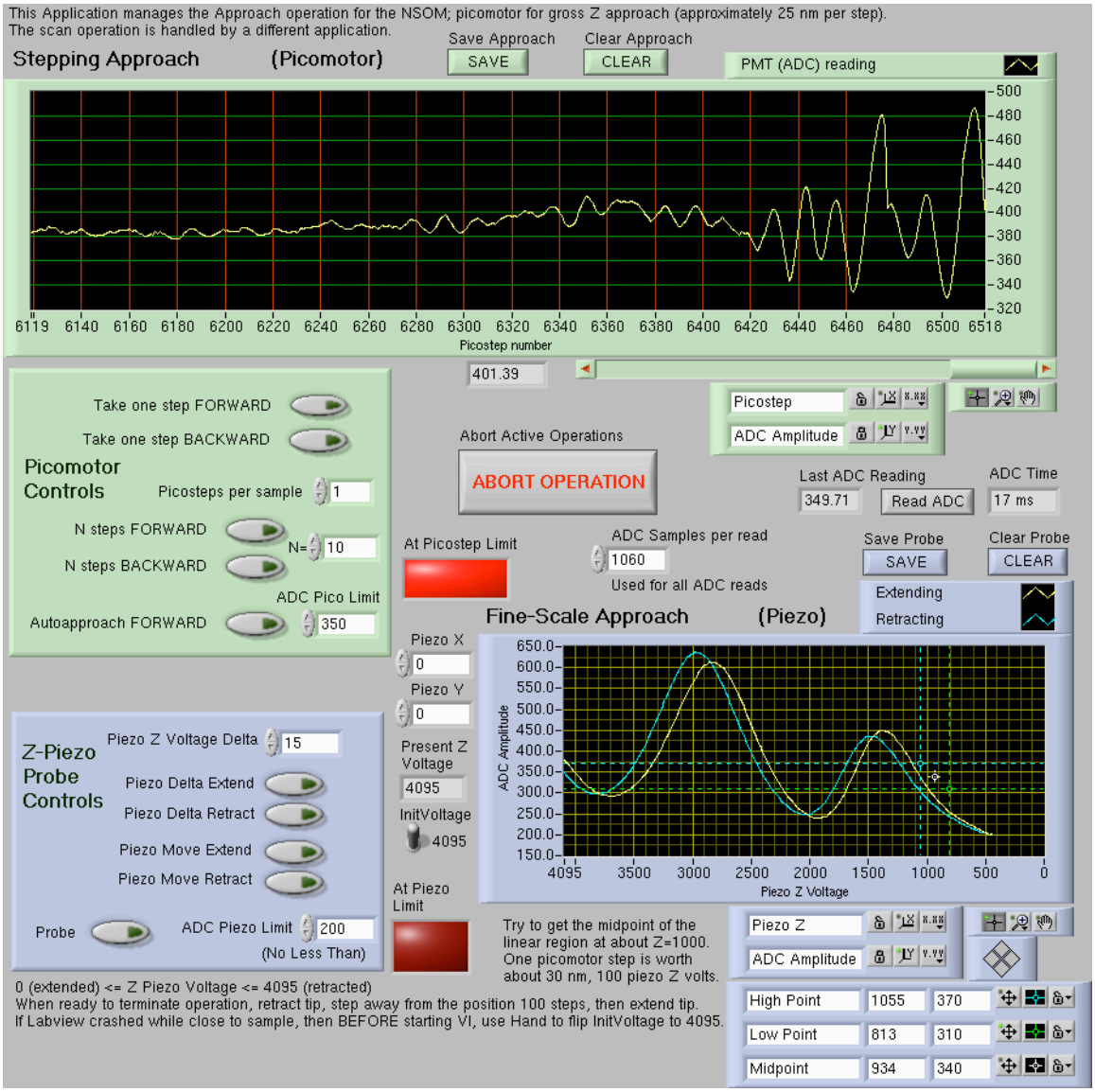

Figure 5.1: The Front Panel for the Approach Application

Common Controls

The common control region is near the center of the window. The "ADC Samples per read" is the number of actual ADC reads that will occur for all sample data requests,

with a single averaged value returned to the caller; this averaging feature is useful for reducing random noise or increasing the time delay. A “Read ADC” button is available to monitor the current ADC value without anything moving; the “Last ADC Reading” monitors the latest ADC value regardless of which function initiated the read. This region includes a large “Abort Operation” button that will attempt to stop all movement operations in progress. It will cease piezo movements and write a zero to the SMC control register. It is not capable of stopping a set of ADC reads, as those are inside a C function call which cannot read the “live” value of the abort button.

The Piezo X and Piezo Y controls will immediately move the tube scanner to a different location in X and Y. This may be useful if you want to do a close approach at a particular location, but the effects of piezo creep make it difficult to be certain where the tip is actually located.

The “Init Voltage” switch has a vital function. Occasionally, the LabView applications may hang, or LabView itself may crash. When the Approach application is initialized, it writes known values to all of its control points; there is no way to find out where the tip is located by interrogating some DAC register. If the probe tip is already close to the sample, then the process of initialization to the extended value may cause the tip to impact the sample. If you are in this situation, then BEFORE starting the Approach application, make certain that the Init Voltage is set to 4095 so that it will be initialized to the fully retracted position.

Picomotor Control

The Stepping Approach graph at the top of the page shows the current ADC reading against the picostep number. As long as the user is continually stepping in the forward direction, this graph is consistent, but if the user mixes forward and backward motion, then the graph can get confusing.

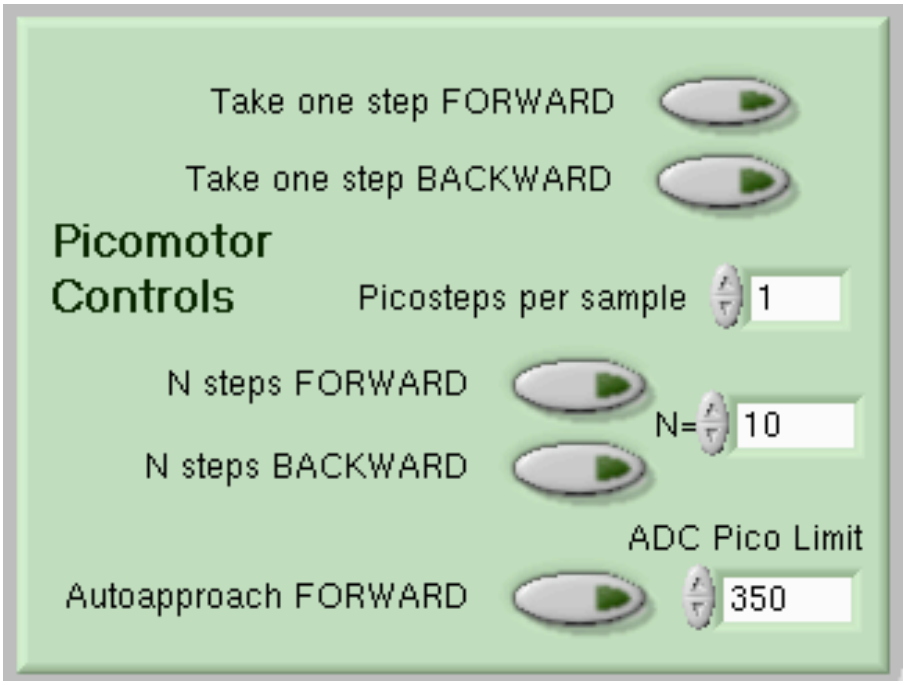

Figure 5.2: Picomotor Controls

The region on the middle-left controls the picomotor. The upper two buttons cause the picomotor to step exactly once, without any precautions. The next box is the number of picosteps between ADC samples; it applies to the next three buttons only. It is used to speed up the process of approaching to within reasonable distances, but if this number is greater than about 6, then you run the risk of aliasing and missing the approach oscillations of the ADC value. The two buttons labeled "N steps" are a useful way to move long distances. They will move the number of steps shown in the numeric box to the right, subject to the ADC Pico Limit control; if the ADC reading is less than the ADC Pico Limit value, then no movement will occur. The "Autoapproach" button is like the "N Steps" buttons, but it will move forever forward, subject both to the ADC Pico Limit and also requiring the latest ADC reading to be within 35% of its long-term average. To properly use this function, you must monitor the latest ADC values and keep the Pico

Limit somewhat close to the baseline of the ADC readings. When the tip is near to the sample, the oscillations of the ADC readings should go low enough to stop the movement; then you can cautiously use the piezo probe function to see how close you really are.

Piezo Control

The region at the bottom of the window deals with the piezo voltages. On the right is a graph of the ADC readings as the piezo voltage changes. The right edge of this window is the fully extended position, and the left side is the fully retracted position. This graph is updated for each piezo movement; different colors are used for retraction and extension.

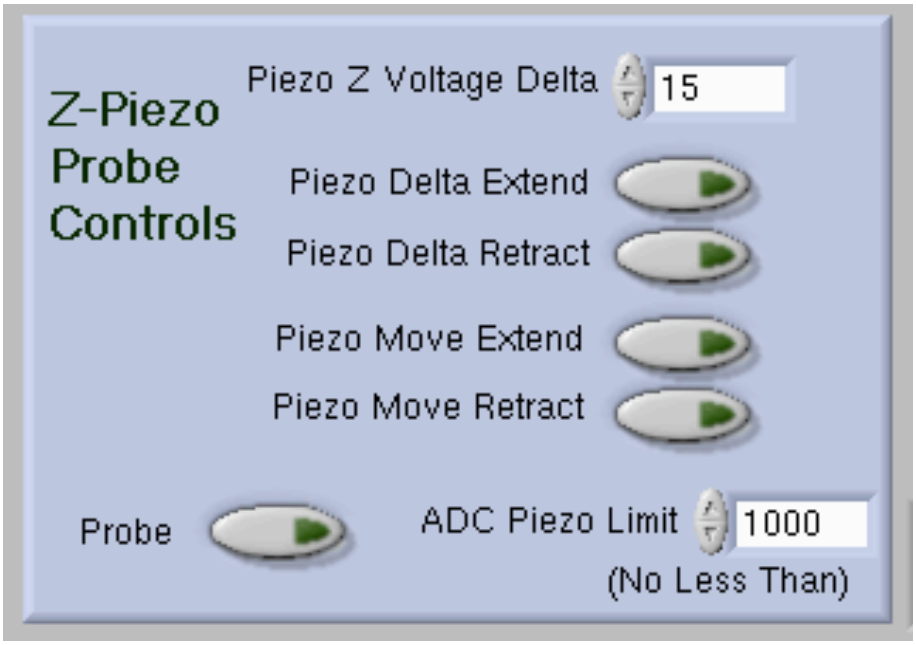

Figure 5.3: Piezo Controls

At the bottom-left of the window are the piezo controls. The "Piezo Z Voltage Delta" parameter is the increment (or decrement) value between samples. The two "Piezo Delta" buttons extend and retract the tube by the delta amount, not subject to the "ADC

Piezo Limit". The two "Piezo Move" buttons extend and retract the tube until either the Piezo Limit or the maximum (or minimum) possible value is reached. The Piezo Limit functions exactly like the Pico Limit for the picomotor; movement is prevented if the current ADC reading is less than the parameter. The "Probe" button will first clear the graph, and then extend the tube until either the Piezo Limit or the maximum extension is reached, then it will retract until the maximum retraction is reached.

The overall goal of this Approach application is to position the tip to within a hundred nanometers of the sample surface while retracted about a quarter of the full range. Once the scan begins, the picomotor cannot be moved, and the Z piezo movement is restricted to be within the 50% of its range nearest the sample (least voltage applied to z) while still allowing maximal X and Y movement. Ideally, you should try to get the optimal tip location near the 25% retracted point, but it is possible that the operator knows that the tip is above an unusually high or low region and can adjust accordingly to obtain a good scan.

Once you are within the correct distance of the surface, it is recommended that you pause for at least 30 seconds at the optimal position. The piezo will creep over this time, and you can adjust the position to remain at the correct distance. Once you are satisfied that the tip has stopped moving significantly, you should make short movements of the tip to ensure your position is still correct. If you anticipate scanning in the "Constant Phase" mode, position the tip near the highest peak of the curve. If you intend to scan in the "Constant Intensity" mode, use the mouse to move the cursor points of the graph to mark the linear region of the approach curve and position the tip at the midpoint.

The last thing to do is to manually stop the Approach application and start the Scan application. If the Approach application is still running, then it will slow the operation of the Scan application.

An Operation Example

Figure 5.1 show a typical approach operation as the tip nears the sample. We begin with the tip in the extended position. The long-term stepping approach graph shows increasing oscillations from the interfering light paths, finally attaining a peak of approximately 1.5 times the average value. At about step 6475, we stopped picostepping and retracted the piezo using the piezo controls (resulting in the discontinuity), and then stepped carefully forward another 43 steps, a few at a time, performing a piezo probe operation repeatedly.

The only way to determine your position is by examining the probe graph. Figure 5.1 also shows the final probe operation before starting the Scan application. The regular sinusoidal oscillations are distorted in the final peak and trough (on the right side of the graph). The reduced amplitude of the signal is of less importance than the peak and trough position changes. The probe shows no sign of an increase in the light at the point where it might be expected from the interference pattern and is therefore within the near-field distance. Note the clear effect of the tube hysteresis as the retracting tube traces out a different Z-position (as determined by the light response) compared to the extending tube for identical voltage values.

5.3 THE GLOBAL VI

As a part of operating the Approach application, the piezo graph has two cursor points that are positioned by the operator to determine the linear part of the approach curve. This information is transferred to the Scan application through the use of LabView global variables. The LabView file is called new_scanner.gbl.vi. The Scan application reads these variables and initializes certain variables of its configuration. It is not essential to position these points, but it is helpful, especially in Constant Intensity scan mode.

5.4 THE SCAN APPLICATION

The Scan application performs a scan of the sample. It does not control picomotor movements; it makes only piezo movements.

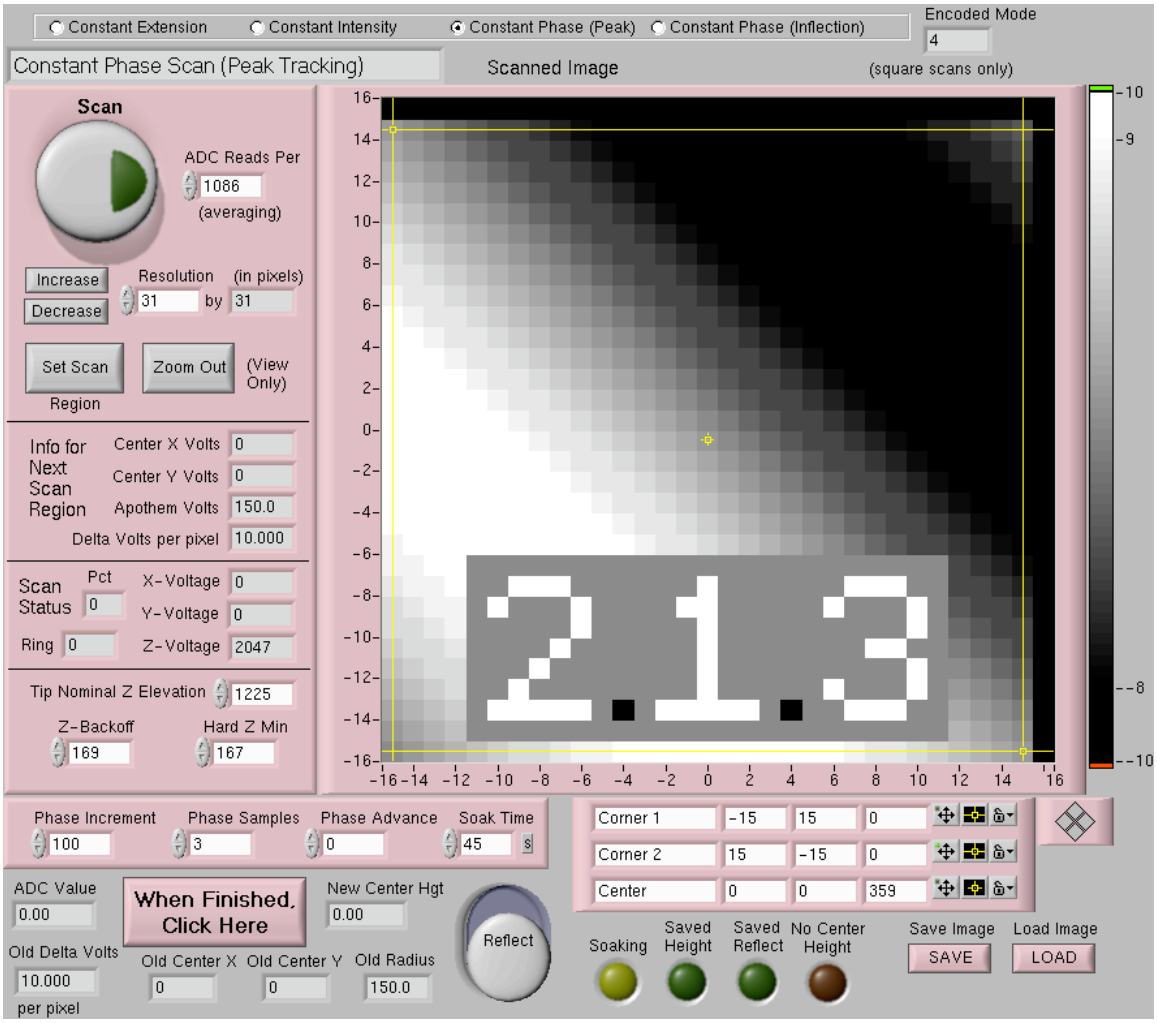

Figure 5.4: The Front Panel for the Scan Application (Version 2.1.3)

At the top of the screen is a selection of the scanning mode. Many NSOM instruments have a “constant height” (above the surface) mode of scanning since they have an independent means of determining the tip height above the surface, but this instrument does not have any such means of closing the feedback loop. Instead, there are

three different modes for scanning: constant extension, constant intensity, and constant phase. These modes are described later in this chapter.

Scan Application Controls

The majority of the front panel is occupied by the image of the scan. On the right side of it is a color bar that is used to alter the colors of particular values of the image. The image shown can be either the intensity of the light or the height of the surface. The large round slider at the bottom-center of the front panel determines which image is visible. The scale at left and bottom are in units of pixels.

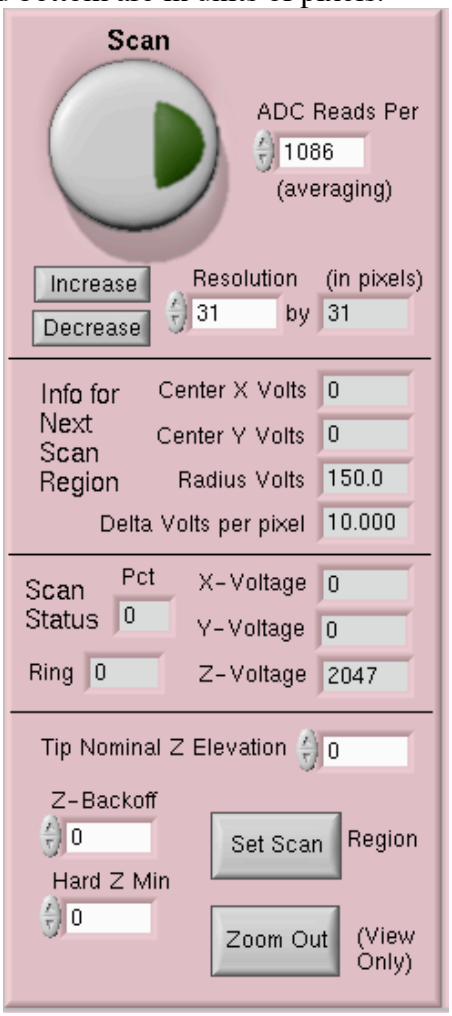

Figure 5.5: Scan Application Controls

The upper left of the front panel controls the resolution and region of the scan. All scans have a square aspect ratio, in terms of both pixels and distance, and all pixels are square. The total scan region is always an odd number of pixels per side. This is because the algorithm for movement in X and Y is a spiral scan around a central pixel. The reason for doing a spiral scan is that every pixel is next to the immediately prior pixel; there are no surprising changes in height nor excessive changes in control voltages. In addition, the first area to be scanned (the center) is likely to be the area that the operator is most interested in. Other NSOM instruments will perform a raster scan, either unidirectional or bidirectional, but such scans always result in the first point at a corner of the scan region with an unknown height. The raster scan voltages also have periodic large changes to accomplish large movements to the beginning of the next scan line, and that results in excessive hysteresis and/or creep of the tip for several seconds after the change in voltage.

There are two buttons in this section that control the scan region boundaries. Pressing “Zoom Out” will show a larger region in the scan image window; it does not alter the actual region of a scan, but only changes the view. Pressing “Set Scan Region” is the ONLY way to alter the X and Y extents of the scan. The operator must first position the cursors in the scan image at the boundaries of the desired scan region, and then press this button. The operator should then inspect the values of the next scan parameters, to see that they are satisfactory, with the outermost ring not exceeding the physical limits of the DAC and the Delta Volts parameter small enough to capture the anticipated minimum feature size.

The next region of the front panel gives information concerning the next scan: the X and Y offsets to the center of the scan region, the apothem distance to the outside of

the scan region, and the control volts per pixel. All units are in terms of the DAC control codes, ranging from -2047 to +2047 for each.

The next region of the front panel shows the status of the current scan in progress: the actual X, Y, and Z values as written to the DAC, the ring number, and the percent complete. Since the scan for a particular ring is handled in a C function, this information is updated only at the end of each ring when control is returned to LabView.

The next region of the front panel restricts the Z-movement of the piezo tube. The value of "Nominal Z Elevation" is the DAC voltage that is interpreted as a surface height of zero; it is assumed that the surface at the center of the scan is at approximately this location. The "Z-backoff" value is the change in Z channel output after reading a pixel; in effect, it is somewhat like a sewing machine needle, retracting from the surface this distance before moving in X or Y, in the hope that the tip will not drag and impact with the surface. The "Hard Z Min" value is an absolute restriction on the voltage applied to the piezo. Should the software calculate a value less than this number, it will abort scanning. The assumption is that some error has occurred, and the values are wildly incorrect, possibly leading to contact with the surface.

Below this section of the front panel is a region that is specific to each scan mode. It is discussed later in this chapter.

At the bottom right are information and controls concerning the location of the cursors in the image. They may be used for fine control of the exact region to be scanned. There are also two buttons that will save and load the visible image, in spreadsheet format, to a file.

At the bottom are four indicator lights. One indicator is that the application is "soaking," or spending an extended period of time, at the nominal tip elevation prior to the scan. It does this to help eliminate distortions in the initial height values due to creep.

Two more lights show if the operator has saved the present image to a file. One light is a warning that the center of the scan region does not have a known height; if the center has a known height, then that value is added to the soaking location to make the soak more likely to be at a more accurate location.

The large button at the bottom left labeled "When Finished, Click Here" should be pressed when you are finished making scans. It will retract the tip halfway, center the X and Y channels, retract fully, make the picomotor step away from the sample a few hundred steps, then extend the tip to its natural position and stop the Scan application. The operator should use the Approach application to continue stepping a few thousand steps away from the surface.

The front panel also has some numerical indicators of the just-completed scan. This is for informational purposes only.

5.5 SCAN MODES DESCRIPTION

The fiber tip has no independent way to determine its height above the surface. Commercial NSOM instruments will use a vibrating fiber to operate in a constant height mode, sensing the approach to the sample by detecting a change in the amplitude of vibration, but that method requires adsorbed water molecules to provide friction with the tip. The instrument described in this thesis is intended for eventual operation in an ultra-high vacuum. All information as to the tip location must be extracted from the light returned from the surface.

Constant Extension Mode Operation

Constant Extension mode simply puts the tip at a particular Z-location and reads the intensity of the light. The data is put into the intensity array; no height information can be returned since all locations are at the same extension. Constant Extension mode

will fail if the surface has a large enough bump which the tip crashes into. This ruins the tip. As the topology of the sample is *a priori* unknown, this is a dangerous mode to use initially. Constant Extension mode has the potential to be the fastest scan mode since it moves the tip the least number of times per pixel.

Figure 5.6: Constant Extension Special Controls

There is no special control parameter for the Constant Extension mode. It simply reads the value at the nominal Z-value, retracts the Z-backoff amount, and moves to the next pixel.

Constant Extension mode as described here is sometimes called constant height mode in the literature.

Constant Intensity Mode Operation

Constant Intensity mode uses the slope of the linear region of the approach curve (as determined in the Approach application) to determine the height of the surface. The tip goes to the anticipated Z-location that will result in an intensity reading that is in the middle of the linear range. It then adjusts its extension according to the actual intensity reading, looking for the nominal intensity. The data is put into the height array; no intensity information can be returned since all locations should have the same intensity. Constant Extension mode fails when the surface has locations with differing reflectivity such that the light intensity is no longer an exclusive function of height. The difference in reflectivity can be caused either by topography changes, directing the reflected light away or toward the pickup fibers, or by the surface intrinsic reflectivity. Any reflectivity

change alters the characteristics of the linear region and changes the linear function that the algorithm depends on. This mode is slower than the Constant Extension mode, as it must seek out the Z location of the correct light intensity; when that is changing radically, the algorithm can "hunt" excessively. It may even fail completely, as when the reflectivity is very low: the algorithm will back away from the surface to get a brighter image, but if it never achieves the reference brightness, then it will back away to the limit. Conversely, if the surface is very bright, then the tip will approach the surface, trying to reduce the brightness; if it reaches the hard limit of motion, it fails.

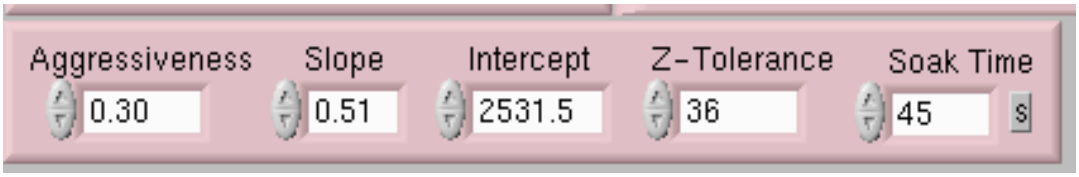

Figure 5.7: Constant Intensity Special Controls

The desired intensity of the light is the value at the nominal Z elevation. The Slope and Intercept parameters are set by the operator in the Approach application by positioning the cursors in the piezo graph to the linear portion of the approach curve. The intensity of the light is read, and the location on the line (as set by these parameters) is determined. If this is not within the "Z-tolerance" value (*i.e.* the light intensity is not within the required range as determined by the line slope and intercept), then it moves toward (or away from) the surface, seeking the nominal intensity of light. The distance to move is reduced by the "Aggressiveness" parameter: a value of 1 will immediately move to the calculated position, but values less than 1 will move proportionally less.

The Constant Intensity mode algorithm can be improved by using the previous pixel's slope and intercept as a starting point and acquiring the new pixel's slope and intercept. This requires enough samples of the intensity curve to reliably locate the linear

region, even when the linear region has shifted in both Z-location and magnitude, and the measurements, being nondeterministic in number and time, are subject to the hysteresis and creep of the piezo tube. There is some doubt about whether this recalibration process would yield consistent images of the surface, and it would undoubtedly be very slow to acquire.

Constant Phase Mode Operation

Over a small enough region of the approach curve near a maxima or minima, it appears to be a parabola. Constant Phase mode will read three (or more) widely separated points of the approach curve and do a curve fit to a parabola. The resulting extremum of the parabola is a known and fixed distance from the surface, since the curve results from the interference between the direct and reflected light paths. The intensity of the light is read from the desired location relative to the extremum, and both intensity and height are simultaneously extracted from the information. In the following discussion, the term "peak" is used for clarity (since that is the usual practice), whereas the actual algorithm will operate with either maxima or minima.

Figure 5.8: Constant Phase Special Controls

The algorithm assumes that the tip is already at the first location for parabolic sampling. The light intensity is read, then the tip is advanced the "Phase Increment" amount and another read occurs, then advanced again until "Phase Samples" points (at least three) are obtained in this way. The operator should adjust the number of phase samples and the phase increment so that the middle of the sample interval is near the

anticipated peak of the curve. The intensities and Z positions are put into a regression, and the least-squares best-fit equation of a parabola is calculated. The peak of the parabola must lie within the sample points, or the algorithm starts over with the previous end point closest to the peak as the new endpoint of a new sample range. Once the peak z-value is determined and inside the sample range, the tip moves to that location plus the "Phase Advance" value; this is a location closer to the sample but still safe. The light intensity is read and placed into the intensity array, while the peak location is placed into the height array. Therefore, both height and intensity readings are returned with this scanning mode. Finally, the tip is retracted the Z-backoff amount and moved in X and Y to the next pixel. The optimal value of the Z-backoff parameter is the sum of half the total sample interval plus the phase advance parameter, *i.e.* to place the next peak (assuming it is at the same location as the current peak) at the midpoint of the sampling range.

As an example, suppose you would like to locate a peak that is near Z location 1210, take the scan pixel from 250 units forward from the peak ("phase advance"), and have a 150 unit spacing ("phase increment") in the three ("phase samples") parabolic sample points. You might set the nominal Z elevation to 1200 and the Z-backoff amount to 400. The soak will occur at 950, and then it will move back to 1350 and make the first parabolic sample. The second sample will be at 1200 and the third at 1050. The parabola has its peak located at 1210, so the Z location for the scan image is from location 960. Finally, the backoff movement will be to location 1360, the X (or Y) location will change, and the next pixel will be acquired in the same manner.

We attempt to keep the curvature of the parabola to the same sign as the previous pixel. Should the calculated peak location be outside the sample range along with a curvature change, then the tip is repositioned to where the endpoint of the sample range closest to the peak becomes the opposite endpoint of the new sample range, *i.e.* it moves

toward the nearest peak of the previous curvature. As a special case, should the extremum location be inside the sample range yet have a curvature of opposite sign, that is taken as a desired change to operate relative to the other extremum of the curve. A warning of this curvature change is printed to the terminal window. The result of these operations is to allow a large change in the height to be compensated for; a pixel-to-pixel change in the peak location by up to ±180 nm can theoretically be accommodated (depending on parameter values). The operator should ensure that the parabola sample points are separated widely enough so that even in the presence of noise, a relatively accurate parabola can be fit to the points.

Our experience is that Constant Phase mode is the most reliable mode and results in the best quality scans. It is somewhat slower than Constant Extension mode because each pixel needs at least four large tip movements. The intensity images that it returns are repeatable and clear.

Constant Phase mode as described here is our method of implementing what is sometimes called “constant gap” mode in the literature.

Chapter 6: Results

6.1 Calibration of the Tube Scanner

The approach curve exhibits interference between the direct and reflected light paths with a presumed period of 376 nm, as calculated by Equation 2.1. Below is a typical result from the probe operation.

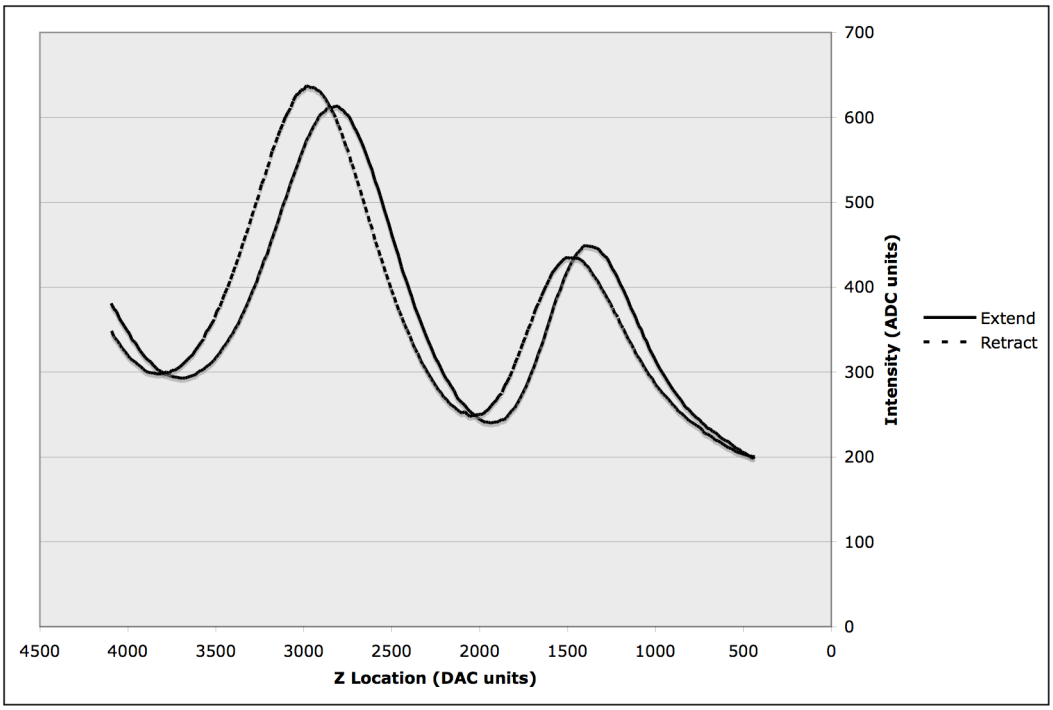

Figure 6.1: A Probe Operation

There are several pieces of information to extract from this graph. First, the amplitude has suddenly increased from the average value (from about 400 to a peak of 600) and is showing large oscillations, therefore the sample must be nearby (and also very reflective). Second, the extending and retracting curves trace different paths, exhibiting the hysteresis of the piezo tube. Third, the period of this oscillation (measured

between the two bottom minima of the extending operation) is approximately 1755 DAC units. The full-scale Z DAC output is 141 V from outer to inner electrodes of the piezo tube, so each DAC unit is 34.4 millivolts, and the period of the oscillation is 60.4 V. Assuming this distance is 376 nm per Equation 2.1, then following Equation 3.1,

$$376 = \frac{d_{31}(0.98)}{0.02}\left(-141 \cdot \frac{1755}{4095}\right), \tag{6.1}$$

the value for d_{31} is -1.27 Å/V, exactly the nominal value given by the manufacturer.

The calibration should occur some distance from the surface, since the curve can become distorted in amplitude and phase when the surface is near.

The approach curve has changed over time and/or use. Some months ago, the d_{31} constant was measured as -1.60 Å/V. It is possible that the large voltages applied in the reverse direction (contracting the tube) are stressing the tube and are slowly reducing the degree of poling in the tube. Most instruments usually operate the tubes in the expansion mode (see Chapter 3).

6.2 Diffraction Grating Target

A diffraction grating, model TDG01 from NT-MDT (www.ntmdt.com) is used as a target for atomic force microscopy. It is made of aluminum on glass and consists of a sinusoidal profile of parallel lines, with 55 nm height and 278 nm period [ntmdt]. The wafer diameter is 12.5 mm with a central effective area 9 mm in diameter.

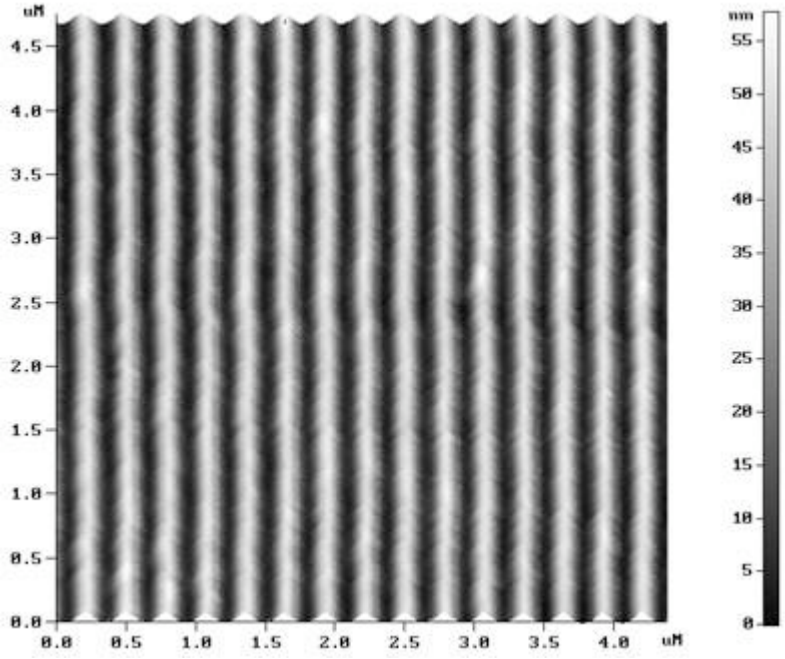

Figure 6.2: TDG01 Diffraction Grating by SPM Semi-Contact Mode

Figure 6.3: Photo of TDG01 Diffraction Grating

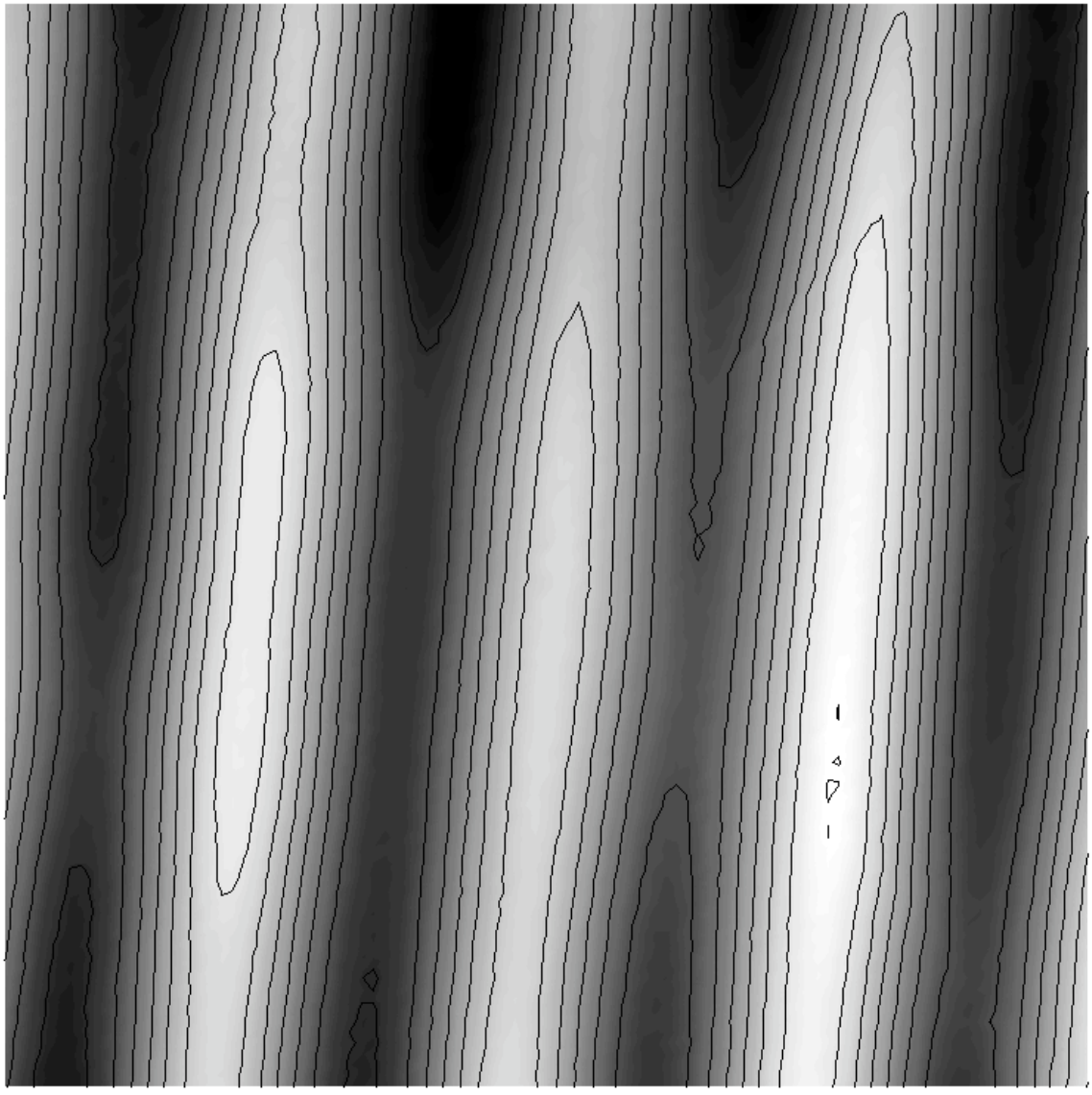

Figure 6.4: Constant Extension Mode Scan, Vertical Orientation (23Apr09)

Figures 6.4 and 6.5 are scans of the same region of the diffraction grating at a resolution of 101×101 pixels and 3.00 DAC units per pixel.

Figure 6.4 is a scan by our NSOM of the diffraction grating done in constant extension mode, so the image is of the detected light. The brightest pixel is 68% brighter than the dimmest. Of note (in comparison to Figure 6.5) is the straightness of the ridges.

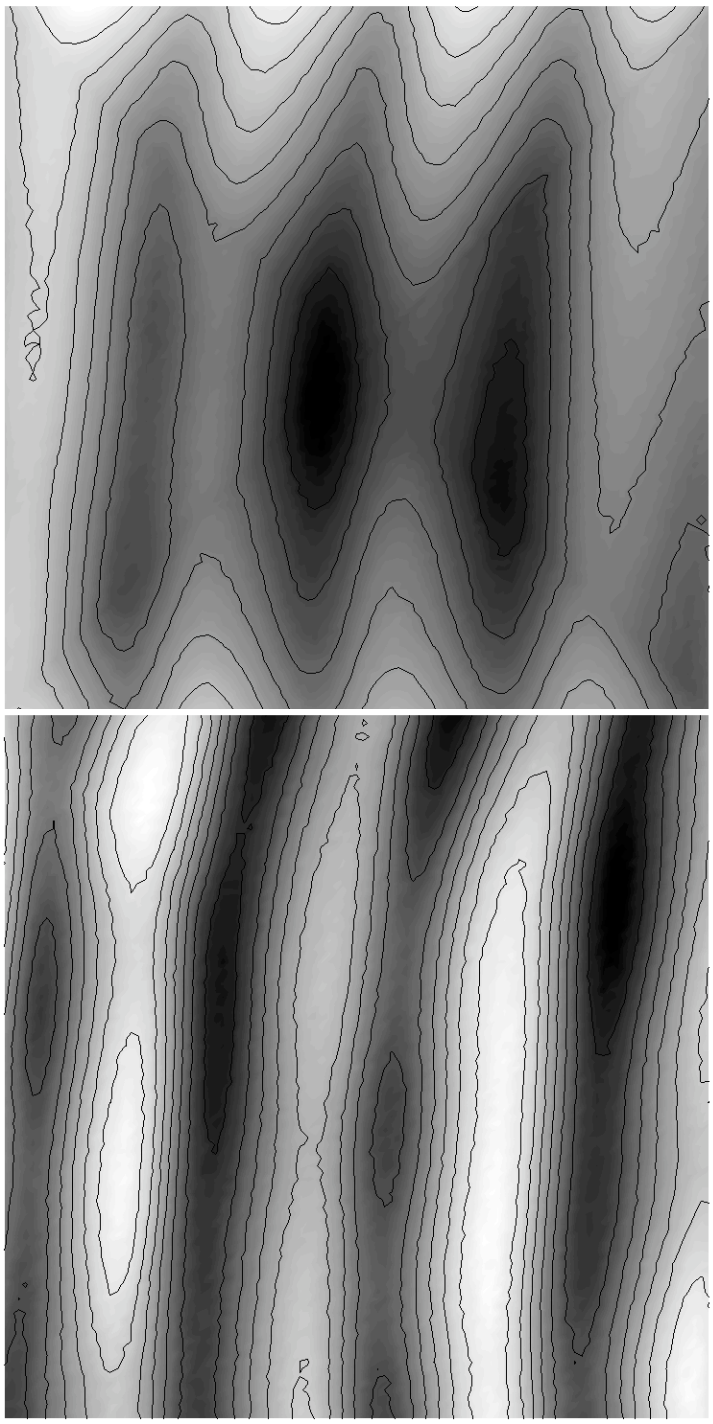

Figure 6.5: Constant Phase Mode Scan in Vertical Orientation (23Apr09) (top) Height (bottom) Intensity

Figure 6.5 is a scan of the diffraction grating done in constant phase mode. The upper scan is the height information, and the lower scan is the intensity of the reflected light, captured 200 Z-DAC units (43 nm) closer to the surface from the peak of the parabola. The grating is oriented vertically; the pickups are receiving light reflecting from the sides of the sinusoidal ridges. The dark color in the height image is farther from the tip. The dark color in the intensity image is dimmer.

Of interest is the intensity and height correlation. It seems that the nadirs of the grating show as brighter, and the crests as dimmer. The grating does not appear as straight as the manufacturer specifies, which is probably an indication that the tube scanner is not perfectly linear in some regions of its movement, probably caused by the hysteresis in the Z-motion necessary to capture the image. The height information also indicates it is "deeper" in the middle, which might be an indication of the spherical surface that the tube scanner moves over; however, the spherical surface should not be visible over the dimensions shown, as that difference is imperceptible from the middle to the edge of the image. It is far more likely that the tube scanner is not maintaining its extension when it is moving in X or Y. It should be possible to calibrate out this distortion from the images, if it is consistent.

As we look at a cross-section across the middle of the scan in Figure 6.6, the sinusoidal grating is clearly visible. The amplitude of the sinusoid is approximately 95 Z-DAC units, or 20 nm according to Equation 3.1. This is considerably different from the nominal 55 nm height. It may be that we do not get the greatest reflection from the nadirs, but rather from some point on the sides of the ridges. This would reduce the apparent relief of the ridges. In addition, we have two pickups, one on each side of the probe tip; the point of greatest reflection, and the interference intensity, can be different on each side, again acting to confuse the true height of the ridges.

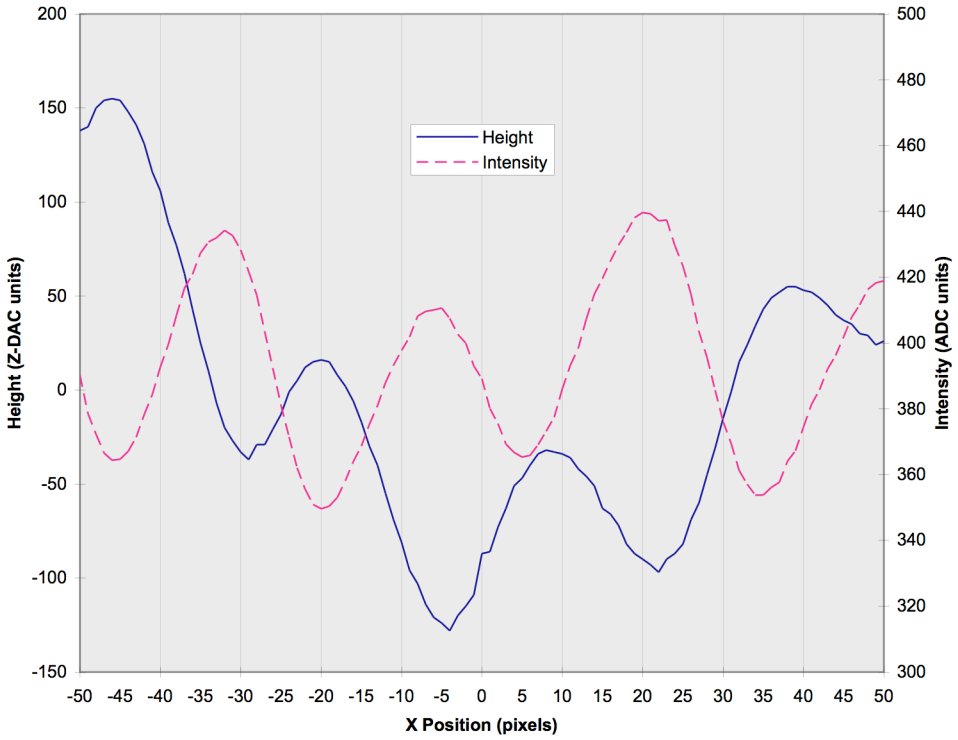

Figure 6.6: Horizontal Section Across the Middle of the Grating (23Apr09)

The period of the grating sinusoid is approximately 26 pixels. According to Equation 3.2, with d_{31} as -1.27 Å/V, the deflection voltage maximum of 152 V, resolution of 3 DAC units per pixel, and remembering the sample holder that adds 60% to the lateral tube movement,

$$\Delta X, \Delta Y = \frac{2\sqrt{2}(-0.127)(0.98)^2}{\pi(0.23)(0.02)}\left(152 \cdot \frac{26 \cdot 3}{2046}\right) \cdot 1.6. \qquad (6.2)$$

This is a distance of 221 nm, 20% less than the nominal 278 nm.

Figure 6.7 below is one of the earliest constant intensity scans of the grating. Getting it to work properly was difficult, and required some editing of the application parameters before it completed. The image is 63×63 pixels at 9.68 DAC units per pixel.

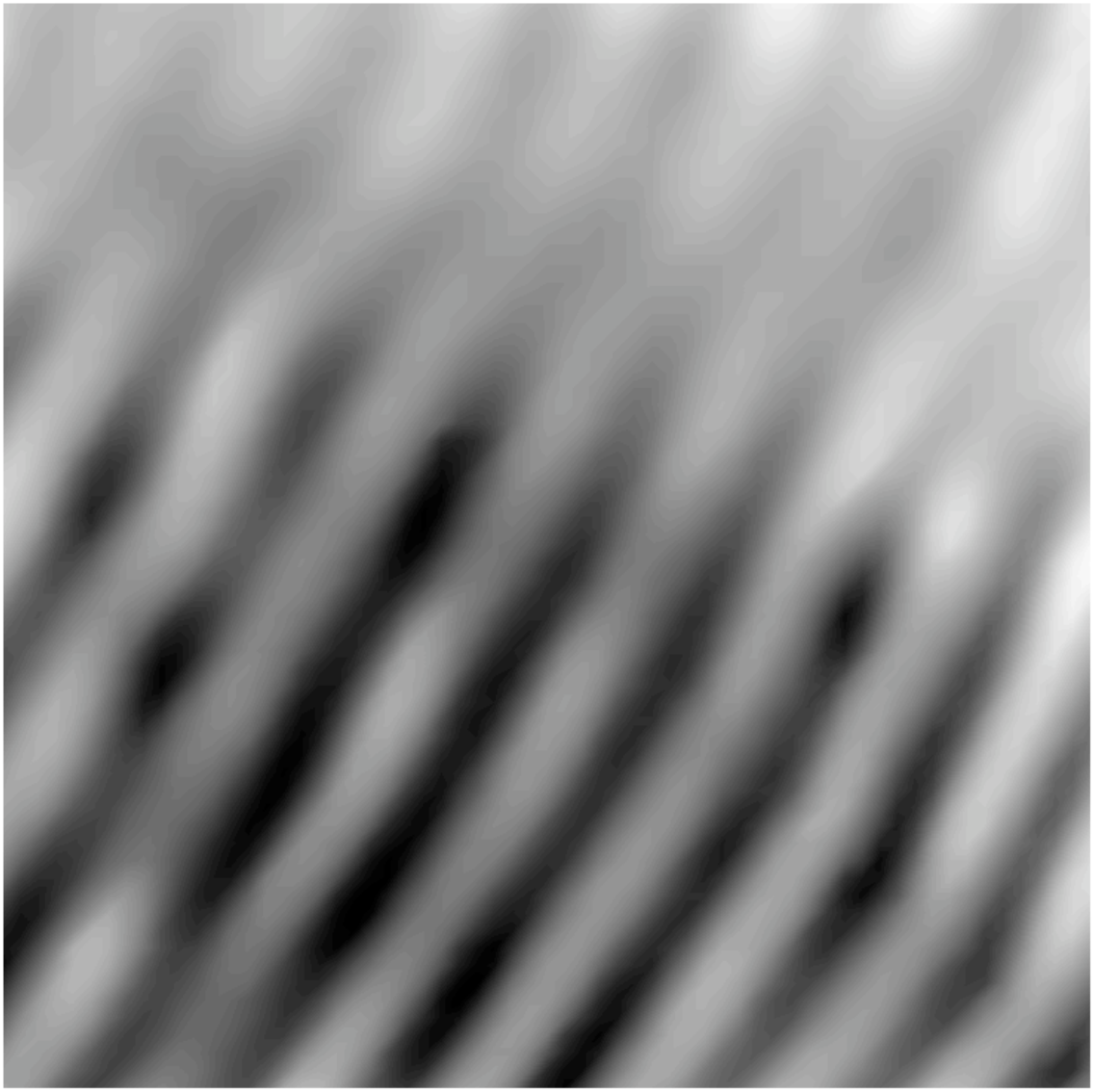

Figure 6.7: Constant Intensity Scan (6Aug07)

6.3 REPEATED AREA SCANS

Addressing issues of repeatability, we conducted multiple scans of the same area at different resolutions and area.

Figure 6.8: Constant Phase Scan (20Aug07s2) (top) Height (bottom) Intensity

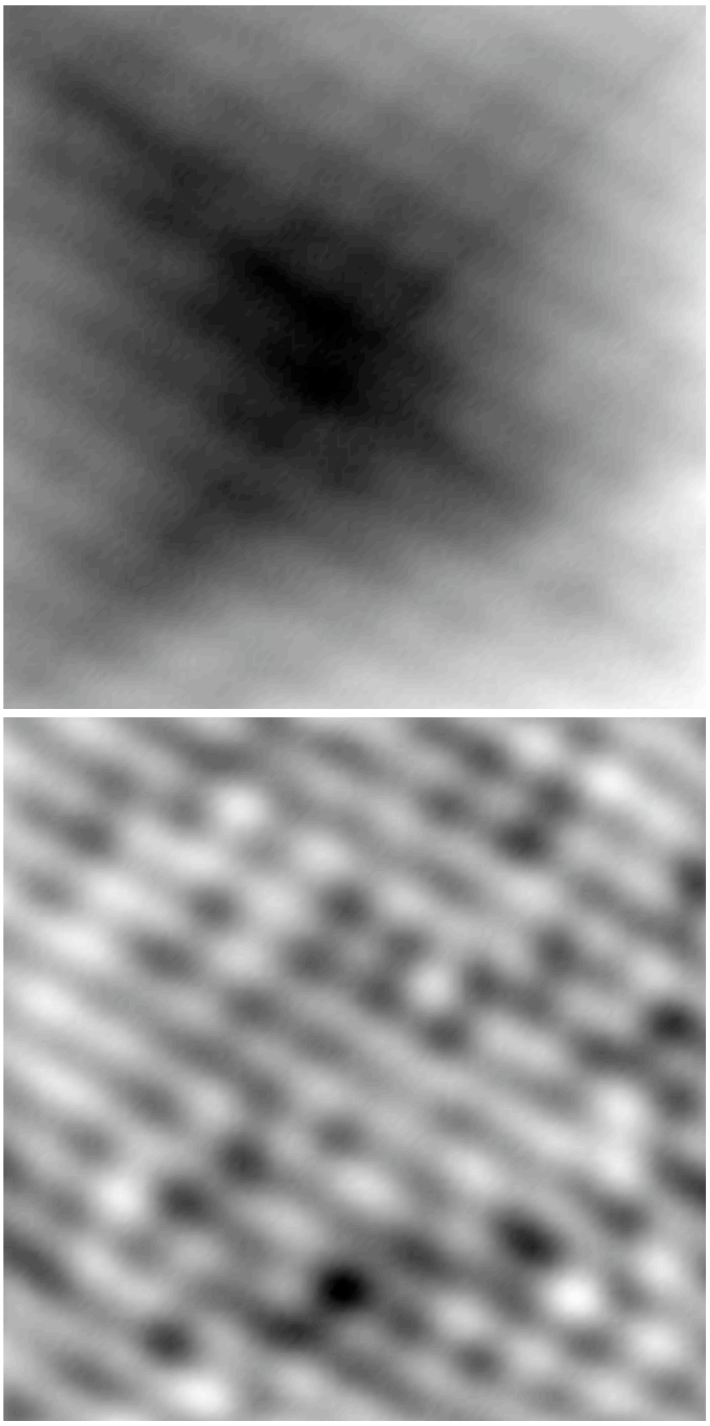

Figure 6.9: Larger Constant Phase Scan (20Aug07s3) (top) Height (bottom) Intensity

Figures 6.8 and 6.9 are centered on the same area. Figure 6.8 is a resolution of 31×31 pixels at 10 DAC units per pixel. Figure 6.9 covers approximately 7.2 times the area with a resolution of 127×127 at 6.38 DAC units per pixel.

The intensity image from Figure 6.8 is clearly the same region in the center of Figure 6.9. What is surprising is the amount of distortion in the height images and how clear and repeatable the intensity images are, even in the presence of the height distortion. If this height distortion is present in the Constant Intensity mode, it is not surprising that that mode has trouble completing scans.

Two faintly darker lines, in an 'X' shape, are visible along the diagonals in the Figure 6.9 (top) Height image. These lines appear frequently in the scans and are obviously an artifact of the spiral scan procedure, as they are at the locations where the scan changes direction. However, we do not know why they appear; there is no physical reason or operation going on that should result in the hardware or software deciding that those particular pixels are deeper than their nearby pixels.

6.4 SHIFTED PHASE LOCATION

The approach curve has multiple parabolic regions. The usual tactic is to begin at the peak closest to the surface, but it is also possible to scan based on the trough of the curve or even the next farther peak. Scans from the next peak are too blurry to get good images; since the surface is more than half a micron from the tip, the reflection takes place over a very large region of the sample, and the image is averaged over the topological details that are the purpose for the NSOM. However, depending on the sample, it may be possible that scanning based on the trough or second peak will yield an acceptable image.

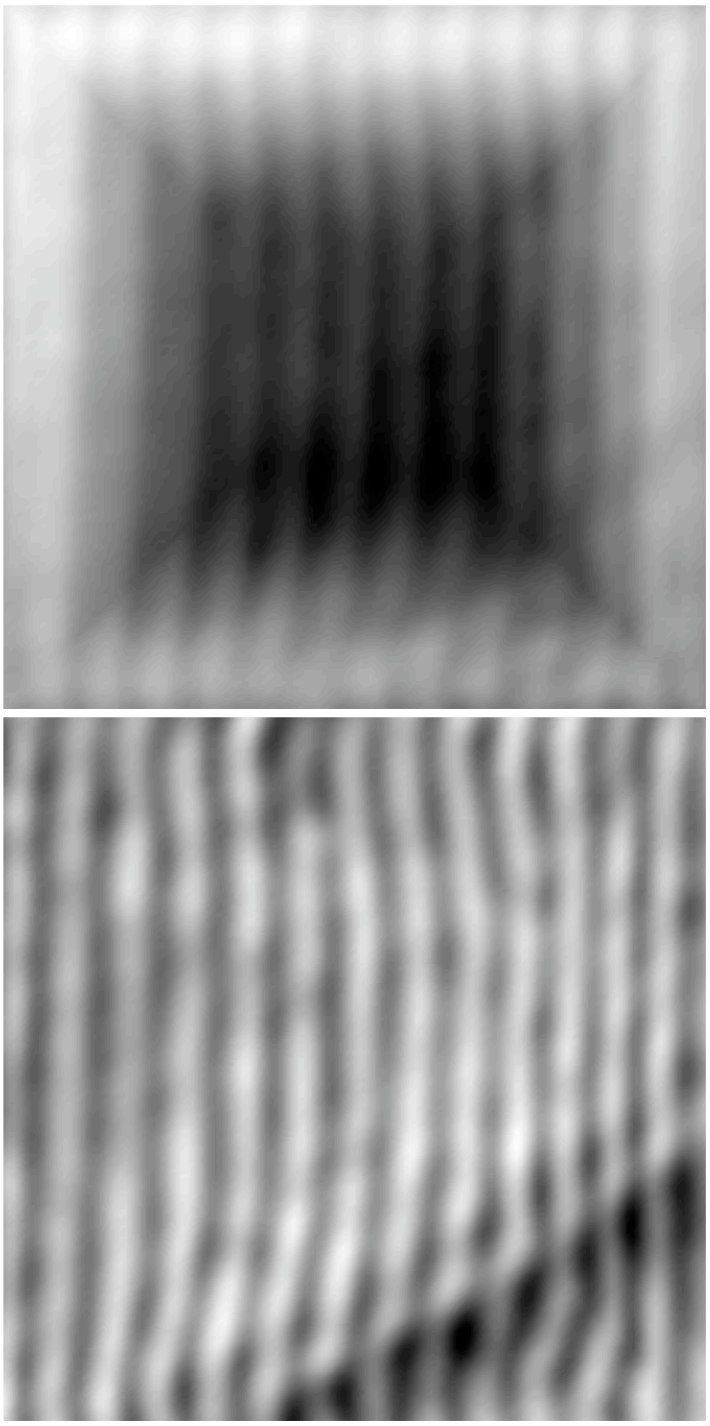

Figure 6.10: Constant Phase Scan from Trough (23Aug07s2) (top) Height (bottom) Intensity

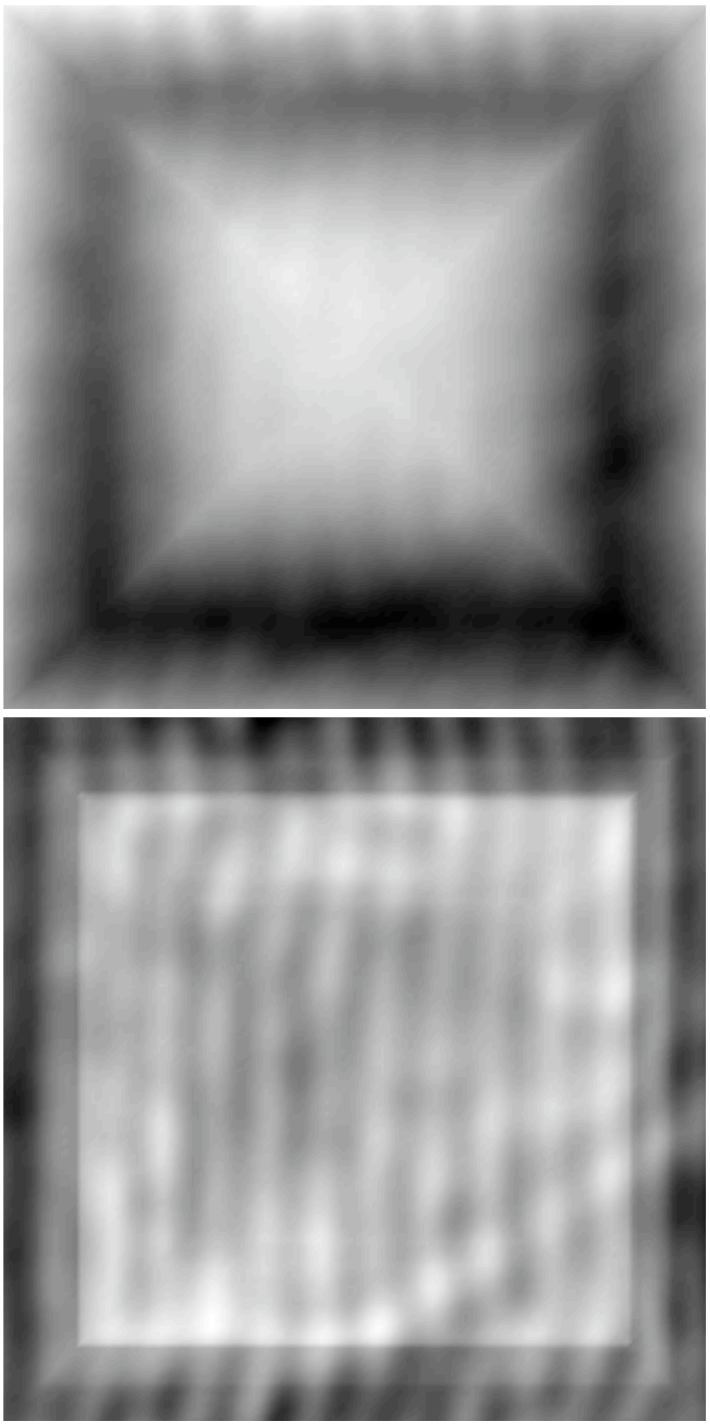

Figure 6.11: Constant Phase Scan from 2nd Peak (23Aug07s3) (top) Height (bottom) Intensity

Figures 6.10 and 6.11 are of the same region and the same resolution. They are 127×127 pixels at 7.94 DAC units per pixel. Figure 6.10 is positioned at the first trough of the approach curve (376 nm sample to tip distance), and Figure 6.11 is from the second peak (564 nm sample to tip distance).

As the tip gets farther from the sample, the intensity images get progressively blurrier. The two figures are of the same region, as can be verified in the intensity images, but the more distant scan is of obviously lower contrast.

One notable feature is in the height images. Figure 6.10 appears to have a large pit in the middle, whereas Figure 6.11 has a moat around a pyramid. Although the algorithm was cuing off a different portion of the approach curve, it should not have made this sort of difference in the height. It is possible that the tube scanner is showing the creep and hysteresis effects as it moves back and forth in Z. Another possible explanation is given in the next section.

The second notable feature is the sudden dimming of the intensity in Figure 6.11. We believe that we picked up a dust particle on our scan, and that obscured the light from the tip or surface. The dust particle may have also affected the height image.

6.5 SEEING THE SURFACE

Figure 6.12 below is a large area scan of the diffraction grating. There appears to be a scratch in the surface. The scan is 255×255 pixels at 7.87 DAC units per pixel, or approximately 5.6 microns square. The image required nearly 1.5 hours to acquire (although it could have been faster with fewer ADC read sample averaging). The final "ring" of the scan did not complete; it failed for unknown reasons near the bottom right corner.

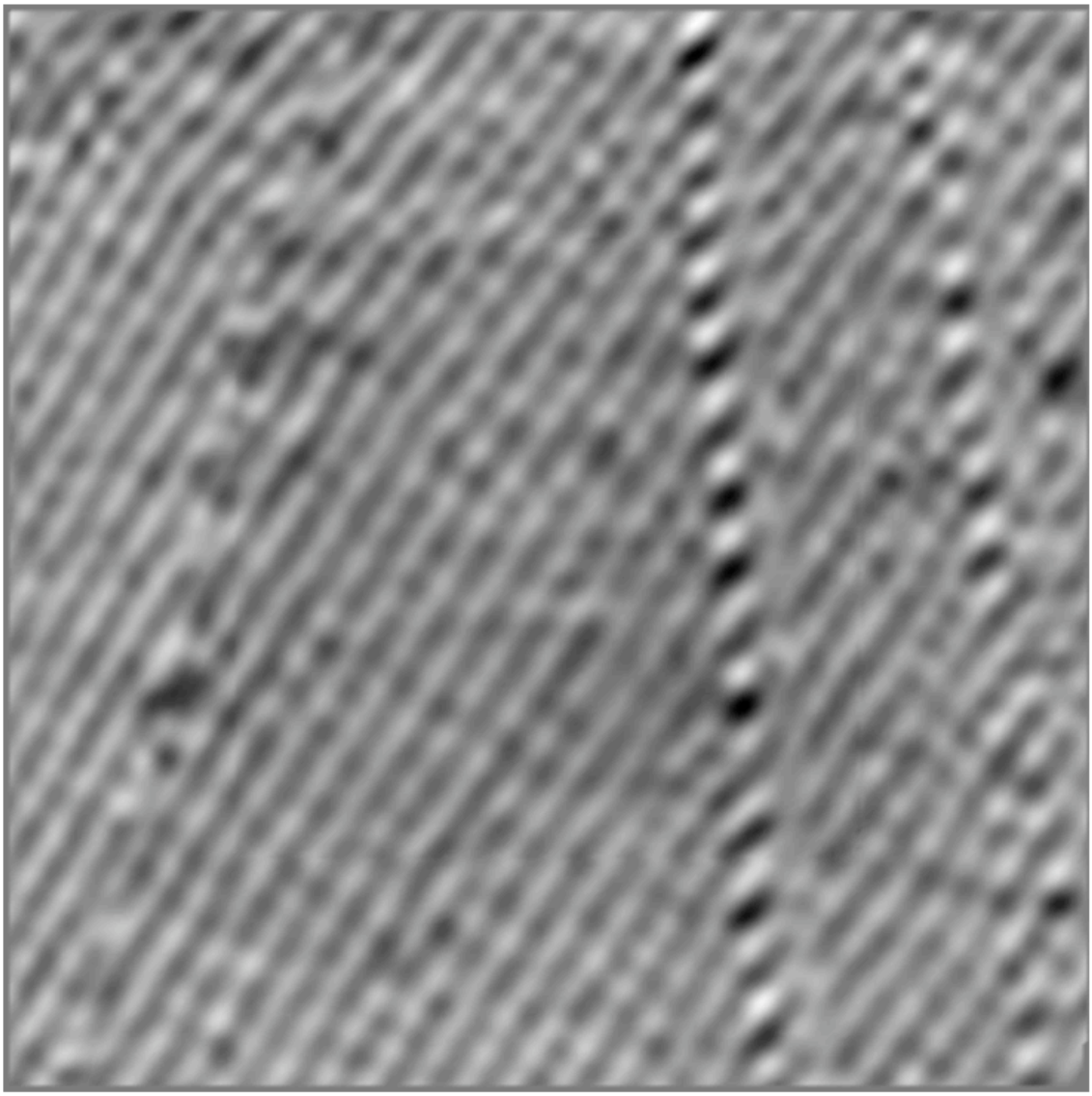

Figure 6.12: Constant Phase Mode Intensity Image of a Scratch (7Sep07s1r)

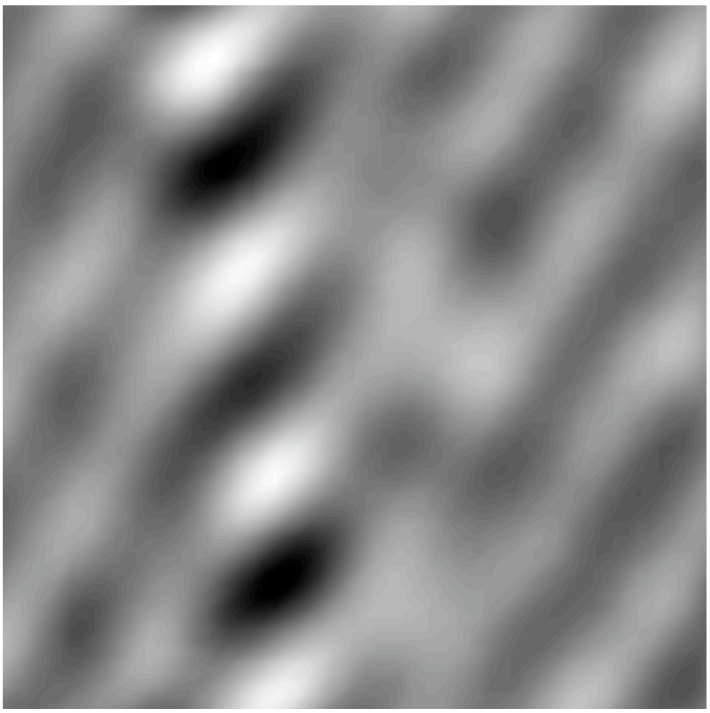

Figure 6.13: Close-up of a Scratch (7Sep07s3r)

Figure 6.13 is a re-scan and close-up of the scratch in the intensity view. Its lower left corner is near the center of Figure 6.12. It is a 63×63 image at 6.73 DAC units per pixel. This scan satisfactorily tested the ability to zoom in on a region of a previous image. The scratch seems to have both the brightest and the darkest pixels of the scan.

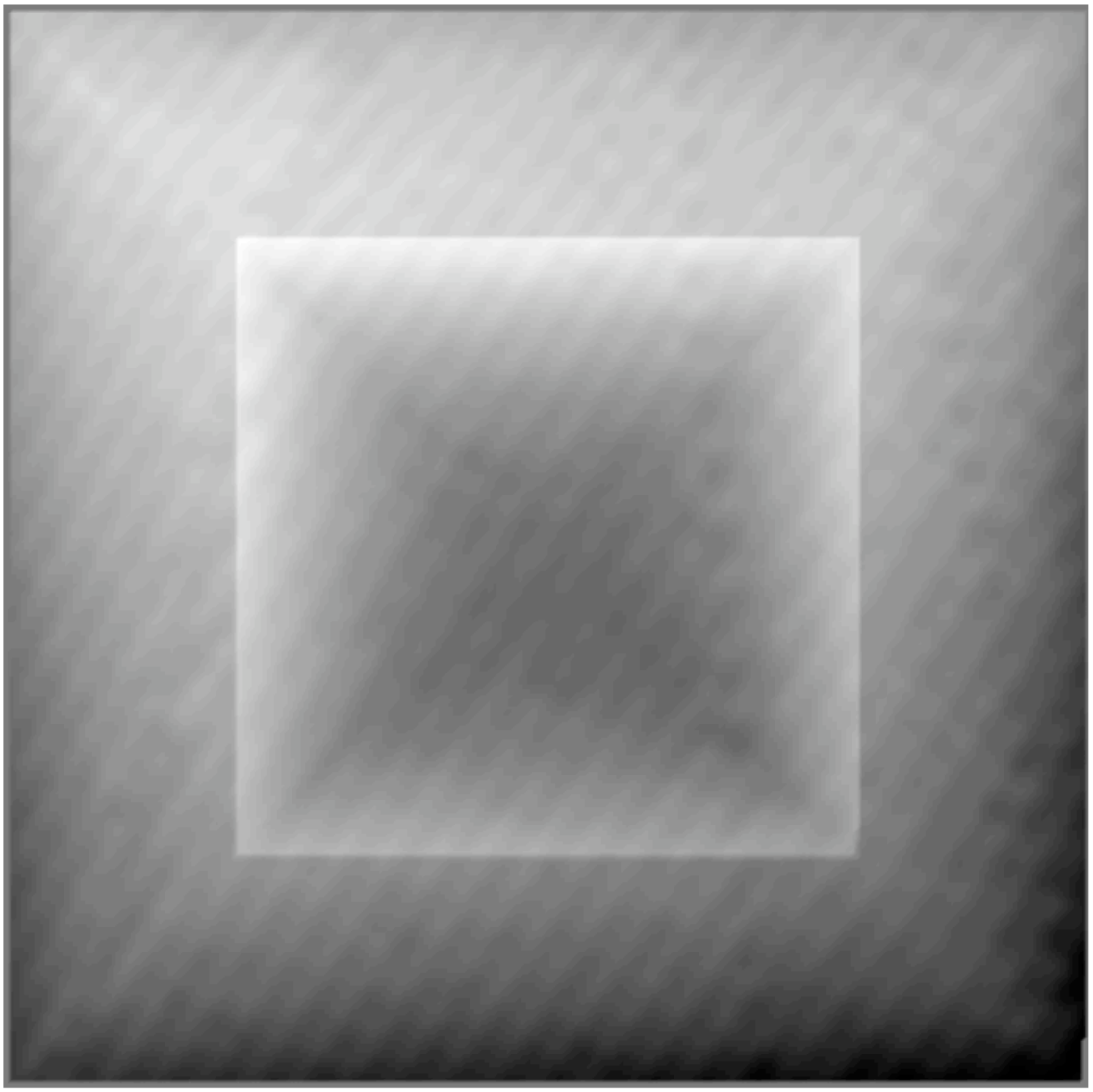

Figure 6.14: Large Area Scratch Height Image (7Sep07s1h)

Figure 6.14 is from the same scan as Figure 6.13, but it displays the height information from the parabolic curve locator. The top of the image is much higher than the bottom, with the difference being linear across the entire image. The central portion of the image shows a discontinuous jump in the height information, whereas the intensity image showed very little difference (yet noticeable) at the same pixels. We have observed

this sort of height discontinuity repeatedly (but not repeatably), in both directions (higher and lower), including multiple incidents during the same scan. Only the Constant Phase mode can cope with this sort of error.

There are two likely causes of the discontinuity. First, the sample holder is a simple friction holder and the sample carrier may be physically moving in its sliding fit (see Figure 4.5) as the sample is repeatedly jerked in and out in the Z direction. Second, the piezo tube may not be glued securely into its carrier, and under the strain of the piezo elongation and contraction, it occasionally jumps to a new position a few nanometers away. Neither possibility can be easily fixed with the current configuration. The sample holder needs to be removable, and the piezo tube cannot be re-glued without risking damage to the tube.

6.6 HORIZONTAL ORIENTATION OF THE GRATING

So far, all the grating images have had the grating oriented vertically, so that the pickup fibers receive light reflected from the sides of the ridges, but when the grating is oriented horizontally, the light reflects essentially equally into each pickup.

Figure 6.15 is at a resolution of 63×63 pixels with 5.60 DAC units per pixel.

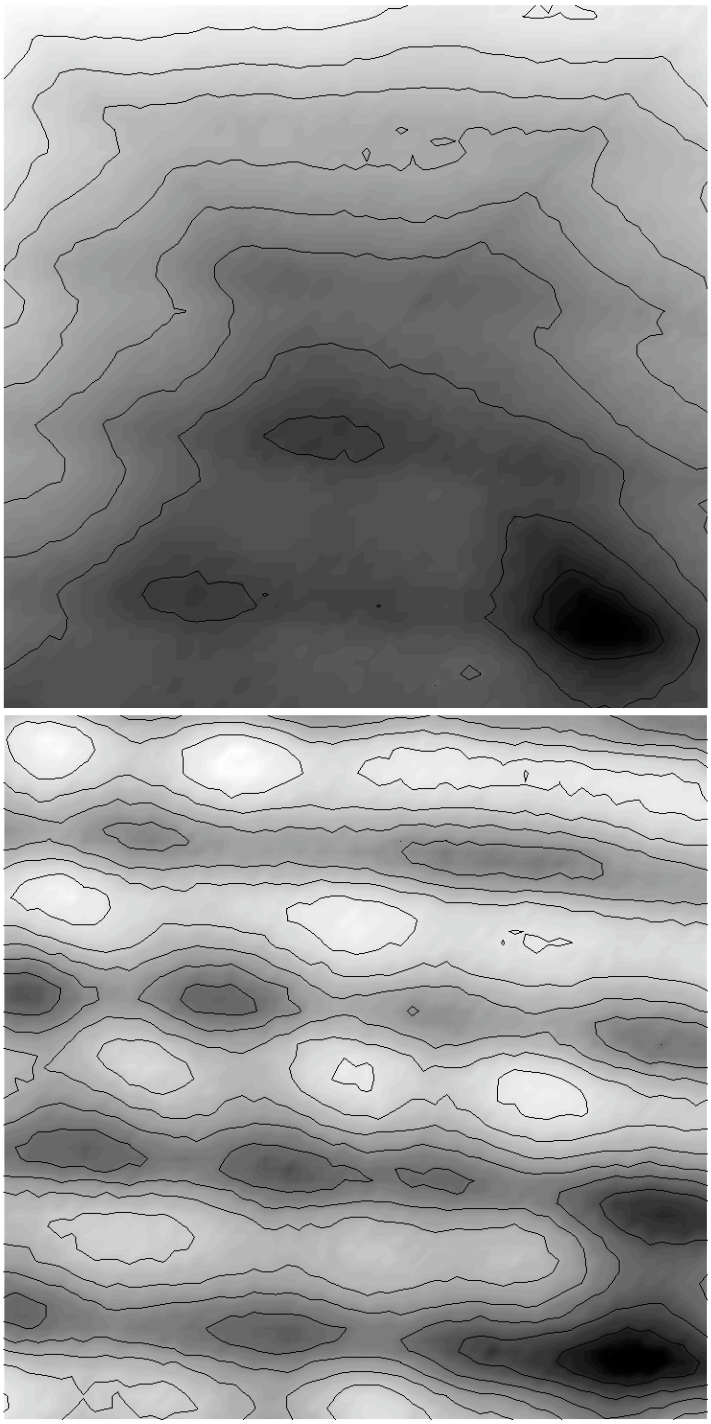

Figure 6.15: Constant Phase Mode in Horizontal Orientation (cp1May09) (top) Height (bottom) Intensity

There are several unique features of this scan. The height data shows a groove depth of only two nanometers (in the presence of a steep, almost planar distortion). The intensity image is more washed-out than usual. Along the vertical centerline, there is only a 14% difference between the brightest and dimmest pixels. The period of the grating is still roughly correct at 246 nm. Notably, the peaks of the grating show up as brighter, not dimmer as was the case for the vertical orientation.

The Constant Phase algorithm needs to locate a parabolic region of the intensity curve for a pixel, and since the scan completed, this must have happened nearly 4000 times. The low apparent depth of the grating must therefore indicate that the light was not reflecting directly into the pickups from the nadirs of the groves, but was instead "banking" into the pickups from the ridges immediately above and below the tip. Since the scan was carried out at the peak of the approach curve, light from the nadirs would experience destructive interference and be much dimmer.

This example serves to highlight the difficulties of obtaining accurate information from the samples. The intensity of the reflected light is a complicated combination of small gaps, surface topology and reflectivity, and destructive and constructive interference. The images can look completely different depending on the precise point of the intensity curve that you chose to examine. If you already know what you are looking at, it will be easier to get a good scan.

6.7 FASTER SCANS

All of the scans discussed so far have used an average of the ADC reading for all sample data points. The ADC value is averaged over 1/60 of a second to remove the small 60 Hz noise component. Since the movements take 3 ms or less, this has the advantage that the majority of the data point is taken from the actual commanded location without introducing a delay for the completion of the movement. However, some

interesting artifacts occur when the ADC is averaged over microseconds instead of milliseconds, without waiting for the movement to complete.

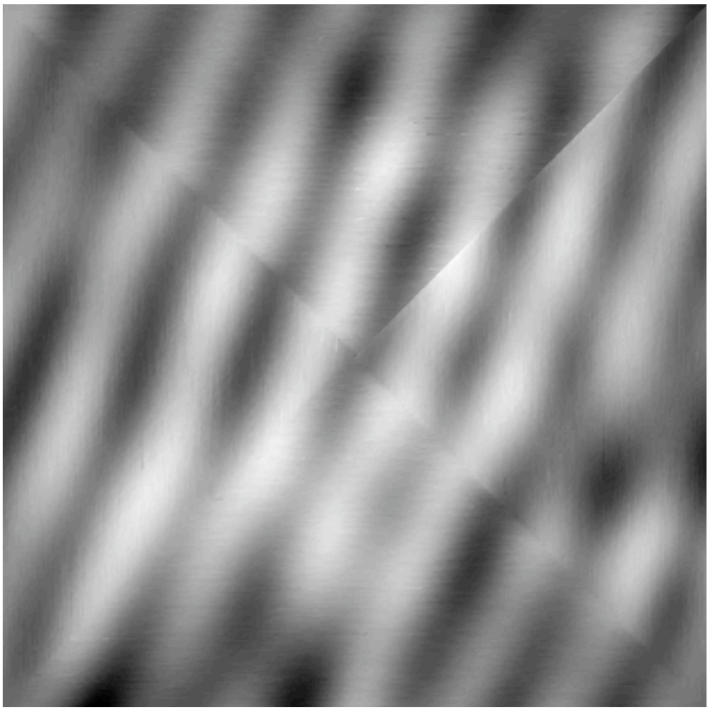

Figure 6.16: Fast Constant-Extension Scan (ce13Apr09_1)

This scan was conducted in constant extension mode, without moving in Z at all, and averaged each sample over only 4 ADC readings, about 60 μs. The image is 309×309 pixels at 2.00 DAC units per pixel (about 1741 nm square). In the intensity image, the turning points of the scan are clearly visible as the X and Y locations that are always "behind" where they are commanded to be; the image is slightly fuzzier than the slower scans. As a positive feature, the scan required only one minute to complete (at approximately 1560 pixels/sec).

A similar scan was made in Constant-Phase mode at 100 samples (1.5 μs) per data point. Although we could see the grating structure, each pixel took two attempts (or more) to locate the parabola, and in the results, alternate pixels were at alternate heights,

as if two images had been interleaved. The intensity image was only slightly better. This demonstrates why the piezo movement should complete before taking data.

Movements of the piezo tube require 2 to 3 ms to substantially complete (see Chapter 3). The flexure stage in the vacuum chamber (see Chapter 7) requires even longer to complete a movement. The 60 Hz noise is so small that it does not meaningfully affect readings, but without a long averaging time, the data points must first wait for movement to complete before initiating the ADC read operations.

6.8 ARTIFACTS IN SCANS

The scans we have made with our NSOM suffer from several artifacts that are not in the actual sample. In many instances, the straight lines of the diffraction grating are wavy, curved, or otherwise distorted. This may be explained by the piezo tube nonlinearity, irregularity, and hysteresis of movement. The Constant Extension mode does not suffer from this problem as much as a mode that moves the sample in the Z direction.

The samples frequently seem to be lower in the center and higher around the sides. This may be due to the nonlinearities of the tube scanner. The sample heights occasionally jump discontinuously. This is likely due to improper gluing of the tube into the carrier, or the sample holder sliding in its fixture.

The scans have artifacts introduced by the spiral scanning method, such that there are apparent height features concentric with the center and along the diagonals of the images. It would be interesting to rewrite the scanning algorithm to perform the more typical raster scan (with suitable cautions for initial extension distances).

If the sample is not exactly in line with the probe tip, then the height information from the scan will be distorted in a plane, as if on a tilting tabletop.

If the data acquisition takes place over much less than 5 ms, then a delay before taking data must be introduced, or the image will not have the data from the desired location.

The scans occasionally suffer from picking up a dust particle. This is obvious from the intensity images, but nothing can be done about this other than to ensure the samples are thoroughly cleaned prior to examination. The dust particles may be scraped off during a scan, just the same as they were picked up.

Chapter 7: The Vacuum Chamber NSOM

7.1 INTRODUCTION

There are a considerable number of changes that must be made to the NSOM system described in the previous chapters so that it can work inside an ultra-high vacuum (UHV) chamber: mostly hardware, but some software too. The software is located in a separate directory, in NSOM_project/vac_nsom. It contains all the files required to operate the vacuum NSOM, including keto_dac.c, the modified vac_routines.c, and the LabView files (vac_approach.vi and vac_scanner.vi). A Makefile is provided to automate the compilation process (simply type "make" while in that directory). The only electronics change is to use the KetoLab DAC (see Chapter 4) to provide the analog control voltages.

7.2 VACUUM CHAMBER

We have a small vacuum chamber constructed by a previous graduate student; it was intended to accommodate a different method of moving in X and Y and large-scale Z from the method we now use. The UHV chamber size should be kept as small as possible, since the ability to sustain the UHV condition is partially dependent on the surface area of the chamber and its contents. Our chamber has interior dimensions of 4"×5"×6". Unfortunately, these dimensions are not large enough to incorporate all the hardware that must be included.

The chamber includes a cold finger port for cooling the sample. The cold finger occupies a substantial portion of the chamber.

The flexure stage (described below) is nearly 4"×4"×2". It is oriented vertically in the chamber. Although it fits completely inside the chamber, the associated hardware

required to hold it and move it are to large to fit inside. The flexure stage must be held in front of a translation stage, not on top (due to the height restriction and cold finger location), and the translation stage has a picomotor to drive it. The combination, forced to its Z position by the cold finger, does not fit inside the chamber (which will now have to be remanufactured).

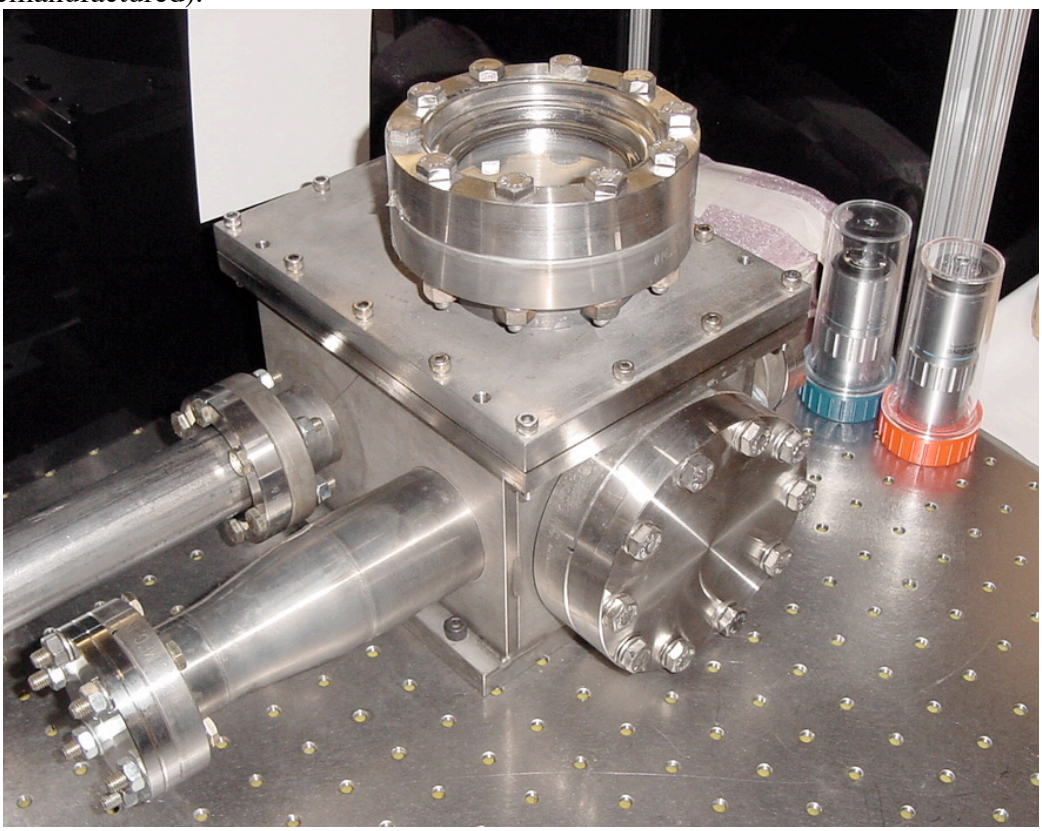

Figure 7.1: UHV Chamber

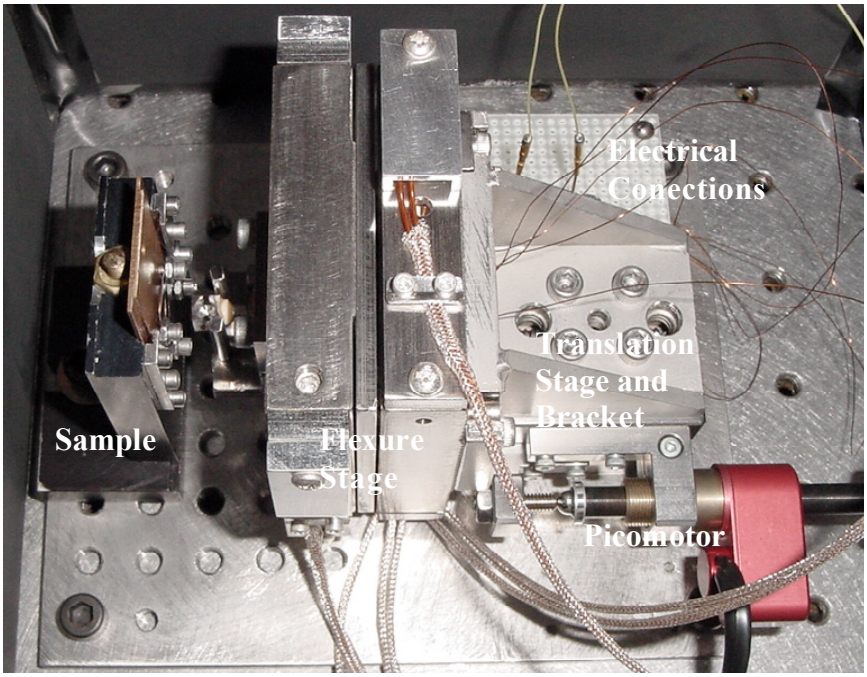

Figure 7.2: Vacuum NSOM in Test Arrangement

7.3 PROBE FIBER

The probe fiber, as mentioned previously, dissipates heat mostly through convection, which does not exist in a vacuum chamber. The amount of light that it can handle without damage is reduced. The amount of reduction must be experimentally determined.

The probe fiber may need to be replaced (after being damaged) without breaking the vacuum seals. Although we attempted to allow for this, the method is clumsy and inadequate; it is very likely to result in damaged tips. In addition, the tip needs to be positioned at the intersection of the pickup fibers, but there is no good way to do this with the current setup.

The probe fiber is aluminized over at least a portion of its length, and it runs on top of the piezo tube that has the possibility of high voltages on its exterior. There should be a shield between the piezo tube and the probe fiber.

7.4 CHAMBER ELECTRICAL PORT

Only one ConFlat port is available for all electrical connections. The flexure stage requires exclusive use of a D15-sized port. Other electrical connections are required for the picomotor on the translation stage (3 or 4) and the tube scanner (2 or 5).

We constructed a custom flange with two D15 electrical ports.

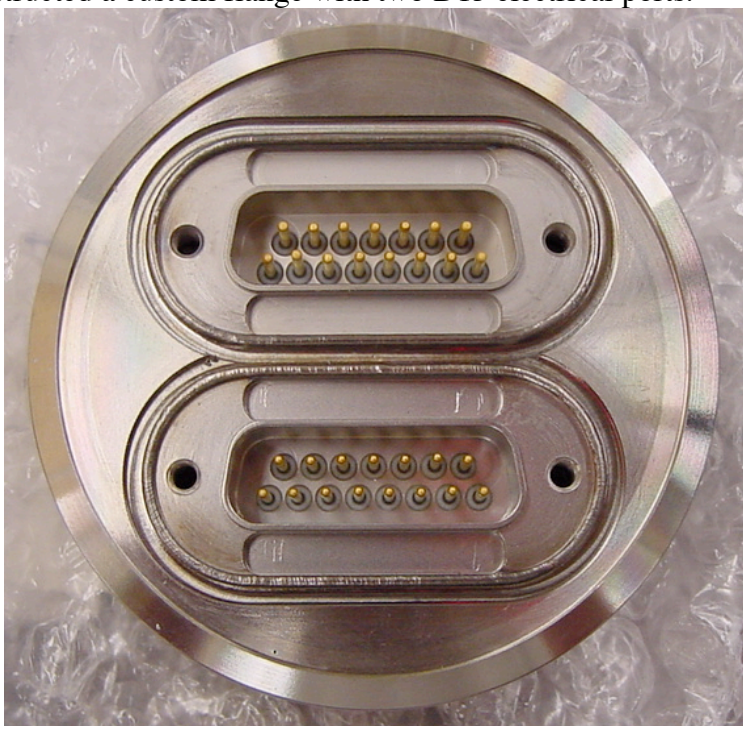

Figure 7.3: Electrical Flange

This ConFlat will need to be modified to allow the pickup fibers to pass from the chamber to the external PMT, unless a channel photomultiplier is used inside the chamber.

7.5 CHAMBER OPTICAL PORT

One ConFlat port is available for the optical probe fibers to pass from the outside (where the laser is) to the inside of the chamber. As probe tips are destroyed during use, they need to be replaced without breaking the vacuum seals. The ConFlat will include multiple fibers, and the tips will be stored inside the chamber so that someone on the outside, using a wobble stick, is able to replace the fiber tip that is on the flexure stage. When all the fiber tips are destroyed, the ConFlat will be replaced with a new set of fibers.

The space between the flexure stage and the sample is too small to permit this sort of tip replacement operation. The translation stage currently used does not permit a sufficient gap to make the replacement.

7.6 FLEXURE STAGE

The Flexure stage allows movement in X and Y. It is model NANO-UHV50 made by Mad City Labs (www.madcitylabs.com), and includes its driver electronics "Nano-Drive". It has a 50 μm range of motion. It is constructed of Invar to reduce temperature effects on position. The drive electronics convert two analog voltages (0 to 10 V) to a position in X and Y, and, through sensor resistors and electronic feedback circuits, it maintains the commanded position without creep or hysteresis.

The stage has a 5 to 10 ms response time, moving from 10% of the commanded motion to 90%. This step response time has not been characterized, although it can be. Knowing this would improve the accuracy of the images and reduce the time to acquire an image.

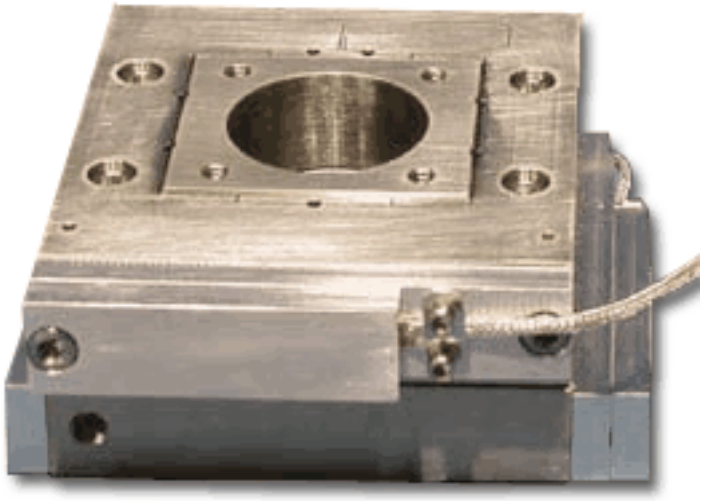

Figure 7.4: Flexure Stage

The flexure stage is mounted on a small translation stage. The small stage was chosen because of the known restrictions on the size of the chamber. Since the flexure stage is large and heavy and can include rapid (if short) movements, we recommend moving to a larger translation stage. This should improve stability and facilitate tip replacement.

7.7 TUBE SCANNER FOR THE CHAMBER

The tube scanner must be held in the position for scanning the sample, which means that it must fit inside the flexure stage. We have a design that allows the chamber to change in temperature without changing the position of the tip.

The tube scanner is designed to extend toward the sample when the control voltage makes the tube contract. The software in the approach application and the scanner application has been modified to accommodate this. It is capable of using the standard quartered-electrodes to conduct rapid small-area XY scans, which should be faster than using the flexure stage.

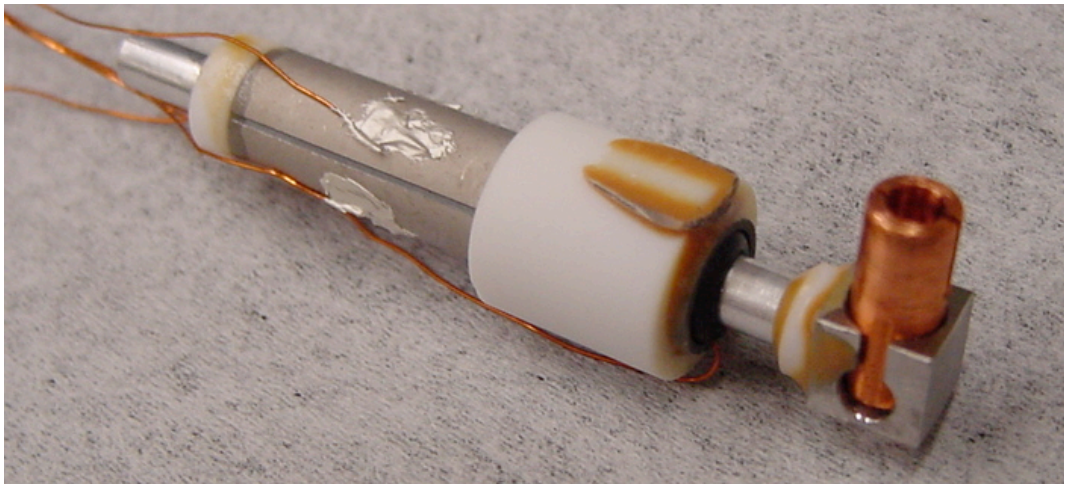

Figure 7.5: Vacuum Chamber Tube Scanner

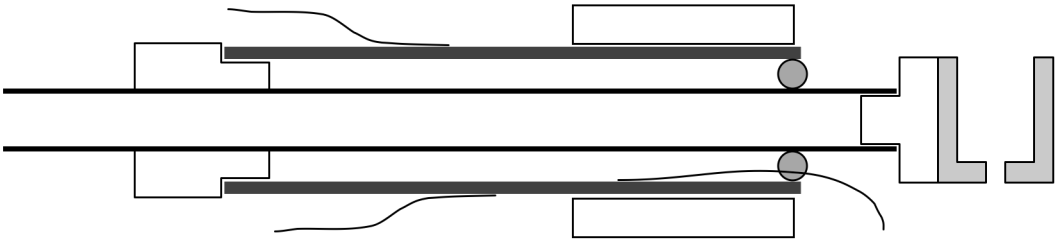

Figure 7.6: Section Through the Tube Scanner Assembly

Our chamber is made of stainless steel 304, with a coefficient of thermal expansion of approximately 18.2×10^{-6} /°C. The other relevant components of the system are composed of Invar (1.2×10^{-6} /°C), aluminum (23.0×10^{-6} /°C), PZT (1.5×10^{-6} /°C), and MACOR (9.5×10^{-6} /°C). The short copper tube in Figure 7.5 is the carrier for the probe fiber; the fiber is glued into it. A small o-ring provides mechanical support for the fiber holder but does not interfere with Z motion.

We would like to have the distance between the sample and the probe tip not change with temperature, even when the temperature is not a fixed value (the cold finger will dramatically change the temperature of the chamber). If the temperature of the

chamber is steady, in the configuration shown a 1.09" length of aluminum holding the fiber from the far end of the tube scanner will compensate for the shrinkage (or lack thereof) in the materials of the chamber and flexure stage and tube scanner. If the temperature is changing, especially if the temperature is changing at different rates between the tube scanner and the chamber floor, then there is no way to compensate for the changes; the distance between the tip and sample is going to change, probably beyond the ability of the tube scanner to compensate for.

7.8 PICKUP FIBERS

The pickup fibers on the original NSOM are far too thick to fit into the flexure stage opening. The opening is only 0.75 inches in diameter, and the pickup fibers need to be able to point at the probe tip, at nearly a 45° angle. The thicker (1 mm) fibers will not bend enough. For the vacuum chamber, we are using 400 μm core diameter multi-mode "Superguide" fibers. They are at approximately a 40° angle to the tip, so the interference in the approach curve has a 347 nm periodicity instead of 376 nm. The fiber bend diameter is smaller than the manufacturer's recommendation.

Based on their NA of 0.39 (estimated since the documentation is missing), the optimal location for these fibers is no more than 0.47 mm from the probe tip.

7.9 RESULTS

We configured the hardware and software for the vacuum chamber version of the NSOM. We obtained a scan that was obviously an image of the diffraction grating, with lines in the image at the nominal spacing, but the scan did not complete. We fixed a software bug, but before we could test it, the flexure stage developed a hardware and/or electronics fault. Before sending the unit out for repair, we obtained several images that, in hindsight, were the diffraction grating, but were greatly distorted by the fault.

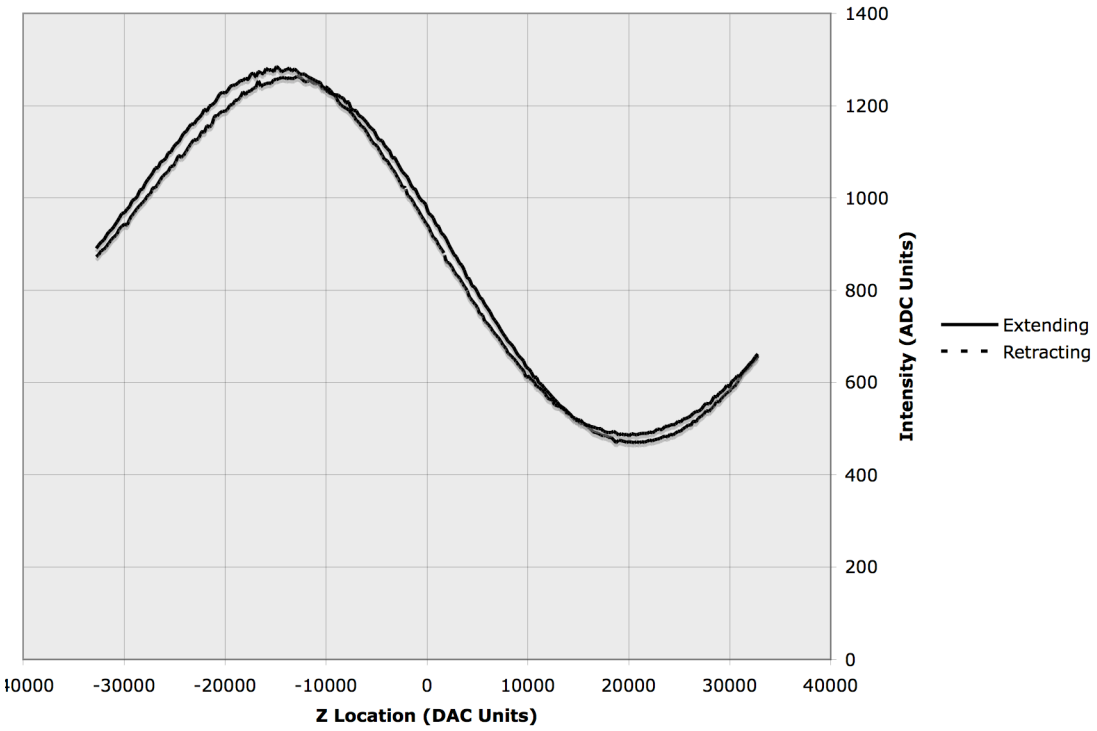

Figure 7.7: Approach Curve for Vacuum Tube Scanner

In Figure 7.7, the sample surface is again to the right, at the maximum extension. The exterior of the tube scanner is grounded, and the interior is at most -84 V. The difference between the high and the low of the extending curve is approximately 33660 (in DAC units). Estimating the angle to the pickup fibers as 40°, from Equation 2.1 the period of the oscillation should be 347 nm, and the real distance between the high and low is 174 nm. Solving Equation 3.1 for the parameter d_{31}, we obtain 0.82 Å/V. This is 35% less than the nominal value as specified by the manufacturer. The tube may have been damaged by heat during the epoxy procedure (attaching the MACOR and the electrode wires). The tube may need re-poling; alternatively, it is perfectly usable just as it is, albeit with a limited ability to cope with height changes. A doubling of the range can be obtained by connecting the negative-Z output of the piezo amplifier to the outer electrode of the tube (taking care not to short the probe fiber to the electrode).

Chapter 8: Conclusions and Future Prospects

8.1 Conclusions

This project has demonstrated the operation of our Near-Field Scanning Optical Microscope. It clearly observes a diffraction grating target and measures the dimensions of the surface topology. It uses 532 nm light to distinguish features on the diffraction grating much less than 278 nm apart. Indeed, differences on the order of 10 nm are visible if the topography is favorable.

We have demonstrated the use of purely optical feedback in the Z-positioning system, in two different algorithms. The system is much faster than commercial instruments that must use shear force microscopy to determine the distance to the sample. The use of optical feedback will be absolutely essential for operation in UHV. Optical feedback also permits operation in a liquid medium, which may have application to the biological sciences.

We have adapted the NSOM to use a flexure stage for better X-Y control. The flexure stage will be used in the vacuum chamber version of the NSOM.

The vacuum NSOM awaits the return of the repaired flexure stage. We anticipate no problems with obtaining good scans.

8.2 Future Prospects

There are multiple opportunities for improving this instrument, especially in the context of the vacuum chamber and cold finger. The mandatory improvement is to increase the size of the vacuum chamber.

The large-scale movement of the probe is very limited. Some way to move it in X and Y, perhaps using multiple picomotors, would permit the scanning of any part of the sample, not just the part that happens to be within 25 μm of the probe.

The mechanical arrangement of the flexure stage and the tube scanner needs improvement. The replacement, from outside the chamber, of a damaged tip would be nearly impossible with the current configuration. To obtain maximal signal levels, the position of the tip needs to be adjustable in relation to the pickup fibers.

The CAMAC system, although useful, is an aging standard. Moving the NSOM to a computer with a high-quality National Instruments DAQ interface would be relatively easy and would ensure continued electronics support. LabView already supports multiple interface standards (*e.g.* IEEE-488) and includes many instrument drivers.

The piezo drive electronics can be converted to a charge amplifier, thus reducing the inherent hysteresis in the tube scanner movement.

The optical fibers, both probe and pickup, need better cleaving and polishing tools. Fiber-to-fiber couplers (outside the chamber) may be useful when changing tips for the vacuum chamber.

The software can be improved with different scanning methods, characterizing and compensating for the tube scanner characteristics, and processing the images to enhance contrast, compensate for tube scanner distortions, or deconvolve the aperture.

Appendix 1: Application for Debugging

To facilitate debugging, and to investigate some mechanical and electrical properties of the NSOM, we developed a small LabView Application called quicktestADC. It is located at NSOMproject/new_nsom/quicktestADC.vi. It uses the old_dac to control the Z piezo. A different version using keto_dac is in the NSOM_project/vac_nsom directory.

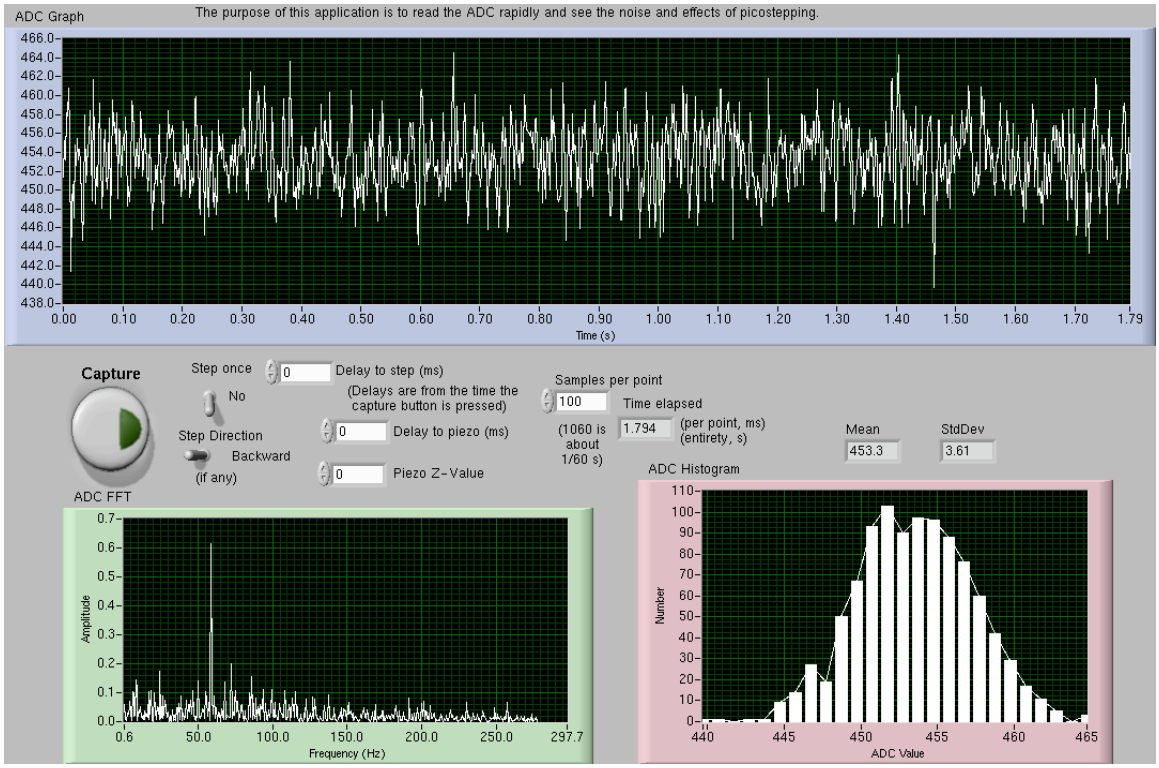

Figure A1.1: Front panel for quicktestADC.vi

The top graph is a time plot, consisting of 1000 ADC samples. Each sample is an average of one or more ADC values, as determined by the "Samples per point" parameter. The application can cause a single picomotor step, in either direction, and/or change the piezo value; each change can have a delay to that action. The bottom left

graph is an FFT of the data (the example shown includes a small amount of 60 Hz noise). The bottom right graph is a simple histogram of the data, with the mean and standard deviation shown above it.

The application does not alter the piezo value (Z, X, or Y) upon initialization. The operator should be very careful about changing the piezo or picostepping near the sample, because there are no safeguards or limits on any operation.

This application was found to be useful in debugging the ADC card switch settings and determining the speed of the piezo movement. It frequently observes small amounts (<1%) of 60 Hz noise from the ADC; we think it is coming from the PMT or its supply since it increases with PMT supply voltage but not with amplification. It helped to discover the point of diminishing effectiveness for the number of ADC samples to average. It also detected intermittent fluctuations in the PMT power supply.

Appendix 2: Mechanical Drawings

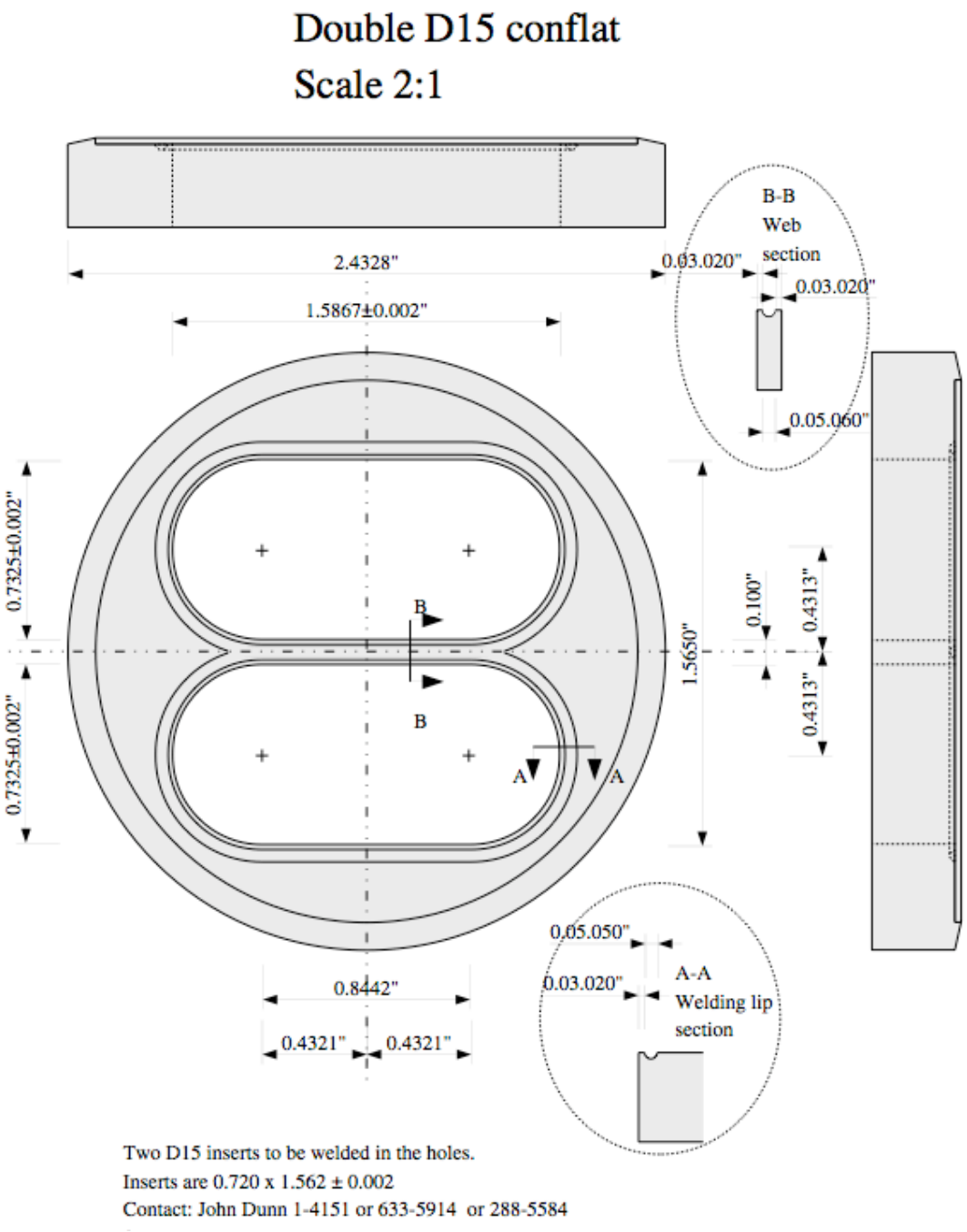

Figure A2.1: Double D15 ConFlat

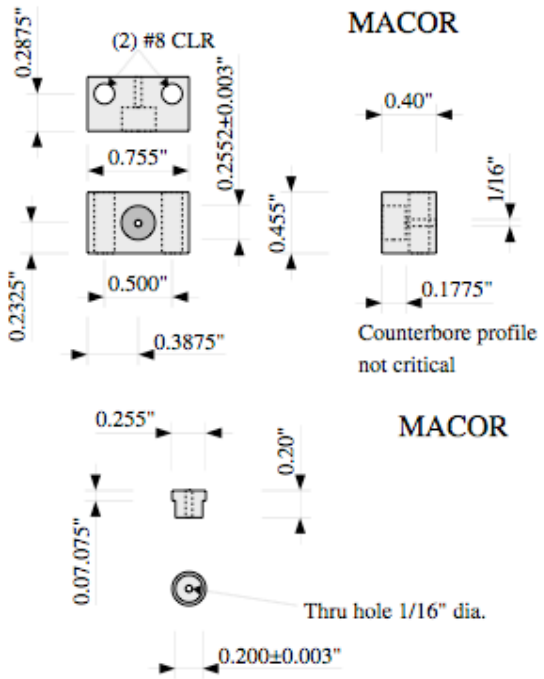

Figure A2.2: New NSOM MACOR Parts (non-vacuum)

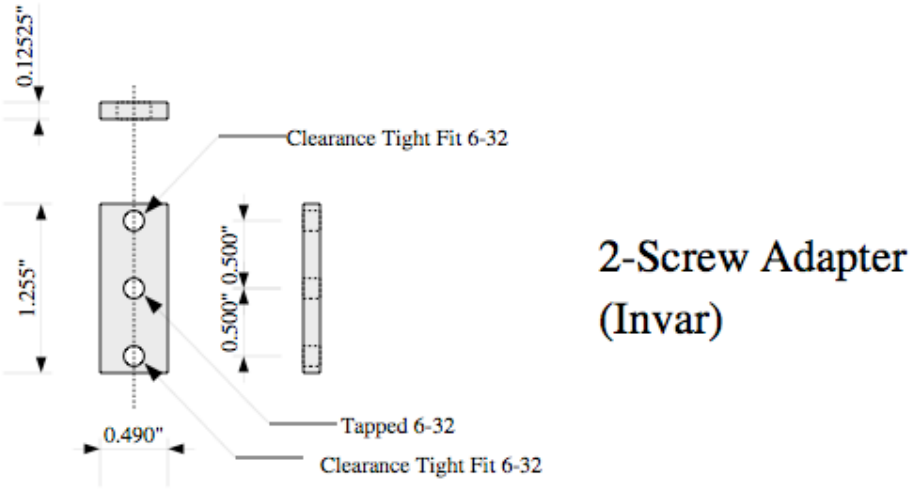

Figure A2.3: Invar Adapter

The flexure stage has a strange mounting hole pattern.

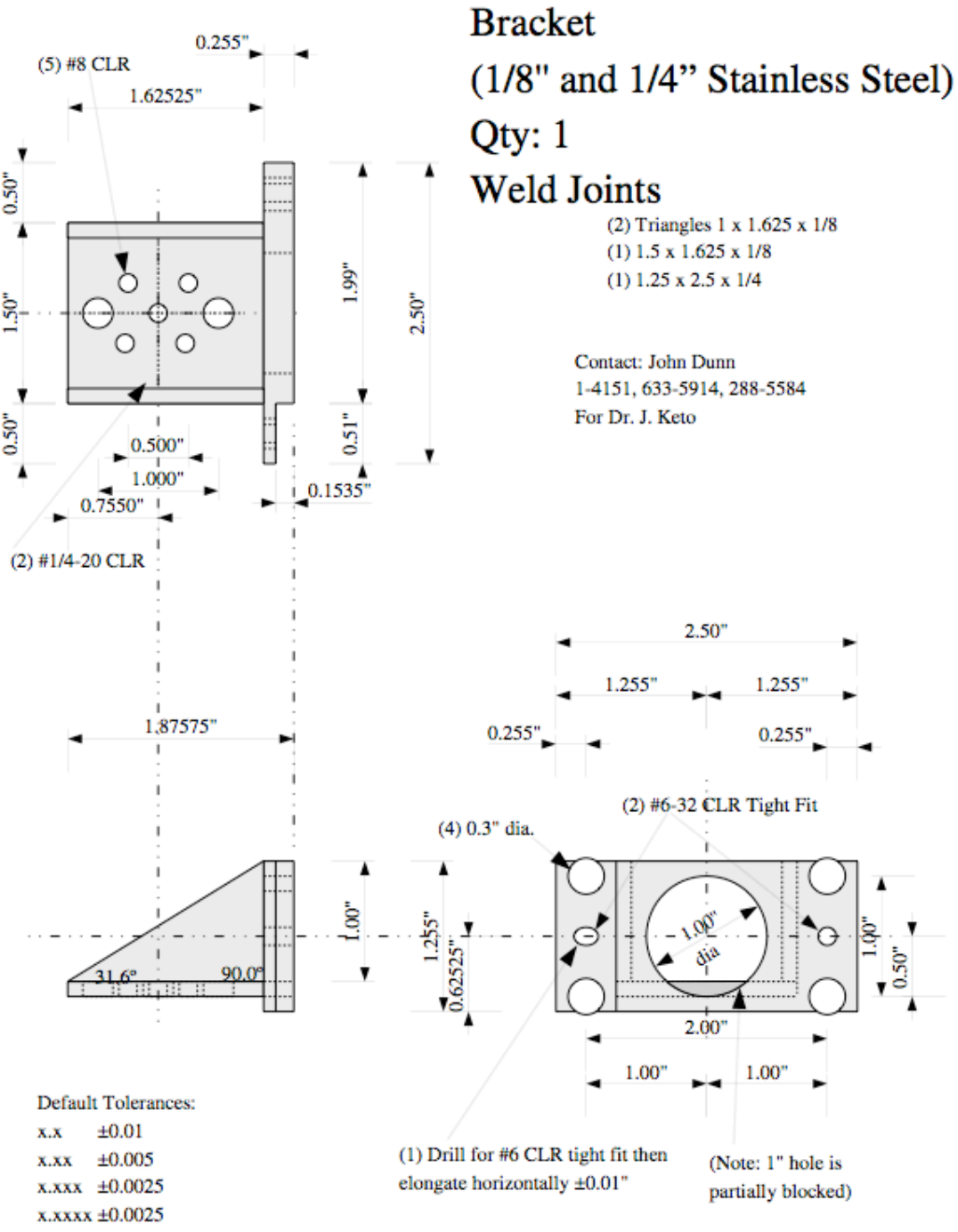

Figure A2.4: Flexure Stage Bracket

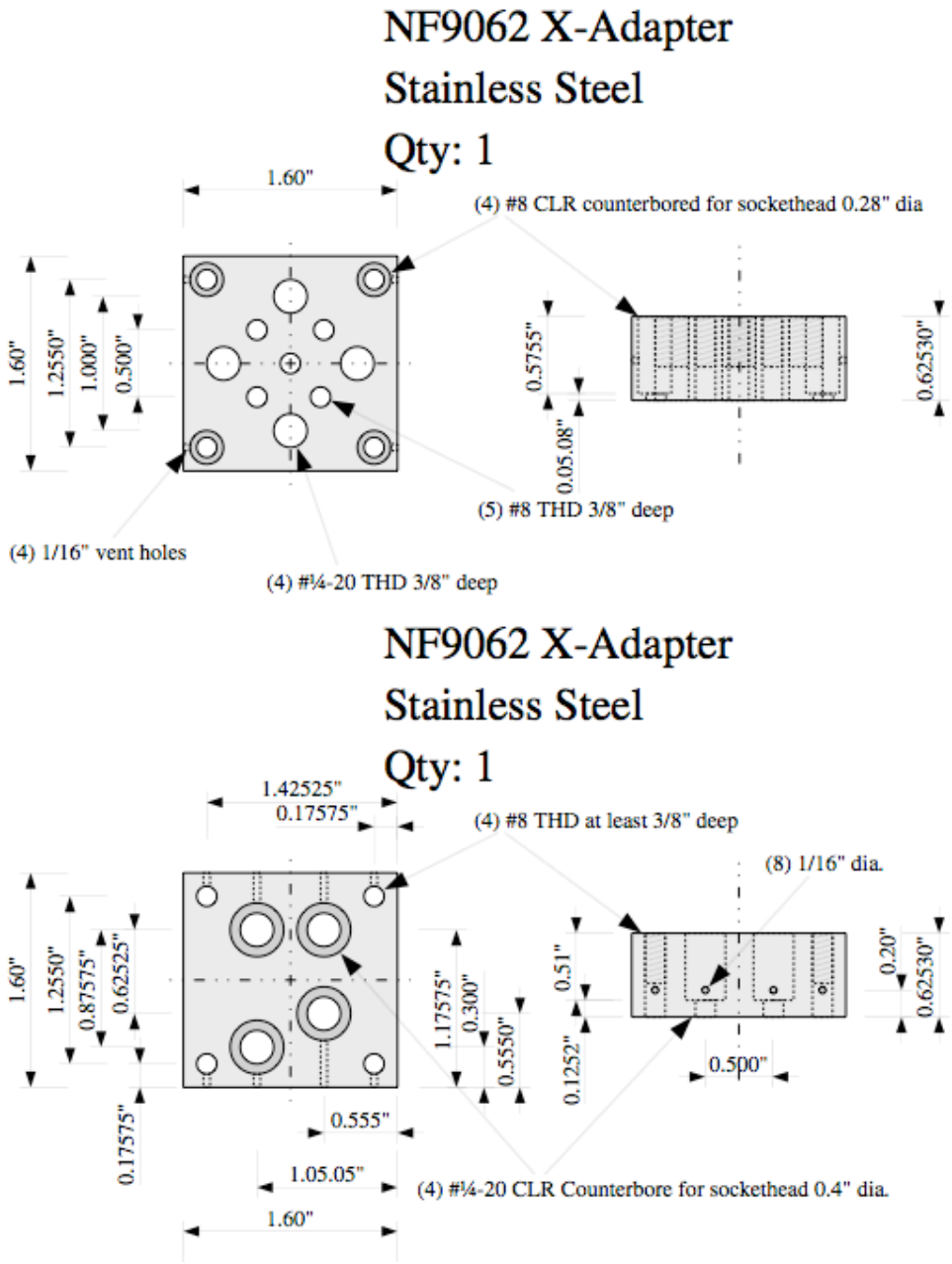

Figure A2.5: Translation Stage Replacements

Two versions depending on the location of the Y-stage (bottom or top). Oddly spaced holes in the second one work with the base plate to allow 1/8-inch adjustments.

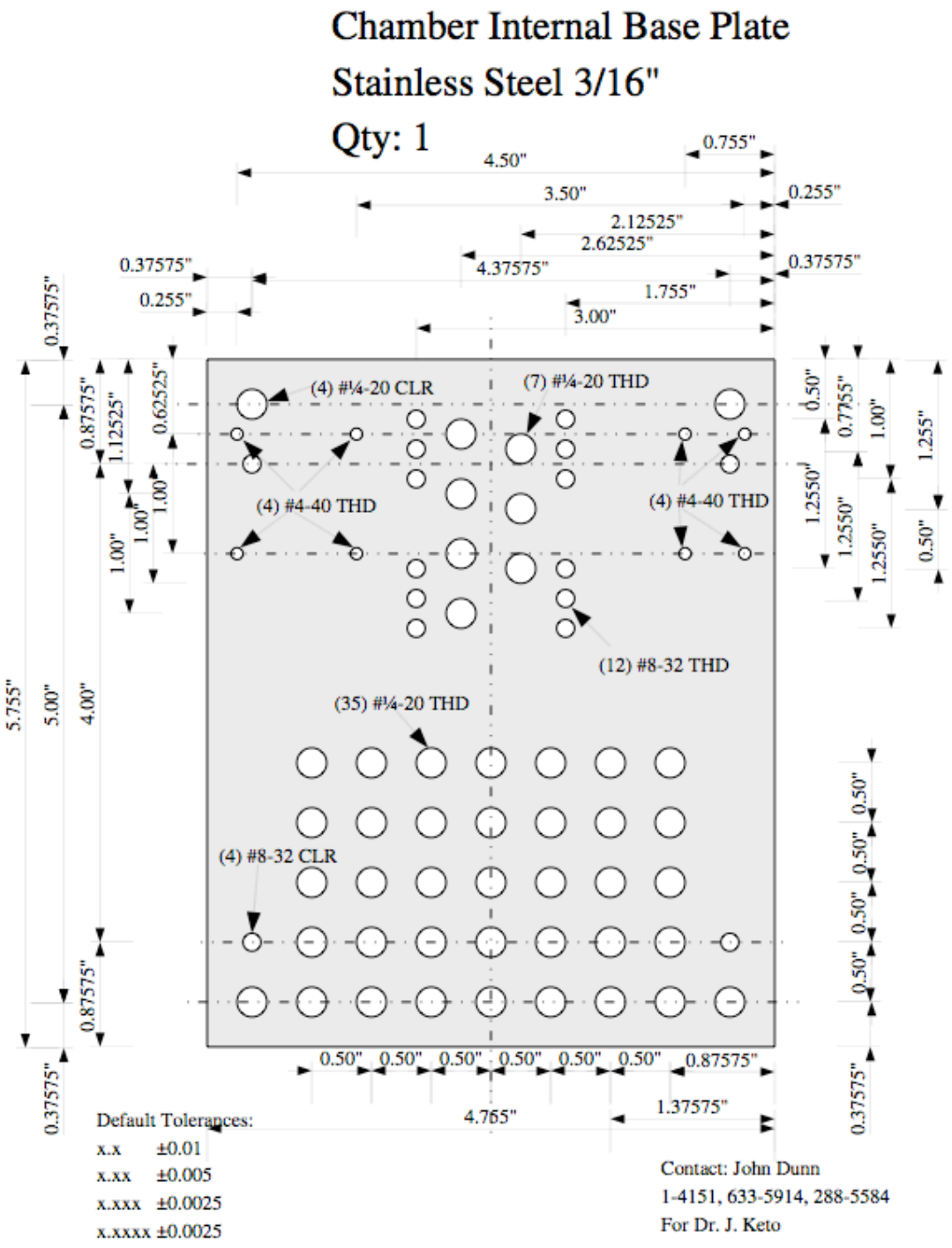

Figure A2.6: Chamber and Mockup Base Plate

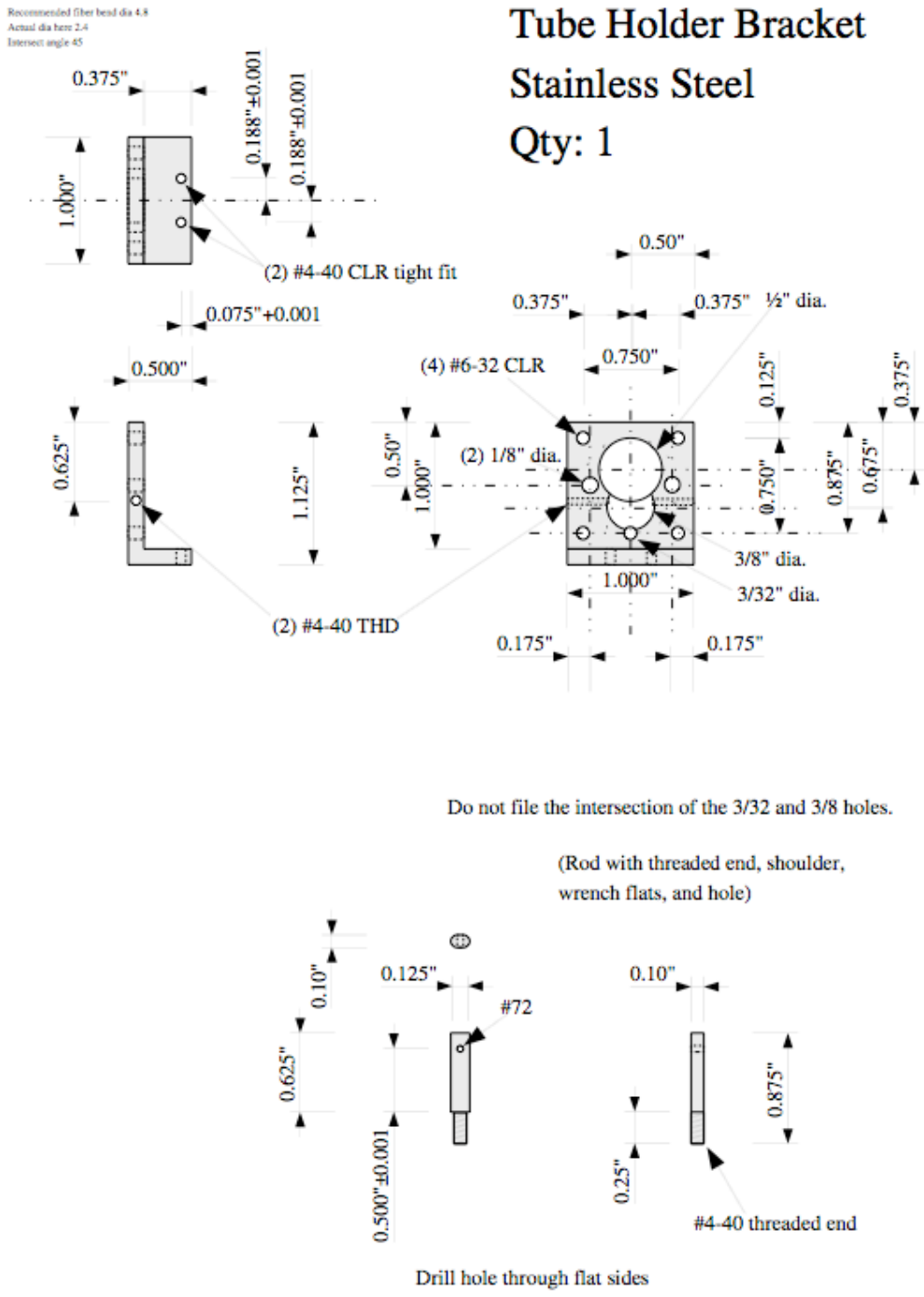

Figure A2.6: Tube Holder Mount and Fiber Guides

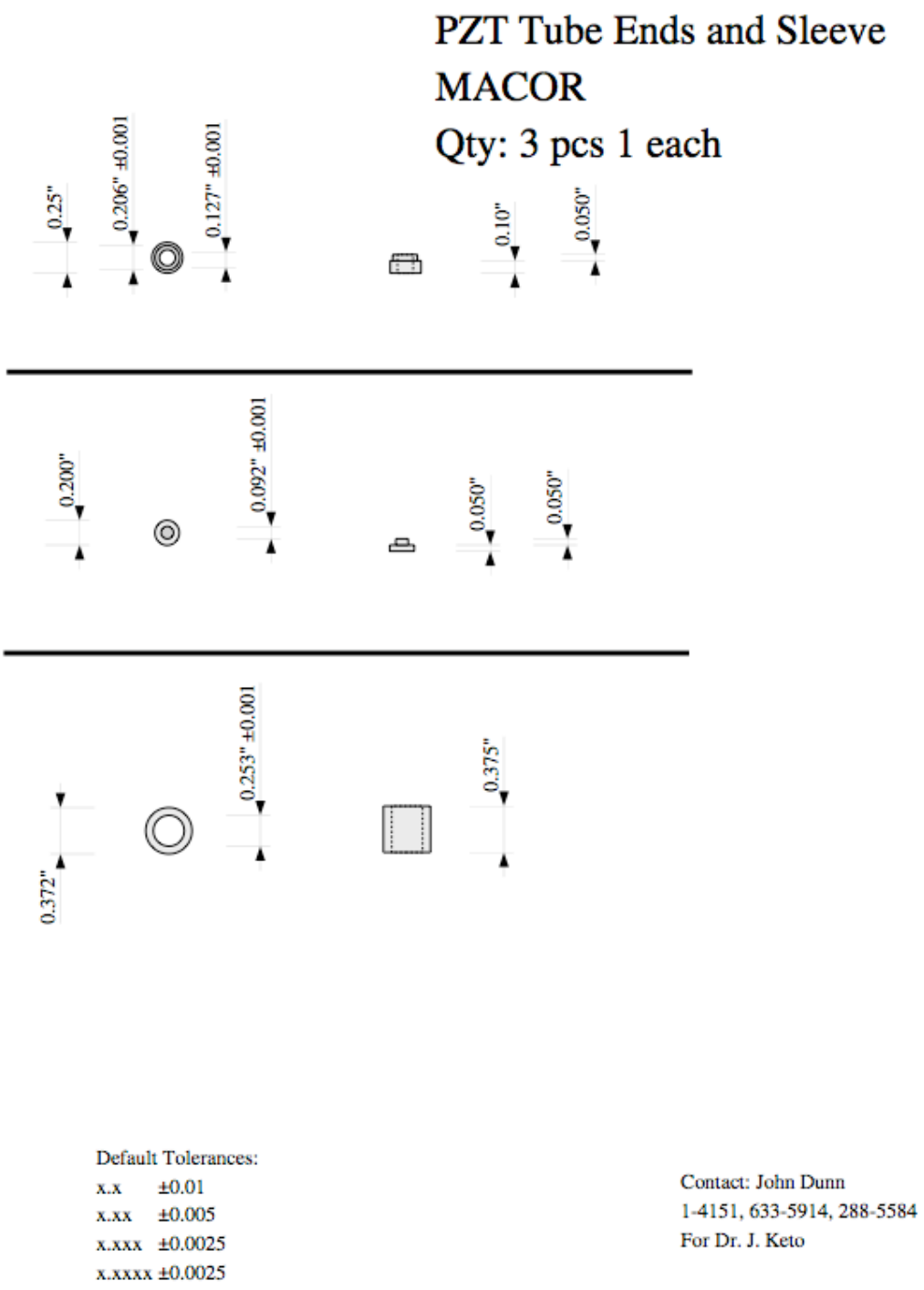

Figure A2.7: Tube Scanner Ends and Sleeve (vacuum chamber)

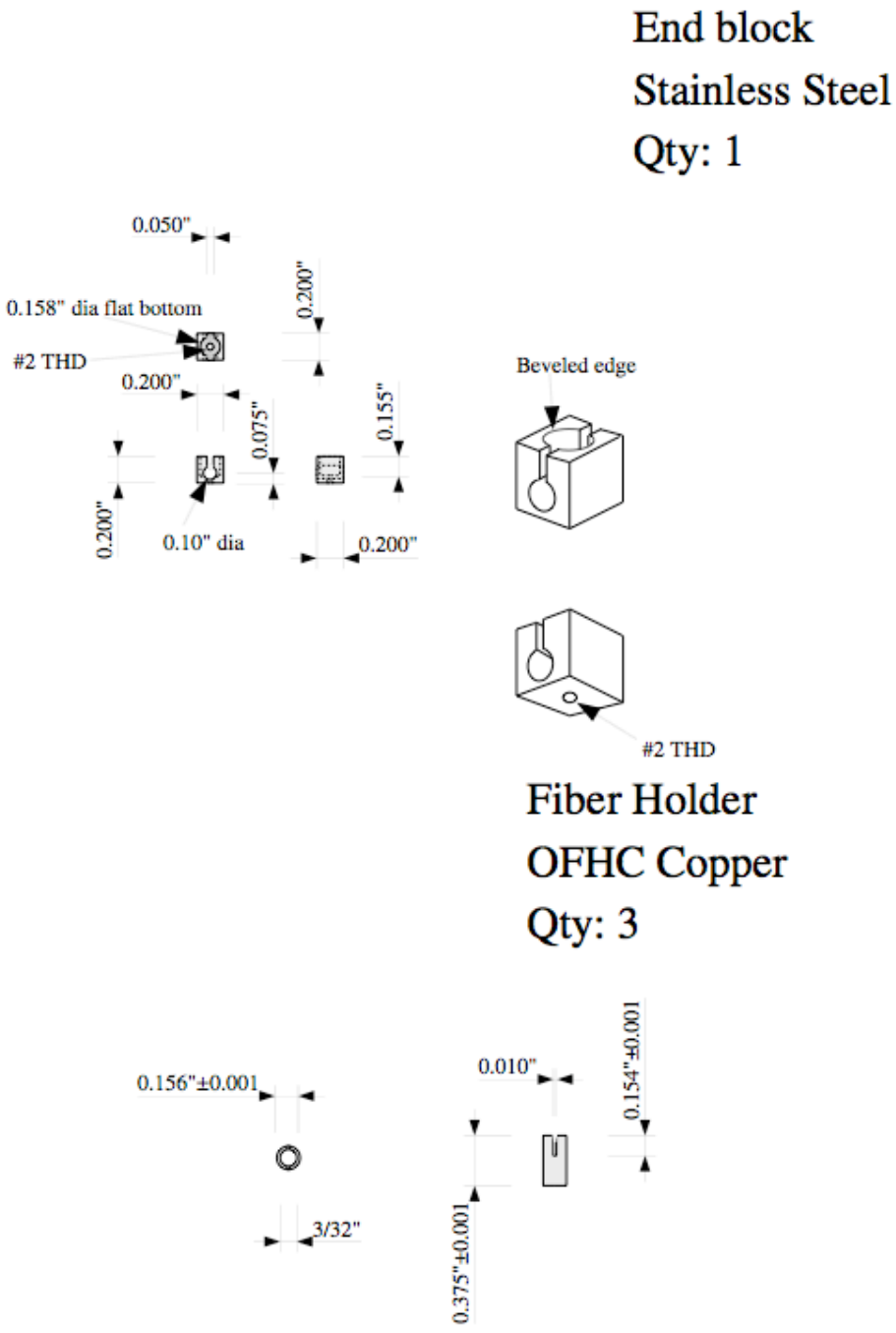

Figure A2.8: Fiber End Block and Fiber Holder

Glossary

ADC	Analog to Digital Converter: converts an analog voltage to a digital value readable by a computer.
CAMAC	Computer Automated Measurement And Control; a standard parallel bus specification for electronics, common in physics and industry.
Cold Finger	An apparatus for cooling a sample without cooling the entire vacuum chamber.
CPM	Channel Photomultiplier: similar to a PMT but smaller and more sensitive with less noise; converts photons to a current.
DAC	Digital to Analog Converter: converts a digital value from the computer to an analog voltage.
DAQ	Data AcQuisition; generic term for a computer interface to the analog world, including sensors and signal conditioning.
LabView	A programming environment for humans interfacing with hardware; made by National Instruments, Inc.
LAM	A CAMAC interrupt; acronym for "Look At Me". The computer will quickly read the data into memory and await software service.
NA	Numerical aperture; the sine of half of the acceptance angle for optics.
Near-Field	A sample so close to an aperture that the light does not propagate as a wave. The far-field regime for a diffracting aperture is where the wavefronts of the light are collimated; this is called Fraunhofer diffraction, and is subject to the diffraction limit. The near-field, or Fresnel diffraction, occurs where $a^2 \ll d\lambda$, with a the diameter of the aperture, d the distance to the sample, and λ the wavelength of the light.

NSOM	Near-Field Scanning Optical Microscope; see Chapter 1.
Picomotor	Uses piezoelectric components to rotate a screw in (approximately) 25 nm steps; made by New Focus, a division of Oclaro, Inc.
Piezo	A piezoelectric component; changes its physical dimension in response to an applied electric field, and *vice versa*.
PMT	Photomultiplier Tube; detects light and converts it to a current.
SEM	A Scanning Electron Microscope uses a raster-scanned electron beam to make an image. The electrons have a shorter wavelength than light and can see features of less than a nanometer. Objects must be electrically conductive, and the scan occurs in a vacuum.
SNOM	see NSOM; an alternative term in some of the literature.
SPM	Scanning Probe Microscopy; NSOM is one type of SPM.
TPI	Threads per inch.
UHV	Ultra-High Vacuum has gas pressures less than 10^{-7} Pascals; UHV reduces sample surface contamination and is especially required in long-duration experiments, but is difficult to establish and maintain.
Wobble Stick	A mechanical device used to manipulate items inside a vacuum chamber from the outside.

References

[Bethe] Bethe, H A, "Theory of diffraction by small holes", *Phys. Rev.* **66**, 163 (1944)

[Bout] Bout, David Vanden, University of Texas at Austin, Department of Chemistry, personal communication 6 May 2009

[Carminati] Carminati, R., Greffet, J., "Equivalence of constant-height and constant-intensity images in scanning near-field optical microscopy", *Optics Letters*, **21**, 16, 15Aug96, p1208-1210

[Chen] Chen, C. Julian, "Electromechanical Deflections of Piezoelectric Tubes with Quartered Electrodes", *Appl. Phys. Lett.* **60** (1) 6 Jan 1992, p132-4

[Comstock] U.S. Patent 4263527 "Charge control of piezoelectric actuators to reduce hysteresis effects" (21 Apr 1981)

[DunnR] "Near-Field Scanning Optical Microscopy", *Chem. Rev.* **1999**, *99*, p2891-2927

[eblproducts] http://www.eblproducts.com (formerly Staveley NDT)

[El Rifai] El Rafai, Osamah M, Youcef-Toumi, Kamal, "Modeling of Piezoelectric Tube Actuators"

[Fleming] Fleming, A J, Mohemani, S O, *IEEE Trans. Control Syst. Technol.* **14**, 33 (2006)

[Gerbracht] Gerbracht, Michael, Near Field Scanning Optical Microscope, Master's Thesis, The University of Texas at Austin, 2004

[Guttroff] Guttroff, Gunther, Scanning Near Field Microscopy and Spectroscopy, Master's Thesis, The University of Texas at Austin, 1995

[Haseno] Haseno, M, Tanaka, Y, Nagasaka, Y, Nagasaki Institute of Applied Science

[Hicks] Hicks, Thomas R, Atherton, Paul D, The NanoPositioning Book, Queensgate Instruments Ltd. 1997

[Koops] Koops, K R, *et.al.*, *Appl. Phys A* **68**, 691-697 (28 Apr 1999)

[Moheimani] Moheimani, S O, *Rev. Sci. Instrum.* **79**, 071101 (2008)

[Novotny] Novotny, L, "The History of Near-Field Optics", *Progress In Optics* **50**, p.137-184, E Wolf (ed.) (Elsevier 2007)

[ntmdt] http://www.ntmdt-tips.com/catalog/gratings/tdg/products/TDG01.html

[Olympus]
http://www.olympusmicro.com/primer/techniques/nearfield/nearfieldintro.html

[physikinstrumente] http://www.physikinstrumente.com/en/products/piezo_tutorial.php

[rdunngroup]
http://www2.chem.ku.edu/rdunngroup/images/Technique_Dev.stuff/NSOM/new_pa11.jpg

[Shiku] Shiku, H., Krogmeir, J., Dunn, R., "Noncontact Near-Field Scanning Optical Microscopy Imaging Using an Interferometric Optical Feedback Mechanism", *Langmuir* **1999**, 15, p2162-2168

[Stahelin] Stahelin, M, et.al. *Appl. Phys. Lett.* **68** (19) 6 May 1996, p2603-5

[Synge] Synge, E H, "A suggested model for extending microscopic resolution into the ultra-microscopic region", *Philos. Mag*. 6:356-362 (1928)

Vita

John P. Dunn was born in Houston, Texas, on July 28, 1961. He is the son of Daniel B. Dunn and Ann S. Dunn. He graduated from Northbrook Senior High School in 1979. He graduated from Texas A&M University in December 1982 with a Bachelor of Science degree in Electrical Engineering. He worked in the integrated circuit and electronics industry for 17 years before pursuing a degree in Physics. He holds 8 US patents and has had 3 publications. He is married to Wendi R. Dunn, and has one son, Steven P. Dunn.

Permanent address: 9604 Dawning Ct.,
Austin, Tx, 78736

e-mail: jwsdunn@austin.rr.com

This thesis was typed by the author.